# Studying the Impact of Infertility Treatment, Maternal Diet and Hyperandrogenemia on Primate Ovarian Follicle, Oocyte, and Preimplantation Embryo Development

By

Sweta Ravisankar

A DISSERTATION

Presented to the Department of Cell, Developmental and Cancer Biology and the Oregon Health & Science University School of Medicine
in partial fulfillment of the requirements for the degree of

Doctor of Philosophy

April 2020

School of Medicine

Oregon Health & Science University

**Certificate of Approval**

**This is to certify that the Ph.D. Dissertation of**

*Sweta Ravisankar*

*"Studying the Impact of Infertility Treatment, Maternal Diet and Hyperandrogenemia on Primate Ovarian Follicle, Oocyte, and Preimplantation Embryo Development"*

**Has been approved**

Mentor: Shawn L. Chavez, Ph.D.

Mentor: Jon D. Hennebold, Ph.D.

Member/Chair: Michael V. Danilchik, Ph.D.

Member: Charles E. Roselli, Ph.D.

Member: Lawrence Sherman, Ph.D.

Member: Sacha A. Krieg, M.D., Ph.D.

Member: Caren Weinhouse, Ph.D.

## TABLE OF CONTENTS

109
110

## LIST OF FIGURES

## LIST OF TABLES

# LIST OF ABBREVIATIONS

| | |
|---|---|
| $\chi^2$ | Chi-square |
| ACSM4 | Acyl-coA synthetase medium chain family member 4 |
| ADAMTS1 | a disintegrin and metalloproteinase with thrombospondin motif 1 |
| ANGPTs | Angiopoietins |
| AREG | Amphiregulin |
| AVPV | Anteroventral periventricular |
| BMI | Body mass index |
| BSA | Bovine serum albumin |
| BTC | Betacellulin |
| C | Control |
| C-OE | Cumulus-oocyte expansion; |
| cAMP | Cyclic AMP |
| CBP | CREB binding factor |
| CBS | Circular binary segmentation |
| CCL | C-C motif ligand |
| CCs | Cumulus granulosa cells / cumulus cells |
| CDKs | Cyclin dependent kinases |
| CEBP | CCAAT/enhancer-binding proteins |
| cGMP | Cyclic GMP |
| CI | Confidence interval |
| CL | Corpus luteum |
| CNP | C-type natriuretic peptide |
| CNV | Copy number variation |
| COC | Cumulus-oocyte complex |
| COS | Controlled ovarian stimulation |
| COv | Controlled ovulation |
| COv | Controlled ovulation |
| CR | Crown-rump |
| CREB | Camp response element binding protein |
| CVs | Coefficients of variation |
| CXCL10 | C-X-C motif ligand 10 |
| DISC1 | DISC1 scaffold protein |
| E2 | Estradiol |
| ECM | Extracellular matrix |
| EGFR | EGF receptor |
| EI | Electron impact ionization |
| EREG | Epiregulin |
| ETC | Endocrine technologies core |
| FF | Follicular fluid |
| FLRT3 | Fibronectin leucine rich transmembrane protein 3 |
| FSH | Follicle stimulating hormone |
| FSHR | FSH receptor |
| GC | Gas chromatography |
| GCs | Granulosa cells |

| | |
|---|---|
| GnRH | Gonadotropin-releasing hormone |
| GO | Gene ontology |
| GR | Glucocorticoid receptor |
| GREs | Glucocorticoid response elements |
| GV | Germinal vesicle |
| GVBD | GV breakdown |
| HA | Hyaluronic acid |
| HABP | HA binding protein |
| HBB | Human hemoglobin beta-chain |
| hCG | Human chorionic gonadotropin |
| HDL | High density lipoproteins |
| HESI | Heated electrospray ionization |
| HILIC | Hydrophilic interaction chromatography |
| HMM | Hidden markov model |
| HOMA-IR | Homeostatic model assessment of insulin resistance |
| HPO | Hypothalamo-pituitary-ovarian |
| hr | Hour |
| HS | High sensitivity |
| HSD11B | 11-β hydroxysteroid dehydrogenase |
| HSD3B2 | 3β-hydroxysteroid dehydrogenase-2 |
| IF | Immunofluorescence |
| IGF | Insulin like growth factor |
| IGFBPs | IGF binding proteins |
| IHC | Immunohistochemistry |
| IL | Interleukin |
| IL-1RA | Interleukin IL -1 receptor antagonist |
| IVF | *In vitro* fertilization |
| ivGTT | Intravenous glucose tolerance testing |
| IVM | *In vitro* maturation |
| KLRG2 | Killer cell lectin like receptor G2 |
| LC-MS/MS | Liquid chromatography-tandem mass spectrometry |
| LDL | Low density lipoproteins |
| LH | Luteinizing hormone |
| LHCGR | Luteinizing hormone-chorionic gonadotropin receptor |
| LIF | Leukemia inhibitory factor |
| MAO | Morpholino antisense oligonucleotide |
| MAPK | Mitogen activated protein kinase |
| mGCs | Mural granulosa cells |
| MI | Metaphase I |
| MII | Metaphase II |
| Min. | Minutes |
| MPF | Maturation promoting factor |
| MS/MS | Tandem mass spectrometry |
| NHPs | Non-human primates |
| NK | Natural killer |
| NMR | Nuclear magnetic resonance |

| | |
|---|---|
| NOTO | Notochord homeobox |
| NPR2 | Natriuretic peptide receptor 2 |
| ONPRC | Oregon national primate research center |
| P4 | Progesterone |
| PCA | Principal component analysis |
| PCOS | Polycystic ovarian syndrome |
| PFA | Paraformaldehyde |
| PGR | Progesterone nuclear receptor |
| PGRMC | P4 receptor membrane component |
| PGS | As pre-implantation genetic screening |
| PGs | Prostaglandins |
| PKA | Protein kinase A |
| PKC | Protein kinase C |
| PLC | Phospholipase C |
| PRAMEF18 | PRAME family member 18 |
| PRKO | PGR knockout |
| PTGER | PGE2 receptor |
| PTGS2 | Prostaglandin synthase 2 |
| REM2 | GEM like GTPase 2 |
| RI | Retention index |
| RP | Reverse phase |
| RT | At room temperature |
| SCD | Standard chow diet |
| sec | Seconds |
| SSTR5 | Somatostatin receptor-5 |
| StAR | Steroidogenic acute regulatory protein |
| STD | Standard control |
| T | Testosterone |
| TALP | Tyrode's albumin lactate pyruvate |
| TCA | Tricarboxylic acid cycle |
| TCs | Theca cells |
| TGF-β | Transforming growth factor-β |
| TLM | *Time-lapse monitoring* |
| TLR7 | Toll like receptor-7 |
| TZPs | Transzonal projections |
| UPLC-MS/MS | Ultrahigh performance liquid chromatography-tandem mass spectroscopy |
| VEGF | Vascular endothelial growth factor |
| WSD | Western-style diet |
| $WSD_L$ | Long-term WSD |
| $WSD_S$ | Short-term Western-Style Diet WSD exposure |
| ZNF750 | Zinc finger protein 750 |
| ZP | Zona pellucida |

**Acknowledgement**

I would like to thank my mentors, Jon and Shawn! They have been incredibly supportive of me since day one. It was my dream to do a PhD in reproductive biology and I met Shawn when I came for recruitment interviews. I am glad she enabled me to complete that dream by taking me into her lab and introducing me to Jon for rotations. Jon and Shawn, thanks for believing in me! A BIG thanks for always encouraging and supporting me to pursue my other profession of Indian classical dancing with the same vigor. Thanks for helping me grow!

Thanks to the Chavez lab and the Hennebold lab members for their support and critique of my work over the past 5 years. A special shout-out to Jimi, Kelsey and Melinda for being super supportive, both experiment-wise and emotionally.

Many thanks to all the members of my DAC committee; Michael Danilchik, Lawrence Sherman, Charles Roselli, and Sacha Krieg. Thanks for being incredibly supportive and encouraging me to think critically throughout my PhD journey. You were especially accommodating with changes in the last moment due to the global Covid-19 pandemic. Thanks to my external examiner, Caren Weinhouse, for being on my defense committee and providing insightful questions during the defense.

Philip Copenhaver, Phil, you have been a pillar of guidance ever since my first semester. Thanks for always being available and ready to talk about things. Lola Bichler, I don't know if any other graduate student has emailed you the amount that I have. Thanks for being patient and coordinating everything so smoothly. Saundra Schlesinger, thanks for being my writing partner and helping me push through the last 5 months of my PhD.

Thanks to the student health center at OHSU and its facilities. They were absolutely invaluable (both in physical and mental health) to me as a graduate student.

Life would be incomplete without friends and family, especially those who constantly motivate you to keep going. Thanks to my friends and family all over the world, my dance teachers, my dancer colleagues and my extended dance community for bringing in the constant positivity that is much needed!

Life would have been a struggle without my family, especially both my sisters and their families who are here in the US. My niece and nephews have been a total stress buster throughout. My parents; amma and appa, thanks for raising me to be this independent and always nurturing me with more confidence and standing by me, come what may! To my husband, Rob, if not for you, I probably wouldn't be in Portland today. It was your encouragement and positive reinforcement that has made this day possible. I would like to thank our entire families for supporting me in this journey.

Last but not the least, I thank each and every one of the people who attended my dissertation defense virtually and made it a memorable one for me, in spite of all that is currently going on in the world!

Thank you!

# Chapter 1: Introduction

## Growth and Development of the Ovulatory Follicle

The follicle is the structural unit within the ovary where endocrine-acting sex steroids and hormones are synthesized and the development of a mature oocyte capable of being fertilized occurs. It is comprised of the oocyte and the surrounding somatic cells, which includes primarily granulosa cells (GCs) and theca cells (TCs). The formation of a mature oocyte requires interactions with these somatic cells, either through direct or indirect means. Follicles initially appear in primates at mid-gestation, when there are approximately 7 million oocytes present in the fetal ovary, of which only 15-20% survive at the time of birth[2,3]. At this stage of development, oocytes reside in large nests of germ cells that are devoid of somatic cells. Each oocyte is subsequently enclosed by a flattened layer of GCs during the third trimester of pregnancy in primates, resulting in the formation of a primordial follicle. At birth, there is a fixed number of primordial follicles that defines the ovarian reserve and reproductive lifespan of an individual[4-6]. Thus, the primordial follicle pool serves as the source of all subsequent mature ovulatory follicles.

After puberty, the growth and development of primordial follicles commences and occurs in both gonadotropin independent and gonadotropin dependent phases. Gonadotropin independent folliculogenesis is a continuous process whereby a cohort of quiescent primordial follicles become activated, with the GCs transitioning to proliferative cuboidal epithelial cells. A single layer of cuboidal GCs surrounding the oocyte is classified as a primary follicle. Initiation of GC proliferation occurs in parallel with the formation of a basement membrane that separates the GCs from the newly formed outer

TC layer, yielding the secondary follicle. With continued growth, a fluid filled cavity develops in the follicle that is termed the antrum. The fluid in the antrum is called the follicular fluid (FF), and it serves as a reservoir of regulatory proteins, extracellular matrix (ECM) proteins, and enzymes. Once formed, antral follicles become dependent upon gonadotropins for their continued growth. Specifically, follicle stimulating hormone (FSH), which is produced by the pituitary and is under the control of signals originating from the hypothalamus, is the major trophic hormone that promotes further follicular development[7-10]. Although there are approximately twenty antral follicles that form following the activation and growth of a cohort of primordial follicles in primates, only one eventually develops into a dominant follicle[11] that ovulates to release an oocyte. From the time primordial follicles become activated and transition to primary follicles, to the point at which a preovulatory follicle forms, is around 120 days[1,12] (**Fig. 1.1**).

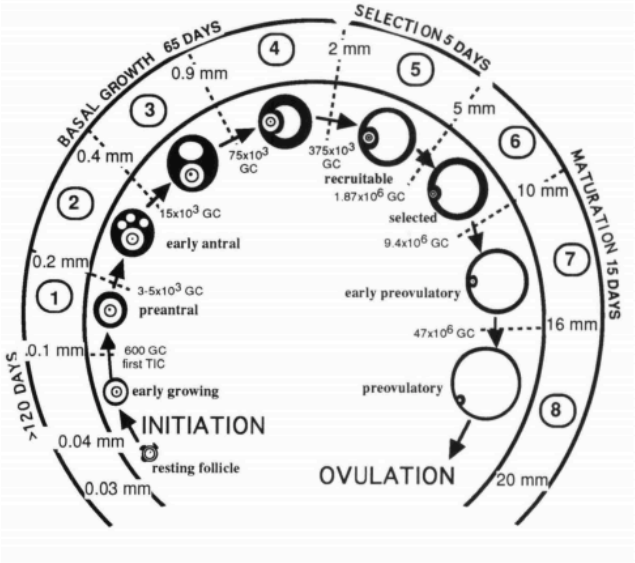


**Figure 1.1. Classification and developmental timeline of folliculogenesis in the human ovary[1].**

After a single follicle in the primate ovary is selected from the cohort of growing small antral follicles to become the preovulatory follicle, its antral cavity size and FF volume increases dramatically over the span of several days. At this stage of follicle development, the GCs secrete factors that are important for synergizing with FSH to

295 promote follicle growth. For example, the transforming growth factor-β (TGFβ)
296 superfamily members activin and inhibin[13] are secreted into the FF and play various roles
297 in follicle growth and development. Activins directly promote GC proliferation[14] and FSH
298 receptor (FSHR) expression[15]. Another set of growth factors, insulin like growth factor
299 (IGF)-I and IGF-II, are critical for the selection and continued growth of the dominant
300 follicle[16,17]. IGF action is regulated at multiple levels in the follicle, including through their
301 synthesis, the presence of binding proteins (IGFBPs) that prevent interaction of IGFs with
302 their receptor, and the action of proteases that degrade IGFBPs, allowing for IGF receptor
303 binding and activation[16-20]. IGF-I is the predominant IGF in the rodent follicle, whereas
304 IGF-II is primarily found in domesticated animal species and primates. IGF action includes
305 promoting follicle growth by inducing GC proliferation and regulating
306 steroidogenesis[17,18,19,21,22].

307 In parallel with the enlargement of the antrum and the development of the
308 preovulatory follicle, the GCs differentiate into two distinct populations that include
309 cumulus granulosa cells (CCs) surrounding the oocyte, forming the cumulus-oocyte
310 complex (COC), and mural GCs (mGCs) that line the wall of the follicle[23]. Within the
311 COC, the immature germinal vesicle (GV) oocyte is itself enclosed in a glycoprotein coat
312 called the zona pellucida. Secreted factors diffuse through the FF, allowing for
313 communication between the TCs, mGCs, CCs, and oocyte[24] (**Fig. 1.2**). FF is rich in growth
314 factors, extracellular vesicles, metabolites, and microRNAs secreted by the mGCs and

oocyte[24-32]. External to the mGCs and the basement membrane, the TCs continue to proliferate and expand in parallel with the growing follicle. As the follicle expands, blood vessels invade the TC layer, but do not traverse the basement membrane.

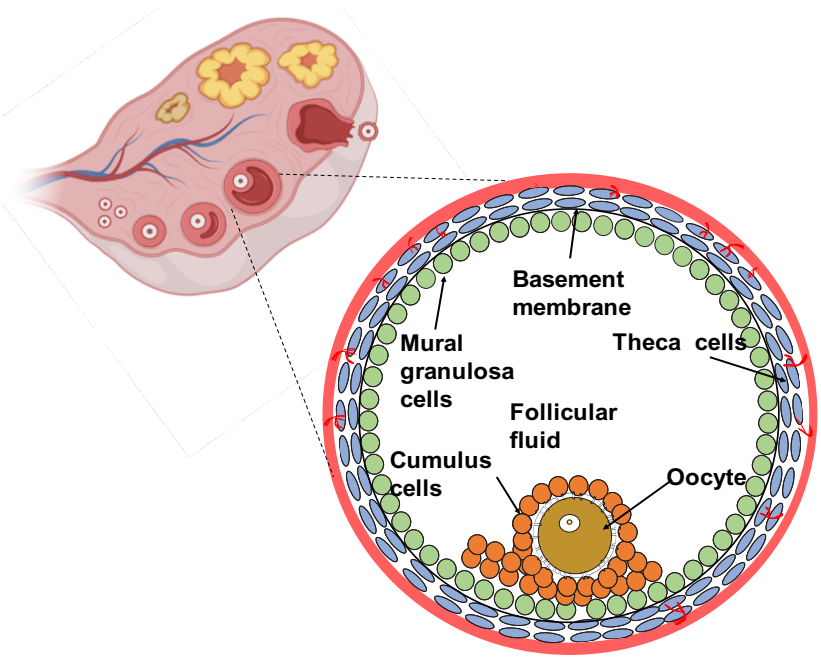


**Figure 1.2. Schematic depicting the cell types and overall structure of the preovulatory follicle.**

Through their close proximity and physical connection to one another, bidirectional communication occurs between the oocyte and the CCs. This direct cell-to-cell communication occurs through transzonal projections (TZPs) originating from the CCs and serves to keep the oocyte arrested at the GV stage. Gap junctions are formed at the site where TZPs make contact with the oocyte[26,33-37], allowing the transfer of nutrients and signaling intermediates to the oocyte for its continued development and sustaining meiotic arrest[19,26-3033,34]. TZPs allow transport of cyclic AMP (cAMP) and cyclic GMP (cGMP) into the oocyte[35,36] and the presence of cAMP inhibits maturation promoting factor (MPF), whereas high cGMP impedes cAMP hydrolysis by inhibiting phosphodiesterase (PDE)3A[37]. C-type natriuretic peptide (CNP) secreted by mGCs binds to its receptor,

338 natriuretic peptide receptor 2 (NPR2), located on CCs to increase production of cGMP,
339 which further contributes to maintaining meiotic arrest[37-39]. cAMP also activates the
340 cAMP-dependent protein kinase A (PKA) that, in turn, inactivates the phosphatase
341 (cdc25/cdc25b) required for activation of the cyclin dependent kinases (CDKs)[40] involved
342 in meiosis. Together, cAMP and cGMP function to inhibit the resumption of meiosis,
343 thereby ensuring that the oocyte remains arrested at the immature GV stage until an
344 ovulatory stimulus is initiated[41].

345 As the antral follicle increases in size, it produces increasing amounts of estradiol (E2).
346 Increased circulating levels of follicle derived E2 leads to the proliferation of uterine
347 endometrial cells and the release of luteinizing hormone (LH) from the pituitary, with the
348 latter being the key event responsible for initiating ovulatory processes[14,42]. Therefore,
349 while FSH is critical for antral follicle growth and development, the pituitary-derived
350 midcycle surge of LH[43-46] is responsible for initiation of events necessary for ovulation[47-
351 49]. In the preovulatory follicle, cholesterol is converted to androstenedione by the TCs and
352 CYP19A1 (aromatase) present within mGCs[50] then converts the available androstenedione
353 to E2. Although E2 supports proliferation and survival of mGCs and maintains oocyte
354 arrest in mice[51,52], it still remains unclear whether it plays a similar role within the primate
355 follicle[53,54]. Despite these potential species-specific differences in the role that E2 plays in
356 follicle development, a conserved critical function in promoting ovulation is mediated
357 through the induction of the midcycle LH surge. Sustained exposure of high concentrations
358 of E2 in the preovulatory phase initiates a positive feedback loop, wherein E2 induces the
359 release of gonadotropin-releasing hormone (GnRH) from the hypothalamus[14,42]. In rodents,
360 E2 is thought to act on the kisspeptin neurons in the anteroventral periventricular (AVPV)

361 regions of the brain, inducing continuous GnRH release from the hypothalamus into the
362 hypophyseal portal system. In other species including guinea pig, sheep, and rhesus
363 macaques, the arcuate nucleus appears to be involved in E2-dependent positive feedback
364 regulation of GnRH neurons[8]. The released GnRH binds to GnRH receptors on the
365 gonadotropes in the anterior pituitary, which stimulates the release of LH[7,42,55]. In addition
366 to follicle-derived E2, the activins and inhibins produced by mGCs[14,56] also serve to
367 regulate the hypothalamo-pituitary-ovarian (HPO) axis and the LH surge. Activins and
368 inhibins serve as positive and negative feedback regulators, respectively, of gonadotropin
369 release at different stages of follicular development. At the LH surge, the mGCs produce
370 more inhibin A than inhibin B or activin. Inhibin A acts on the pituitary gland in a negative
371 feedback loop to inhibit FSH production and further growth of follicles[14,57]. Within the
372 follicle, inhibins can also act in a paracrine manner on the TCs to increase the androgen
373 production, further increasing the E2 production by aromatization[15,58].
374 The above-noted steroidal and non-steroidal hormones/growth factors prepare the follicle
375 for the upcoming events initiated by LH surge. This resulting LH surge itself directly
376 affects the cells of the follicle, leading to initiation of a cascade of autocrine and paracrine
377 signaling events that promotes ovulation as described in the sections below.
378

379 **LH and the Initiation of Events Leading to Ovulation**

380 LH binds to the luteinizing hormone-chorionic gonadotropin receptor (LHCGR), a G
381 protein couple receptor, on mGCs and TCs[59]. In addition to altering cellular function
382 directly, LHCGR activation also results in the synthesis of paracrine or autocrine acting
383 factors, including
384 steroids, growth
385 factors, cytokines,
386 and lipid-derived
387 inflammatory
388 intermediates that
389 play unique roles in
390 events involved in
391 ovulation (**Fig.**
392 **1.3**). The direct and
393 indirect effects of
394 LH on the follicle
395 result in four major
396 processes that

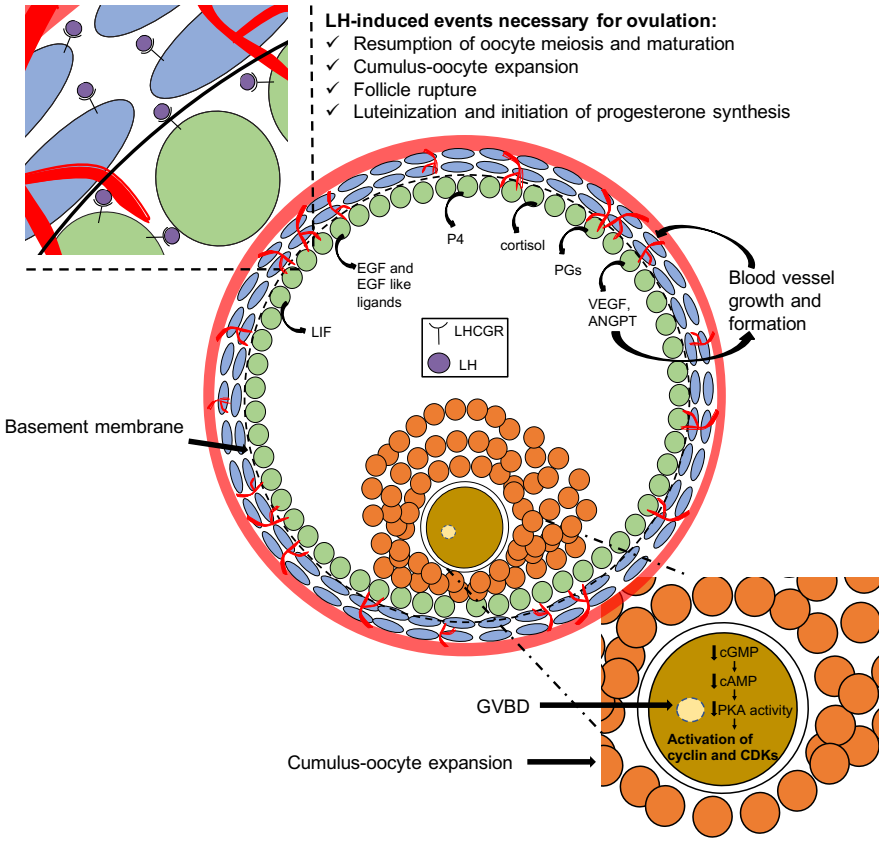


**Figure 1.3. Schematic of the direct and indirect actions of LH on the periovulatory follicle.**

397 collectively comprise ovulation, including re-initiation of oocyte meiosis, expansion of the
398 cumulus cells surrounding the oocyte (cumulus-oocyte expansion; C-OE), follicle rupture,
399 and differentiation (i.e., luteinization) of the remaining GCs and TCs into the corpus luteum
400 (CL). If fertilization occurs, the CL is responsible for sustaining pregnancy through the
401 large amounts of progesterone (P4) it produces.

402

403 **Direct effects of LH on the Periovulatory Follicle**

404 LH binding to LHCGR in the mGCs activates the G proteins, $G\alpha_s$ ($G_s$) and $G\alpha_q$ ($G_q$).
405 $G_s$ is reponsible for stimulating adenylate cyclase to increase cAMP levels, whereas $G_q$
406 activates phospholipase C (PLC), leading to diacylglycerol and calcium release. Although
407 the importance of cAMP signaling is well studied in the context of the ovulatory follicle,
408 the role that the $G_q$ pathway plays is less understood[59,60]. The elevated cAMP levels activate
409 the cAMP-dependent protein kinase, PKA. LHCGR signaling also leads to the activation
410 of the mitogen activated protein kinase (MAPK) pathway, specifically ERK1/2[59,61,62]. Both
411 these pathways converge independently to phosphorylate and activate the transcription
412 factor, cAMP response element binding protein (CREB)[63]. In rodents, PKA activation was
413 demonstrated to induce AKT phosphorylation of CREB in GCs[64], whereas the MAPK
414 pathway was able to activate CREB independent of PKA[63]. CREB phosphorylation leads
415 to its dimerization and binding to CREB binding factor (CBP). Through its ability to
416 regulate transcription, CREB-CBP controls proliferation, growth, survival, and
417 differentiation of mGCs[63].

418 Direct action of the LH surge induces cessation of mGC proliferation in primates and
419 non-primates[51,62,65-68]. The main drivers of mGC proliferation are the cyclins and the
420 CDKs, which are further regulated through the action of CDK inhibitor proteins. LH
421 directly downregulates cyclin D2 and cyclin E whilst upregulating the CDK inhibitors, p27
422 and p21 in mGCs, thus inhibiting the G1-S phase transition in mitosis and proliferation[62].
423 Although the direct actions of LH on mGCs and TCs, as noted above, are important for
424 ovulation, it is the regulation of paracrine or autocrine acting factors that allows for the

425 coordination of critical events across distinct cells types. The tight regulation of this
426 cascade of effectors is necessary for regulating critical ovulatory events including
427 steroidogenesis, angiogenesis, COC expansion, and oocyte maturation leading to release
428 of the mature oocyte.

429

430 **Indirect Effects of LH on the Periovulatory Follicle**

431 *LH effects on steroid synthesis and action*

432 LHCGR signaling leads to dramatic changes in steroid, bioactive lipid, and protein
433 content in the periovulatory follicle, with the periovulatory interval being defined as the
434 period from the peak of the LH surge to follicle rupture and the release of the oocyte. LH-
435 dependent autocrine-paracrine acting factors consequently alter mGC, CC, and oocyte
436 function, leading to oocyte maturation and ovulation of a fertilizable oocyte. Changes that
437 are known to occur in the follicle in response to an ovulatory stimulus include a shift in the
438 types of steroids that are produced (P4, cortisol), increased synthesis of lipid-derived
439 biologically active factors (prostaglandins; PGs), and production of an array of growth
440 factors and cytokines[51,59,62]. The following section highlights how such LH-inducible
441 factors are critical for coordinating the events necessary for ovulation.

442 LH signaling in the follicle leads to a switch from E2 to P4 synthesis. A key event
443 in this change includes increased cholesterol uptake in the mGCs to account for the large
444 amount of P4 that is eventually produced by the fully developed CL that forms from the
445 antecedent ovulatory follicle. The LH surge causes the mGCs to undergo hypertrophy due
446 to an increase in their lipid content, leading to the formation of the granulosa-lutein cells[69-
447 71]. Circulating low density lipoproteins (LDL) are the key source of cholesterol for

448 steroidogenesis in primates, whereas rodents derive most of their cholesterol form high
449 density lipoproteins (HDL)[72]. Increased expression of steroidogenic acute regulatory
450 protein (StAR) mobilizes cholesterol transport from the outer mitochondrial membrane to
451 the inner mitochondrial membrane, where the first step in steroidogenesis occurs. The LH
452 surge, via cAMP, induces the expression of mitochondrial P450scc (CYP11A1) in the
453 mGCs[73], the enzyme responsible for converting cholesterol to pregnenolone.
454 Pregnenolone, the upstream precursor for all steroid hormones, is then converted by 3β-
455 hydroxysteroid dehydrogenase-2 (HSD3B2) to P4[70,74]. HSD3B2 gene expression is also
456 upregulated in mGCs in response to LH action[70].

457 The P4 that is produced within the follicle through the periovulatory interval binds
458 to and regulates gene transcription through a classical progesterone nuclear receptor (PGR)
459 expressed in mGCs. P4 binding and activation of PGR results in its translocation to the
460 nucleus where it regulates the expression of target genes that control processes critical for
461 ovulation in non-primate and primate species[75-81]. In addition to increasing P4 synthesis,
462 the LH surge induces PGR mRNA levels in the follicle of all mammalian species studied,
463 where it plays an essential role in ovulation[82,83]. In PGR knockout (PRKO) mice
464 undergoing a simulated estrous cycle (i.e., a superovulation protocol), administration of
465 human chorionic gonadotropin administration (hCG; acts like LH by also binding to the
466 LHCGR) failed to induce ovulation as was observed in wild type mice[84-86]. After hCG
467 stimulation, PRKO mice possessed only unruptured follicles with entrapped oocytes[79,87].
468 Thus, in the absence of PGR, follicles were able to mature, but unable to undergo ovulation.
469 Studies using rhesus macaques also demonstrated that P4 is involved in primate
470 ovulation[75]. Blocking P4 action by administering trilostane, a HSD3B inhibitor, in

471 gonadotropin-stimulated rhesus macaque females prior to receiving an ovulatory bolus of
472 hCG prevented follicle rupture and led to the presence of trapped oocytes. Administration
473 of a synthetic PGR agonist that initiates a physiological response when combined with the
474 PGR, to rhesus macaques receiving trilostane restored ovulation. To define the downstream
475 factors important for ovulation that were regulated by PGR, the expression of genes in wild
476 type and PRKO mouse ovaries were identified by differential display PCR. From these
477 studies, it was determined that a disintegrin and metalloproteinase with thrombospondin
478 motifs 1 (ADAMTS1) is a P4-dependent metalloproteinase that is necessary for follicle
479 rupture[87]. It is important to note that in addition to the nuclear PGR, P4 can also act through
480 membrane associated receptors, including P4 receptor membrane component proteins
481 (PGRMC1 and PGRMC2), both of which were reported to be involved in P4 mediated
482 signaling post-LH surge. Both PGRMC1 and PGRMC2 are associated with cell survival
483 and have anti-apoptotic properties[88], with PGRMC1 being reported in cattle as essential
484 for mGC proliferation and meiotic maturation of the oocyte[89,90].

485 The LH surge also leads to a significant increase in intrafollicular levels of the
486 biologically active glucocorticoid, cortisol, by altering the expression of key glucocorticoid
487 metabolizing enzymes. Cortisol and cortisone, the active and inactive forms of
488 glucocorticoids, respectively, are interconvertible through the action of two 11β-
489 hydroxysteroid dehydrogenase (HSD11B) enzymes; HSD11B1 and HSD11B2[91].
490 HSD11B1 converts cortisone to cortisol, which binds to and activates glucocorticoid
491 receptor (GR), whereas HSD11B2 coverts cortisol to cortisone, a compound that has low
492 to minimal affinity for GR[92,93]. Increased HSD11B1 expression and a concomitant decrease
493 in HSD11B2 expression was observed in rat GCs *in vitro* and in rhesus macaque GCs both

494 *in vivo* and *in vitro*[94,95]. In response to hCG administration, it was also shown that
495 HSD11B1 mRNA expression increased, while HSD11B2 mRNA expression decreased, in
496 rhesus macaque periovulatory follicles as early as 12 hr post-hCG injection and stayed at
497 low levels through the subsequent 36 hrs[96]. An increase in the ratio of HSD11B1 to
498 HSD11B2 expression has been observed in the rhesus macaque periovulatory follicle[95] and
499 bovine COCs[97]. CCs obtained just prior to ovulation in women undergoing infertility
500 treatment predominantly express mRNA for HSD11B1[98], which may also contribute to the
501 increase in intrafollicular cortisol levels after an ovulatory stimulus[99,100].

502 The increased conversion of cortisone to cortisol after the LH surge would lead to
503 an increased potential for GR activation, with GR being detected in various cells of the
504 ovarian follicle throughout its development and ovulation, as well as in the CL[94,101]. In
505 bovine follicles, GR mRNA levels are greatest in TCs, but also notable in GCs[102]. GR
506 expression was also in bovine and rat GCs obtained from periovulatory follicles, as well as
507 in rodent and human luteal cells[94,103,104]. Recently, GR expression was also demonstrated
508 in pig and mouse CCs and oocytes[105]. Nuclear GR protein was localized by
509 immunohistochemistry to human CLs, luteinized GCs, stromal fibroblasts, pericytes,
510 macrophages and endothelial cells[104]. In bovine oocytes undergoing *in vitro* maturation
511 (IVM) and *in vitro* fertilization (IVF), HSD11B1expression and cortisol concentration
512 increased during IVM and remained increased through IVF. Cortisol levels and HSD11B1
513 expression were associated with increased bovine oocyte maturation and fertilization[97].
514 Increased intrafollicular levels of cortisol in rhesus macaque FF after an ovulatory stimulus
515 was also observed in the studies included in this dissertation (see Chapter 2 below). Cortisol
516 in human FF was hypothesized to influence human follicular development and oocyte

517 maturation[106]. Higher cortisol, presumably resulting in GR activation, was associated with
518 lower HSD11B2 activity and oocyte maturation in women undergoing IVF cycles[107].
519 Blocking cortisol synthesis in zebrafish also resulted in reduced GV breakdown (GVBD)
520 and oocyte maturation[108]. In contrast, other studies reported that glucocorticoids may
521 mediate an inhibitory effect on meiotic maturation of oocytes[109]. Due to these conflicting
522 studies and incomplete analyses of GR, further experiments are warranted to understand
523 the function and potential role GR signaling plays in ovulation.
524
525 *LH induction of prostaglandin synthesis*
526 In parallel with the rise in P4 and cortisol, there is a concomitant increase in
527 intrafollicular production of PGs. LH induces phospholipase A2 activity in mGCs that
528 leads to arachidonic acid release from membrane associated phospholipid stores[110-112].
529 Prostaglandin synthase 2 (PTGS2) expression increases dramatically in mGCs in response
530 to LHCGR activation and serves to convert arachidonic acid to PGH2, which is then further
531 converted into different PG isoforms by specific enzymes[113]. PGE2 and PGF2α are the
532 predominant PGs in the follicle; their concentration rises several fold after the LH surge in
533 the periovulatory follicle of rodents, domesticated animal species, and rhesus
534 macaques[111,114].
535 PGE2 is regarded as the primary PG involved in ovulation[115,116] and acts through
536 one of four receptors PGE2 receptors (PTGER1-4)[117,118], whose activation is necessary for
537 follicle rupture[114,119]. PTGS2 or PTGER2[120] null mutant mice fail to ovulate in response to
538 an ovulatory stimulus. The administration of a PTGS2 inhibitor[121] in rats was also shown
539 to impair ovulation. Similarly, inhibiting PG synthesis in the primate follicle prevented

540 follicle rupture from occurring[122]. In addition, administration of a selective PTGER2
541 antagonist into the rhesus macaque follicle inhibited C-OE. Signaling via PTGER2 in
542 primate COCs leads to hyaluronic acid production, an event critical for C-OE and release
543 of the COC from the follicle wall[118]. Moreover, oral administration of the PTGER2
544 antagonist significantly reduced pregnancy rates in a contraceptive trial using cynomolgus
545 macaques[118]. PGR signaling pathway inhibitors reduced the production of PGs post-LH
546 surge, demonstrating a role for P4 in also regulating PG production[123].
547
548 *LH-induced synthesis of growth factors and cytokines*
549 LH also stimulates mGCs and TCs to secrete a number of growth factors and
550 cytokines, the best studied of which includes members of the EGF family.
551 Amphiregulin (AREG), betacellulin (BTC), and epiregulin (EREG) synthesis increase in
552 the follicle after an ovulatory stimulus and bind to EGF receptors (EGFRs) on CCs and
553 oocytes[59,124-134]. EGFR signaling triggers phosphorylation and activation of MAPK family
554 members, ERK1/2, which in turn regulates the ability of the transcription factors,
555 CCAAT/enhancer-binding proteins (CEBP)-A and -B[47,135], to control events necessary for
556 C-OE and re-initiation of oocyte meiosis[47,136]. EGFR activation directly inactivates
557 connexin 43 within gap junctions of the TZP[40,137,138] by phosphorylating key serine
558 residues[139,21]. Gap junction closure prevents the transfer of cAMP from the CCs to the
559 oocyte. AREG also causes a reduction in CNP production, leading to lower cGMP[38,39]
560 levels and maximum cAMP hydrolysis within the oocyte[37]. The net effect of EGF ligand
561 action is the reduction in cAMP leading to activation of the CDKs required for re-initiating
562 meiosis[40,137,138]. Additionally, activation of ERK1 and ERK2 through EGFR signaling also

563 increase P4 and reduce E2 production in mouse mGCs *in vitro*[140], demonstrating that the
564 EGF ligands participate in follicle luteinization.

565 More recently, members of the interleukin (IL) cytokine superfamily, including
566 leukemia inhibitory factor (LIF) and IL-6 were discovered in the FF of the periovulatory
567 follicle in rodents and humans[141,142]. LIF was demonstrated to directly induce C-OE in
568 mouse and human COCs and promoted the first cleavage division in mouse embryos[143].
569 Delivery of a LIF-specific antagonist directly to the rhesus macaque follicle blocked
570 ovulation without impacting subsequent luteal development[144]. Along with IL-6 family
571 members, other cytokines including IL-8 and IL-1, were detected in FF obtained from
572 women undergoing ovarian stimulations for IVF[142]. IL-8 is purported to increase the
573 proteolytic enzymes needed for follicle rupture, is secreted by human mGCs *in vitro*[145],
574 and increases in FF after an ovulatory stimulus[145,146]. IL-1 has been predicted to mediate
575 and/or assist in gonadotropin action on C-OE[141]. Inflammatory mediators such as
576 bradykinin is involved in promoting angiogenesis, maintaining a positive intrafollicular
577 pressure, and inducing a breakdown of the periovulatory follicle wall[147,148], leading to
578 ovulation[149].

579 The LH surge causes a dramatic increase in new blood vessels that coincides with the
580 breakdown of the basement membrane separating the mGCs and the TCs. Nascent blood
581 vessels come into contact with the hypertrophying mGCs, thereby increasing the diffusion
582 of nutrients and gonadotropins into the cells and the progesterone they synthesize into the
583 circulation[150]. Two major angiogenic factors induced by LH, vascular endothelial growth
584 factor (VEGF) and angiopoietins (ANGPTs), play a critical role in ovulation[116,151-157].
585 VEGF synthesis by the mGCs increases through the periovulatory interval and is found in

586 high concentrations in the FF post-LH surge[151]. Among the various isoforms of VEGF,
587 VEGF-A promotes blood vessel development by stimulating endothelial cell proliferation.
588 Two isoforms of ANGPT are involved in the process of vascularization. ANGPT1
589 promotes blood vessel maturation, whereas ANGPT2 destabilizes the vessels, thus
590 allowing VEGF to form additional blood vessels[151]. ANGPT1 is expressed and produced
591 in primate mGCs in response to an ovulatory stimulus. Blocking VEGF in the periovulatory
592 follicle by intrafollicular delivery of a VEGF antagonist inhibits ovulation and P4
593 synthesis[158,159]. Intrafollicular injection of ANGPT2 into the primate periovulatory follicle,
594 which is effectively a functional ANGPT1 antagonist, blocked ovulation and a subsequent
595 rise in circulating P4 levels[159,160]. Collectively, these studies demonstrate that LH induction
596 of angiogenesis and new blood vessel formation is tightly linked with processes necessary
597 for ovulation.
598
599 *Paracrine factors direct ovulatory events in cells that do not express LHCGR*
600 The LH responsive cells of the follicle, primarily the mGCs, communicate with LH
601 nonresponsive cells (e.g., the CCs and the oocyte) through paracrine factors, including the
602 examples detailed above. A prominent example of indirect LH actions includes changes in
603 CC function that leads to PKA and protein kinase C (PKC) activation in the oocyte, which
604 are essential for the resumption of meiosis[161]. PKA activity within the oocyte decreases
605 after the LH surge, leading to the activation of cyclin and CDKs, such as cyclin B and
606 CDK1, that triggers MPF activity and progression through metaphase I[129,162-164]. In mouse
607 oocytes, PKC activation accelerates GVBD and possible activation of the MAPK
608 pathway[165]. GVBD and chromosome condensation results in the formation of metaphase I

609 (MI) oocyte. After completing the first meiotic division and the release of the polar body,
610 the oocyte arrests at the metaphase II (MII) stage[166] until fertilization occurs.

611 The direct actions of LH on the cells of the follicles, coupled with LH-inducible
612 autocrine and paracrine factors, allows for the complex and highly orchestrated events that
613 are required for the re-initiation of meiosis, C-OE, follicle rupture and luteinization.
614 Although the aforementioned secreted factors induced by LH are known to be important
615 for ovulation, including P4, PGs, EGF family members, as well as select cytokines and
616 angiogenic factors[7,8,167-173], the entire complement of LH-dependent intrafollicular
617 autocrine or paracrine acting substances have yet to be identified[76,96,117,144,174-179]. Thus,
618 identifying and characterizing LH-induced intrafollicular factors and their
619 autocrine/paracrine activities will help us understand the processes that are critical for the
620 release of an oocyte that can undergo successful fertilization and preimplantation
621 development.

622 Apart from the direct and indirect signalling pathways mediated by LH surge, there
623 are external or environmental factors (i.e., exogenous hormones, diet) that also have a
624 negative impact on the ovarian follicular environment and oocyte competency. By looking
625 at how these factors influence the intrafollicular environment and the resident oocyte, we
626 will be able to better understand how these different processes are integrated to ensure
627 proper ovarian function. Importantly, such studies will also yield insight into novel
628 therapies for the treatment of reproductive dysfunction that results in subfertility or
629 infertility.

630

631 **The Effect of Endocrine, Metabolic, and Nutritional Disruptions on the Ovulatory**
632 **Follicle**

633 It is known that certain metabolic and endocrine disorders, external factors such as diet,
634 as well as gonadotropin stimulation as part of current infertility treatments can lead to
635 ovulatory dysfunction. Under current clinical practice, exogenous gonadotropins are
636 administered for 7 or more consecutive days to promote the growth and development of
637 multiple follicles from which oocytes are obtained for IVF. Although this approach can
638 allow for the collection of large numbers of oocytes, sometimes up to 50 or more, there is
639 also a concomitant increase in oocyte heterogeneity due to the continued growth of follicles
640 that would normally undergo atresia during the natural selection process[180-183]. Oocyte
641 heterogeneity occurs wherein, not all oocytes are competent to undergo fertilization,
642 cleavage divisions, and successful preimplantation stage blastocyst formation, either due
643 to their varying stages of maturity or even within the same stage of maturity due to
644 unknown reasons. This phenomenon manifests in a significant number of collected oocytes
645 that, after fertilization, arrest prior to blastocyst formation or yield blastocysts that have
646 reduced potential to yield a pregnancy.

647 The consumption of high fat diet Western-style diet (WSD) can lead to both endocrine
648 and metabolic disruption and, in turn, negatively affect female fertility[184-186]. Maternal
649 obesity associated with WSD consumption can give rise to intrafollicular changes that
650 results in reduced fertility and oocyte competency[184,187]. In mice, maternal obesity is
651 associated with higher numbers of degraded oocytes, chromosomal abnormalities, and
652 mitochondrial dysfunction[185,188,189]. A prolonged exposure to WSD in primates can lead to
653 increased metabolic dysregulation in addition to an inflammatory intrafollicular

654 environment[186,190]. Understanding how WSD consumption by itself or through the
655 subsequent development of obesity impacts events in the follicle that are necessary for
656 ovulation has important clinical ramifications as the incidence of obesity continues to
657 increase globally[191].

658 Genetic, environmental, endocrine, and metabolic dysfunction also contribute to
659 the disease, polycystic ovarian syndrome (PCOS). PCOS is common endocrine disorder in
660 women[192], with symptoms commonly appearing in adolescent or peripubertal teenage girls
661 and young women of reproductive age[193]. Diagnosis of PCOS is based on the presence of
662 at least two out of the following three features: hyperandrogenism (elevated circulating
663 levels of testosterone; T), oligo-anovulation (infrequent or irregular ovulation) or
664 anovulation, and polycystic ovaries (the presence of multiple persistent small antral
665 follicles)[194]. It has been associated with increased incidence of insulin resistance, type II
666 diabetes[195,196], and infertility. Though there are correlations between disease progression
667 and severity with changes in the intrafollicular factors and oocyte competency, the
668 individual and combined effects of diet, metabolic disorders, and hyperandrogenemia on
669 periovulatory events is not well understood.

670 Female macaques share numerous biological similarities with women, including
671 their menstrual cycle duration (~28 days on average), development and ovulation of a
672 single oocyte per menstrual cycle, similar timing of key developmental events such as
673 embryonic genome activation (occurs 2-3 days post fertilization), and an analogous
674 percentage (~30-50%) of embryos that will successfully reach the blastocyst stage[197]. By
675 studying these processes in a clinically relevant animal model such as the rhesus macaque,
676 insight can be gained on how disruptions in the intrafollicular processes can impact oocyte

677 competency in the periovulatory follicle. The studies that comprise this dissertation
678 specifically focus on the effects of infertility treatments, short-term diet changes, and long-
679 term diet and/or hyperandrogenemia on the ovarian follicular microenvironment and the
680 ability of the resident oocyte to undergo meiotic maturation, fertilization, and development
681 to a preimplantation stage embryo.
682
683

684 **Chapter 2:**

685 **Metabolomics Analysis of Follicular Fluid Coupled with Oocyte Aspiration Reveals**

686 **Importance of Glucocorticoids in Primate Periovulatory Follicle Competency**

687 Sweta Ravisankar[1,2], Kelsey E. Brooks[2], Melinda J. Murphy[2], Nash Redmayne-Titley[2],

688 Junghyun Ryu[2], Jason M. Kinchen[4], Shawn L. Chavez[2,3,5], Jon D. Hennebold[2,3*]

689

690

691 [1]Department of Cell, Developmental & Cancer Biology; Graduate Program in Molecular

692 & Cellular Biosciences; Oregon Health & Science University School of Medicine;

693 Portland, Oregon

694 [2]Division of Reproductive & Developmental Sciences; Oregon National Primate Research

695 Center; Beaverton, Oregon

696 [3]Department of Obstetrics & Gynecology; Oregon Health & Science University School of

697 Medicine; Portland, Oregon

698 [4] Metabolon, Inc., Morrisville, NC 27560

699 [5]Department of Molecular & Medical Genetics; Oregon Health & Science University

700 School of Medicine; Portland, Oregon

701

702 *Corresponding author: henneboj@ohsu.edu

703

704

705 Submitted to Scientific Reports for Review on April 7th 2020

706 **Abstract**

707 Exogenous gonadotropin administration during infertility treatment stimulates the
708 growth and development of multiple ovarian follicles, yielding heterogeneous oocytes with
709 variable capacity for fertilization, cleavage, and blastocyst formation. To determine how
710 the intrafollicular environment affects oocyte competency, 74 individual rhesus macaque
711 follicles were aspirated and the corresponding oocytes classified as failed to cleave, cleaved
712 but arrested prior to blastulation, or those that formed blastocysts following *in vitro*
713 fertilization. Metabolomics analysis of the follicular fluid (FF) identified 60 unique
714 metabolites that were significantly different between embryo classifications, of which a
715 notable increase in the intrafollicular ratio of cortisol to cortisone was observed in the
716 blastocyst group. Immunolocalization of the glucocorticoid receptor (GR) revealed
717 translocation from the cytoplasm to nucleus with oocyte maturation *in vivo* and correlation
718 to intrafollicular expression of the 11-hydroxy steroid dehydrogenases that interconvert
719 these glucocorticoids was detected upon an ovulatory stimulus *in vivo*. While GR
720 knockdown in oocytes had no effect on their maturation or fertilization, expansion of the
721 associated cumulus granulosa cells was inhibited. Our findings indicate an important role
722 for GR in the regulation of follicular processes via paracrine signaling. Further studies are
723 required to define the means through which the FF cortisol:cortisone ratio determines
724 oocyte competency.

725

726 **Introduction**

727 Since the advent of human *in vitro* fertilization (IVF) in 1978, the resultant live-
728 birth rates have remained relatively constant at ~35%, although the demand has been
729 steadily growing (cdc.gov/art). IVF requires the use of controlled ovarian stimulation
730 (COS) to obtain sufficient quantities of eggs by administering pharmacological levels of
731 exogeneous hormones to stimulate the development of multiple follicles. However, this
732 causes a concomitant increase in oocyte heterogeneity due to the continued growth of
733 follicles that would normally undergo atresia during the natural selection process[180-183].
734 This oocyte heterogeneity, as well as the certainty that less than half of cultured human
735 embryos will form blastocysts capable of implantation, contributes to the consistently low
736 birth rate following IVF. Thus, it is essential to accurately and non-invasively identify those
737 oocytes that possess the greatest potential to fertilize, undergo cleavage divisions, and
738 reach the blastocyst stage in development to improve IVF success and pregnancy
739 outcomes.

740 Ovarian follicle maturation leading to the ovulation of a fertilizable oocyte involves
741 complex intracellular interactions between the oocyte itself, surrounding somatic cells,
742 and the follicular fluid (FF)[61,198-200]. The mid-cycle surge of luteinizing hormone (LH), the
743 master regulator of ovulation, triggers direct LH/chorionic gonadotropin receptor signaling
744 and the production of autocrine or paracrine factors responsible for the resumption of
745 meiosis and the transition from an immature germinal vesicle (GV) to a mature metaphase
746 II (MII) oocyte[47-49]. This includes the synthesis and secretion of certain fatty acid-derived
747 and steroid-based hormones, cytokines, chemokines, as well as growth factors by the cells
748 comprising the periovulatory follicle, which in turn, regulate oocyte maturation and

749 fertilization potential. Due to species-specific differences in follicle size, processes
750 involved in selection, and growth rates, there is limited information defining the optimal
751 follicular microenvironment that can be extrapolated to women[197]. Therefore, assessing the
752 ovarian follicular microenvironment in rhesus macaques, an animal model that is more
753 similar to humans in terms of ovarian physiology, as well as response to COS protocols
754 based on the number of oocytes produced and percentage of fertilized oocytes that typically
755 reach the blastocyst stage, is likely to be more clinically relevant.

756 Although IVF success depends on multiple factors, much of the research has
757 focused on the correlation between IVF outcomes and somewhat subjective assessments
758 of embryo quality for selection and transfer[201,202]. Non-invasive technologies, including
759 time-lapse imaging of embryo development and analysis of spent culture media, as well as
760 more invasive techniques such as pre-implantation genetic screening (PGS), have been
761 implemented into clinical practice for this purpose, but not without limitations and
762 controversy[83,203-209]. More recently, studies have concentrated on the cellular and molecular
763 processes occurring in the ovarian follicle at the time of aspiration and oocyte collection.
764 Reports detailing the use of genomic, transcriptomic, and metabolomics approaches to
765 non-invasively assess the intrafollicular microenvironment have begun to emerge and have
766 yielded insight into oocyte competency within the naturally selected follicle and following
767 environmental or pathological insults[210-215]. Most of the metabolomics studies, however,
768 used methods that were only capable of identifying a select number of metabolites involved
769 in known cellular processes. Because the metabolome constitutes inputs from genomic,
770 transcriptomic, and proteomic processes, it is essential that metabolomics analyses be as
771 thorough as possible for the discovery of important, but yet to be characterized, metabolic

772 pathways. Thus, non-targeted mass spectrometry of FF obtained from individual follicles
773 from rhesus macaque females undergoing COS was performed here to define the follicular
774 metabolome relative to the developmental outcome of each resident oocyte following
775 fertilization. Our findings demonstrate that an unbiased metabolomics analysis of FF
776 provides a comprehensive assessment of the intrafollicular signaling pathways and
777 identifies important downstream mediators in follicles containing oocytes with the greatest
778 potential of yielding a normal term pregnancy.
779

780 **Materials and Methods**

781 *Rhesus macaque oocyte, somatic cells and FF collection*

782 All protocols involving animals were approved by the ONPRC Institutional Animal
783 Care and Use Committee and conducted in accordance with the National Institutes of
784 Health Guidelines for the Care and Use of Laboratory Animals. The housing and general
785 care of rhesus macaques (*Macaca mulatta*) was previously described[144].

786 Female rhesus macaques (N=17) of reproductive age [~7-8 years (yrs) old]
787 underwent COS protocols as previously described over a period of 2 yrs to stimulate the
788 development of multiple ovarian follicles[180]. Female rhesus macaques were anesthetized
789 for laparoscopic follicular aspirations 36 hours (hr) after the administration of human
790 chorionic gonadotropin (hCG) to induce events necessary for the re-initiation of meiosis.
791 Individual ovarian follicles (N=10 per ovary) were manually aspirated and collected into
792 separate sterile 1.5 ml Eppendorf tubes with a low dead-space 3ml syringe with a 22-gauge
793 X 1.5-inch needle (Ulticare, UltaMed Inc., Excelsior, MN) for each aspirate. The tubes
794 were spun down to separate the FF from the cumulus-oocyte complex (COC) and the

795 granulosa cells (GCs). COCs were then examined for presence of an oocyte under a
796 stereomicroscope by dilution with Tyrode's albumin lactate pyruvate (TALP)-HEPES
797 media with 0.3% bovine serum albumin (BSA; Sigma-Aldrich, St. Louis, MO) and
798 transferred to a pre-equilibrated IVF dish containing 100 µl drops of (0.3% BSA and
799 0.006% sodium pyruvate) covered by mineral oil (Sage™, Trumbull, CT). Each oocyte
800 from an individual aspirate was isolated form the COCs by gentle micropipetting and
801 placed in a separate drop. The FF and the cumulus cells (CCs) were kept in separate tubes,
802 flash frozen in liquid nitrogen, and stored at -80ºC until future use.
803
804 *IVF and assessment of pre-implantation development*
805 Fresh semen from adult male rhesus monkeys of reproductive age (6-9 yrs) was
806 collected according to established ONPRC protocols[216] and used for IVF at a final
807 concentration of $2x10^6$ sperm/ml in TALP-Complete media. Semen was collected only
808 from males that were proven breeders. IVF for mature MII oocytes was performed the
809 evening of the collection as previously described[216]. IVF dishes were incubated at
810 5% $CO_2$ and 37ºC overnight and fertilized oocytes separated from excess sperm the next
811 morning by micropipeting. The zygotes (identified by two pronuclei and/or two polar
812 bodies) were cultured in separate wells containing 100µL of one-step commercial media
813 supplemented with 10% serum protein (LifeGlobal, Guildford, CT) under mineral oil at
814 37°C with 6% $CO_2$, 5% $O_2$. Embryo development was individually tracked through day 8
815 post-IVF. Media was changed on day 3 post-IVF and the embryos were left to continue
816 developing to the blastocyst stage up until day 8. Arrested (pre-blastocyst stage) embryos
817 and blastocyst development outcomes were recorded. Based on their fertilization and

818 developmental outcome, embryos were categorized as uncleaved (MII oocytes that did not
819 fertilize or those that appeared to fertilize, but did not cleave), cleavage stage arrested group
820 (those that cleaved, but ceased dividing prior to forming a blastocyst), or blastocyst (those
821 that progressed to form a blastocyst). The percentage of uncleaved oocytes/embryos,
822 cleaved embryos, and blastocysts formed were calculated as follows: percentage of
823 uncleaved oocytes or embryos = (number of oocytes that remained unfertilized or those
824 that appeared to fertilize, but did not cleave/number of mature MII oocytes that underwent
825 IVF) *100, percentage of cleaved embryos= (number of embryos that cleaved/number of
826 zygotes formed) * 100, and percentage of blastocyst formed = (number of blastocysts
827 formed/number of cleaved embryos) *100 and compared between follicles that had greater
828 or less than 35µl FF volume.
829
830 *FF sample preparation for metabolomics analysis*
831 A total of 255 oocytes were isolated from individual follicles, fertilized via
832 conventional IVF and allowed to undergo pre-implantation development. Out of these, a
833 total 74 individual FF samples (33 from year 1 and 41 from year 2) were categorized based
834 on the corresponding oocyte's development into the above embryo groups, were shipped
835 in separate batches on dry ice to Metabolon Inc. (Durham, NC,
836 U.S.A.; www.metabolon.com).These FF samples were chosen based on a required FF
837 volume of greater than or equal to 40µl for the metabolomics analysis. Further processing
838 and metabolomics analyses were conducted using the automated MicroLab STAR®
839 system from Hamilton Company[217]. Recovery standards were added prior to the first step
840 in the extraction process to assess variability and verify performance of extraction and

841 instrumentation. To remove protein and recover chemically diverse metabolites,
842 dissociated small molecules bound to protein or trapped in the precipitated protein matrix,
843 were precipitated in methanol with vigorous shaking (Glen Mills GenoGrinder 2000) for 2
844 minutes (min.) followed by centrifugation. The resulting extract was split and used by
845 separate reverse phase (RP)/ultrahigh performance liquid chromatography-tandem mass
846 spectroscopy (UPLC-MS/MS) methods with negative ion mode electrospray ionization
847 (ESI), one for analysis by hydrophilic interaction chromatography (HILIC)/UPLC-MS/MS
848 with negative ion mode ESI, and either one or two aliquots for analysis with UPLC-MS/MS
849 with positive mode ESI (depending on year of acquisition).For the first run, a gas
850 chromatography (GC)/MS instrument was also used – samples were dried under vacuum
851 for a minimum of 18 h prior to being derivatized under dried nitrogen using bistrimethyl-
852 silyltrifluoroacetamide. Derivatized samples were separated on a 5% diphenyl/95%
853 dimethyl polysiloxane fused silica column (20 m x 0.18 mm ID; 0.18 um film thickness)
854 with helium as carrier gas and a temperature ramp from 60° to 340°C in a 17.5 min period.
855 Samples were analyzed on a Thermo-Finnigan Trace DSQ fast-scanning single-quadrupole
856 mass spectrometer using electron impact ionization (EI) and operated at unit mass
857 resolving power. The scan range was from 50–750 m/z.
858
859 *Quality assessment of metabolomics analysis*
860 Several types of controls were analyzed in concert with the experimental samples:
861 a pooled matrix sample generated by taking a small volume of each experimental sample
862 served as a technical replicate throughout the data set; extracted water samples served as
863 process blanks; and a cocktail of QC standards that were carefully chosen not to interfere

864 with the measurement of endogenous compounds were spiked into every analyzed sample,
865 allowing instrument performance monitoring and chromatographic alignment.
866 Experimental samples were randomized across the platform run with QC samples spaced
867 evenly among the injections[217], as outlined in **Supplementary Fig. S2. 1**.
868
869 *Ultrahigh performance liquid chromatography-tandem mass spectroscopy*
870 Molecules were separated using a Waters ACQUITY UPLC system and identified
871 using a Thermo Scientific™ Q Exactive™ Hybrid Quadrupole-Orbitrap mass spectrometer
872 interfaced with a heated electrospray ionization (HESI-II), operating at 35,000 mass
873 resolution. The sample extract was dried and then reconstituted in solvents compatible with
874 each of the four different methods. Each reconstitution solvent contained a series of
875 standards at fixed concentrations to ensure injection and chromatographic consistency.
876 Aliquots were analyzed using acidic positive ion conditions chromatographically
877 optimized for hydrophilic compounds, hydrophobic compounds, acidic positive ion
878 conditions as well as hydrophobic compounds and basic negative ions optimized
879 conditions using a separate dedicated C18 column with negative ionization. The analysis
880 alternated between MS and data-dependent $MS^n$ scans using dynamic exclusion and the
881 scan range varied slightly between methods, covering 70-1000 m/z.
882
883 *Metabolite identification, quantification, and visualization*
884 Raw data was extracted, peak-identified, and QC processed as previously
885 described[217]. Compounds were identified by comparison to library entries of purified
886 standards or recurrent unknown entities. Biochemical identification was based on three

887 additional criteria: retention index (RI) within a narrow RI window of the proposed
888 identification, accurate mass match to the library +/- 10 ppm, and the MS/MS forward and
889 reverse scores between the experimental data and authentic standards. The MS/MS scores
890 were based on a comparison of the ions present in the experimental spectrum to the ions
891 present in the library spectrum. While there may be similarities between molecules
892 according to one of these factors, the use of all three data points was utilized to distinguish
893 biochemicals. More than 3,300 commercially available purified standard compounds were
894 acquired and registered into LIMS for analysis on all platforms and determination of their
895 analytical characteristics. Additional mass spectral entries were created for structurally
896 unnamed biochemicals, which have been identified by virtue of their recurrent nature (both
897 chromatographic and mass spectral). Library matches for each compound were checked
898 for each sample and corrected if necessary. Peaks were quantified using area-under-the-
899 curve. For studies spanning multiple days, a normalization step was performed to correct
900 variation resulting from inter-day instrument differences. For purposes of data
901 visualization, values were normalized in terms of raw area counts.
902
903 *Measurement of cortisol and cortisone concentrations in FF by LC-MS*
904 FF was retrieved from one follicle in each ovary of female rhesus macaques
905 undergoing a COS protocol without (0 hr; N=5 animals) hCG administration or 36 hr after
906 hCG administration (N=5 animals) and stored at -80 C until analysis. Cortisol and cortisone
907 concentrations were determined using a LC-MS system (Shimadzu Nexera-LCMS-8050)
908 in the ONPRC Endocrine Technologies Core as previously described[218]. All samples were

909 simultaneously analyzed in a single run for each analyte. Accuracy and intra-assay
910 coefficient of variation (CV) for cortisol was 98.0% and 5.8%, respectively.
911
912 *Immunohistochemistry (IHC) of ovarian follicles*
913 Ovaries were collected from female rhesus macaques undergoing a controlled
914 ovulation (COv) protocol both prior to (0 hr) or after (12 hr, 24 hr, and 36 hr) injection
915 with a bolus of hCG as previously described[219]. The COv protocol allows for the continued
916 development of the naturally selected follicle and the initiation of ovulation at a specified
917 time. Ovaries were fixed in 4% paraformaldehyde (PFA; Alfa Aesar, Ward Hill, MA)
918 overnight, placed in 5% sucrose for 24 hr, dehydrated in a series of ethanol solutions (50%,
919 70%, and 100%), embedded in paraffin, and serial sectioned as reported previously[220].
920 Ovarian sections (5μm) were incubated with a rabbit polyclonal antibody that recognizes
921 GR (Abcam, Cambridge, MA, catalog #ab3579, RRID: AB_303925, 1:200), HSD11B1
922 (Thermo Fisher, Waltham, MA, catalog #PA5-79397, RRID: AB_2746513, 1:100), or
923 HSD11B2 (Thermo Fisher, Waltham, MA, catalog #PA5-79399, RRID: AB_2746513,
924 1:100). Primary antibodies were detected using a biotinylated anti-rabbit IgG secondary
925 antibody (Vector Laboratories, Burlingame, CA, BA1000, RRID: AB_2313606) and a
926 peroxidase substrate kit (ABC Elite Kit; Vector Laboratories, Burlingame, CA, PK6100).
927 A rabbit IgG isotype control (Abcam, Cambridge, MA, catalog #ab172730) was used to
928 determine background levels by performing white balance in Adobe Photoshop uniformly
929 across all images. Images for IHC were taken using a Nikon Ti-U inverted microscope with
930 20, 40 or 100X objectives.
931

932 *Immunofluorescence (IF) of oocytes and CCs for GR detection*

933 Oocytes and CCs were collected from female rhesus macaques undergoing COS
934 protocols as describe above at 0 hr and 36 hr post-hCG administration. A small number of
935 oocytes were also obtained from a 0 hr COS and underwent in vitro maturation (IVM) as
936 described below for 24 hr to compare GR localization in oocytes post-IVM versus those
937 that matured in vivo from a 36 hr COS. Removal of the zona pellucida was accomplished
938 by incubating oocytes in EmbryoMax Acidic Tyrode's Solution (EMD Millipore,
939 Burlington MA) for ~30 seconds (sec). The oocytes were washed in 0.1% BSA (Sigma-
940 Aldrich, St. Louis, MO) plus 0.1% Tween 20 (Sigma-Aldrich, St. Louis, MO; PBS-T) and
941 fixed by incubation in cold 4% PFA in PBS for 20 min. at room temperature (RT). Oocytes
942 were washed with PBS-T to remove any fixative and permeabilized in 1% Triton-X
943 (Calbiochem; Burlington, MA) for 30 min at RT. Non-specific binding sites were blocked
944 by incubation in 4% donkey serum (Jackson ImmunoResearch Laboratories, Inc.; West
945 Grove, PA) for 30 min at RT. Oocytes were incubated with the primary antibody for GR
946 (Abcam, Cambridge, MA, catalog #ab3579, RRID: AB_303925, 1:200 in PBS-T)
947 overnight at 4$^{o}$C and washed with PBS-T. As a negative control, oocytes were incubated
948 with the rabbit IgG isotype control antibody described above. Primary GR antibody binding
949 was detected by incubating samples in a donkey anti-rabbit antibody conjugated with Alexa
950 Fluor 488 for GR (Thermo Fisher, Waltham, MA, A-21206, RRID: AB_2535792, 1:100)
951 for 2 hr at RT. All antibodies were diluted in PBS-T +1% donkey serum. DNA was stained
952 with 1 μg/ml DAPI (Thermo Fisher, Waltham, MA, D1306, RRID: AB_2629482, 1:1000)
953 for 10 min. In between each step, the oocytes were washed with PBS-T three times for 5
954 min. each. Oocytes were transferred to glass bottom petri-dishes (Mattek; Ashland, MA)

955 and GR immunolocalization visualized on a Leica SP5 AOBS spectral confocal system
956 using the 10x and 20 x objective. Z-stacks 1-5 μM apart were imaged sequentially to avoid
957 spectral overlap between channels.
958
959 *GR morpholino antisense oligonucleotide (MAO) design and oocyte microinjection*
960 A GR specific MAO was designed to bind the 5'UTR upstream of the translation
961 initiation site in the rhesus macaque GR gene (XM_015141112.1:
962 TGGAGTCCATCAGTGAATATCAACT), thereby inhibiting the translation of the GR
963 protein. A MAO recognizing a splice site mutant of the human hemoglobin beta-chain
964 (HBB) gene (AY605051: CCTCTTACCTCAGTTACAATTTATA) was used as a
965 standard control (STD). Both the GR and STD MAOs were synthesized with a 3'-
966 carboxyfluorescein tag to aid in visualization during embryo microinjection. Oocytes were
967 collected at 6 hr or 36 hr following hCG injection from rhesus macaque females undergoing
968 a COS protocol. The MAOs were reconstituted in embryo grade water (Sigma- Aldrich,
969 W1503) and microinjected using a CellTram vario, electronic microinjector and
970 Transferman NK 2 Micromanipulators (Eppendorf, Hauppauge, New York, USA). The
971 MAO concentration (0.3 mM) was chosen based on previous reports that this concentration
972 of STD MAO did not impact blastocyst formation rates in both mice[221] and rhesus
973 macaques[222].
974
975 *IVM and IVF of microinjected oocytes*
976 Injected oocytes from the 6 hr post-hCG COS were allowed to undergo IVM for 24
977 hr to allow progression to the MI/MII stage of meiosis in 100 μl drops containing

978 preequilibrated maturation medium (IVF Bioscience, UK, 61002 BO-IVM) and cortisol at
979 a concentration of 64 ng/µl, which was based on the data from the LC-MS analysis of
980 periovulatory follicle FF obtained at 36 hr post-hCG administration. The IVM oocytes from
981 the 6 hr COS and the injected *in vivo* matured oocytes from the 36 hr COS underwent
982 conventional IVF as described above to ascertain if there were differences in GR MAO-
983 injected oocytes matured under different conditions. Maturation and fertilization rates were
984 calculated as follows: percentage of mature oocytes = (number of mature MII oocytes/total
985 number of oocytes) *100, percentage of fertilizated oocytes= (number of zygotes
986 formed/number of mature MII oocytes that underwent IVF) *100, while the percentage of
987 cleaved embryos and blastocyst were determined as described above.
988
989 *Cumulus cell expansion assay*
990 Individual follicles were aspirated 6 hr post-hCG to isolate immature oocytes and
991 their surrounding CCs. Oocytes were microinjected with either STD MAO or GR MAO as
992 described above and re-incubated with their surrounding somatic cells (primarily CCs).
993 Reconstructed COCs were allowed to undergo IVM in preequilibrated maturation medium
994 with cortisol as described above for 24 hr after which, CC expansion was recorded by
995 stereomicroscopic imaging. To determine if there were differences between embryo
996 treatment groups, hyaluronic acid (HA)-induced extracellular matrix breakdown, an
997 indicator of CC expansion, was examined in reconstituted COCs by IF. Using a
998 biotinylated HA binding protein (HABP; Sigma-Aldrich, catalog #385911, 1:200) and the
999 appropriate streptavidin conjugated Alexa 488 secondary antibody (Thermo Fisher
1000 Scientific, S32354, RRID: AB_2315383, 1:200), the absence or presence of HA in

1001 CC/mGCs was visualized in Z-stacks at 4-5 μM apart by confocal microscopy as described
1002 above.
1003
1004 *Statistical analysis*
1005 To determine whether the FF volume in a periovulatory follicle was related to the
1006 post-IVF outcome of the oocyte, we performed a Chi-square ($\chi^2$) test with $p<0.05$
1007 considered significant. In the metabolomics assessment, statistical analyses were
1008 performed in ArrayStudio on natural log transformed data. Each biochemical in OrigScale
1009 was rescaled to set the median equal to 1. Values for each sample were normalized by
1010 sample volume and following normalization to sample mass, log transformation, and
1011 imputation of missing values, if any, with the minimum observed value for each compound.
1012 A mixed model ANOVA with post-hoc tests (incorporating same-subject sampling as a
1013 random effect term) was performed to identify biochemicals that differed significantly
1014 between experimental groups. Data from different run batches were run-aligned by setting
1015 the median of each group to 1 to correct for batch effect. An estimate of the false discovery
1016 rate (*q*-value) was calculated to consider the multiple comparisons that normally occur in
1017 metabolomics-based studies[217]. Analysis of the cortisol:cortisone ratio in the 74 FF samples
1018 was performed by the mixed effects model and Bonferroni multiple testing adjustment.
1019 One-way ANOVA was used to test for significant differences in concentration in FF
1020 between 0 hr and 36 hr COS cycles by LC-MS.
1021
1022

1023 **Results**

1024 *Classification of post-fertilization developmental outcomes and association with FF*
1025 *volume*

1026 Our first objective was to collect both the oocyte and FF from individual follicles
1027 of rhesus macaque females (N=17) undergoing COS protocols and compare the FF
1028 metabolites to the corresponding oocyte's developmental potential post-IVF. 255 oocytes
1029 were isolated and the corresponding FF samples were categorized as uncleaved, cleavage
1030 stage arrested group, or blastocyst as explained in the methods. A higher percentage of
1031 blastocysts formed and a lower percentage of cleaved embryos was observed from the
1032 oocytes aspirated from follicles with a FF volume greater than 35 μl, compared to a lower
1033 percentage of blastocysts formed and a higher percentage of cleaved embryos detected
1034 from follicles with a FF volume less than 35 μl. The uncleaved rate, however, remained
1035 unchanged (**Supplementary Fig. S2. 2**). A chi-square test ($\chi^2$) revealed a significant
1036 correlation between FF volume and the post-IVF outcomes of resident oocytes ($\chi^2$=15.921,
1037 $p<0.001$), which suggested that FF volume can be used as an indicator of oocyte
1038 competency.

1039 Out of the 255 oocytes that were obtained from individual follicle aspirations,
1040 fertilized via conventional IVF, and underwent pre-implantation development, 74 FF
1041 samples with a volume of 40μl or greater were chosen for further analysis and categorized
1042 as uncleaved (N=22), cleavage stage arrested group (N=21), and blastocysts (N=31) as
1043 defined in the methods and **Figure 2. 1a**. To minimize the bias towards any single female,
1044 we selected embryos from as many rhesus macaque females as possible, including 9
1045 females in the uncleaved group, 12 females in the cleavage stage arrested group group, and

1046 most importantly, 14 females in the blastocyst group. The distribution of animals in each
1047 group is represented in **Supplementary Fig. S2. 3.**
1048
1049 *Metabolomics analysis of FF and identification of signaling pathways indicative of oocyte*
1050 *competency*
1051 Once the oocytes were categorized according to post-IVF outcome, non-targeted
1052 metabolomics profiling was performed on the corresponding 74 FF samples to determine
1053 whether there were differences in the intrafollicular microenvironment between groups.
1054 While two separate metabolomics assessments were initially performed for each year, the
1055 final results were batch-normalized to generate a dataset with greater statistical power and
1056 to avoid potential heterogeneity amongst females. A total of 382 biochemicals were
1057 identified in the FF, of which 348 had a known identity (named biochemicals) and 34 had
1058 both unknown structural identity and biological function (unnamed biochemicals).
1059 Statistically significant differences of FF biochemicals were noted between the three
1060 embryo groups, with the greatest difference observed in FF obtained from follicles that
1061 yielded an oocyte that arrested at the cleavage stage versus those that progressed to the
1062 blastocyst stage (**Fig. 2. 1b**). Interestingly, the majority (~93%; N=28/30) of these
1063 metabolites were downregulated in the blastocyst group compared to those embryos that
1064 arrested at the cleavage stage.
1065 After combining all the identified biochemicals from each embryo category, we
1066 performed pathway enrichment analysis, which revealed entire molecular pathways that
1067 were differentially represented between embryo groups (**Table 2. 1**). As shown in **Figure**
1068 **2. 1c**, the sphingomyelin pathway was the most enriched in the FF from follicles with

1069 oocytes that did not cleave following IVF versus FF associated with oocytes that produced
1070 arrested cleavage stage embryos. With the exception of uracil-derived orotate
1071 (**Supplementary Fig. S2. 4**), the majority of these metabolites were at higher levels in
1072 follicles yielding oocytes that led to cleaved embryos. In contrast, the guanido and
1073 acetamido amino acid metabolism pathways were enriched in the FF containing oocytes
1074 that did not cleave relative to those that developed into blastocysts. The greatest pathway
1075 enrichment differences observed by pairwise comparison were between embryos that
1076 arrested at the cleavage stage versus those that formed blastocysts, which included long
1077 chain monosaturated fatty acid, the tricarboxylic acid cycle (TCA), and glutamate
1078 metabolism (**Fig. 2. 1c**).
1079
1080

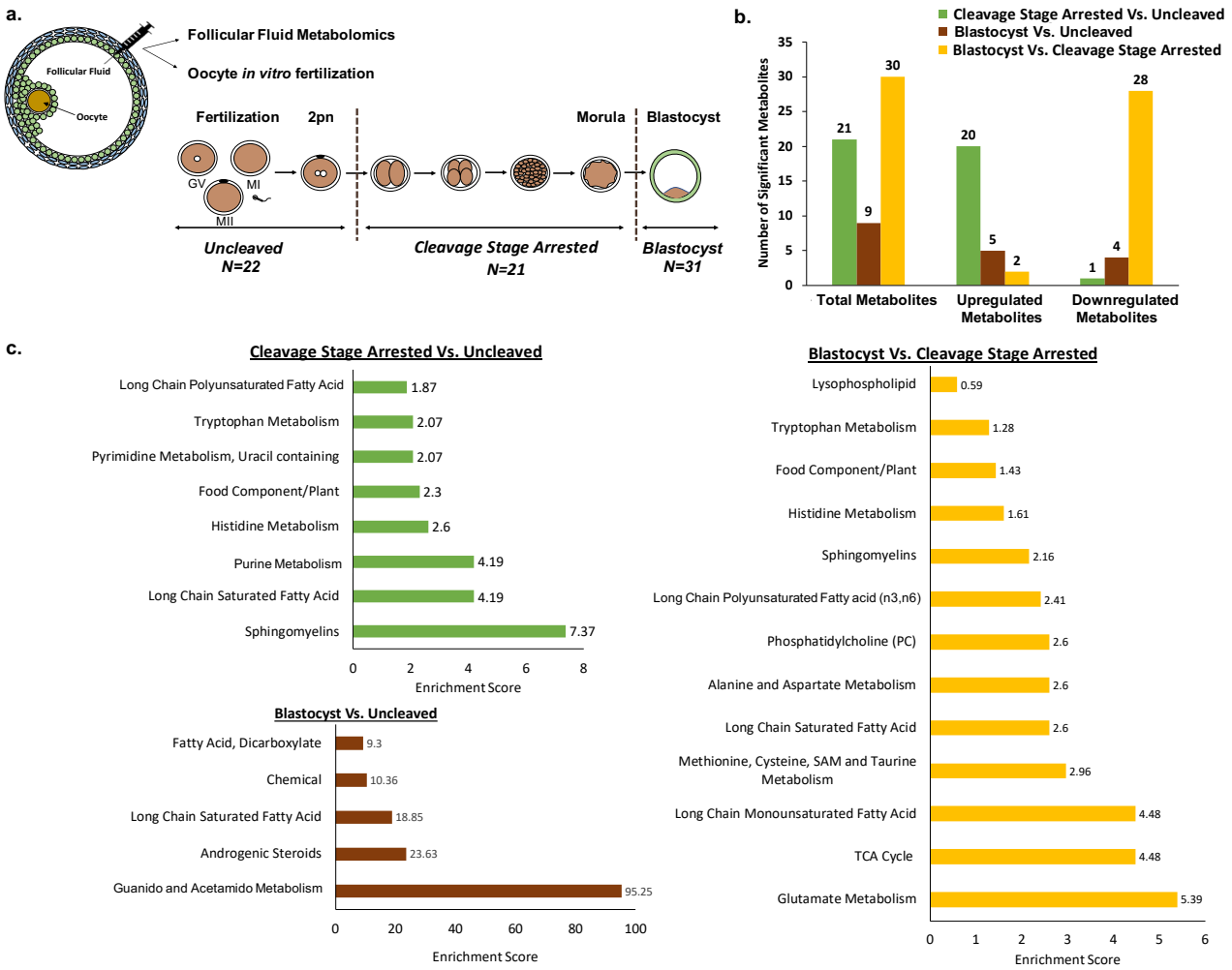


1081 **Figure 2. 1.** Metabolomics assessment of follicular fluid constituents.

**(a)** Schematic depicting the experimental design of the study with the collection of FF for metabolomics analysis and the corresponding oocyte for IVF. Resultant embryos were classified as uncleaved (N=22), cleavage stage arrested (N=21), or blastocyst (N=31). **(b)** The total number of significant metabolites ($p \leq 0.05$) that were upregulated or downregulated in the FF between the embryo groups was determined through pairwise comparisons. Note that the majority of metabolites that were statistically different between the blastocyst and cleavage stage arrested embryo groups were downregulated in blastocysts. **(c)** Pathway enrichment analysis of the metabolites in the FF shown as pairwise comparisons identified multiple fatty acid and metabolism pathways as well as the TCA cycle components that were different between the embryo groups. Enrichment score= (k/m)/((n-k)/(N-m)) where m = number of metabolites in the pathway, k = number of significant metabolites in the pathway, n = total number of significant metabolites and N = total number of metabolites.

1082 Box plots of the significantly different metabolites between the blastocyst and
1083 cleavage stage arrested groups were constructed and are shown in **Figure 2. 2,** whereas the
1084 uncleaved versus cleaved or blastocyst comparisons are shown in **Supplementary Fig. S2.**
1085 **4**. In addition, there were several metabolites belonging to same molecular pathway that
1086 showed a trend between the embryo groups, but were not statistically significant
1087 (**Supplementary Fig. S2. 5**). These metabolites included alanine, threonine, asparagine,
1088 tyrosine, proline, and methionine from the amino acid pathway and prostaglandin E2, 1-
1089 linoleoyl-GPC, 1-oelyl-GPC, 1-palmitoyl-GPC, 3-hydroxyadipate of the lipid pathway,
1090 which should be further investigated in additional cohorts of individual follicles.
1091
1092

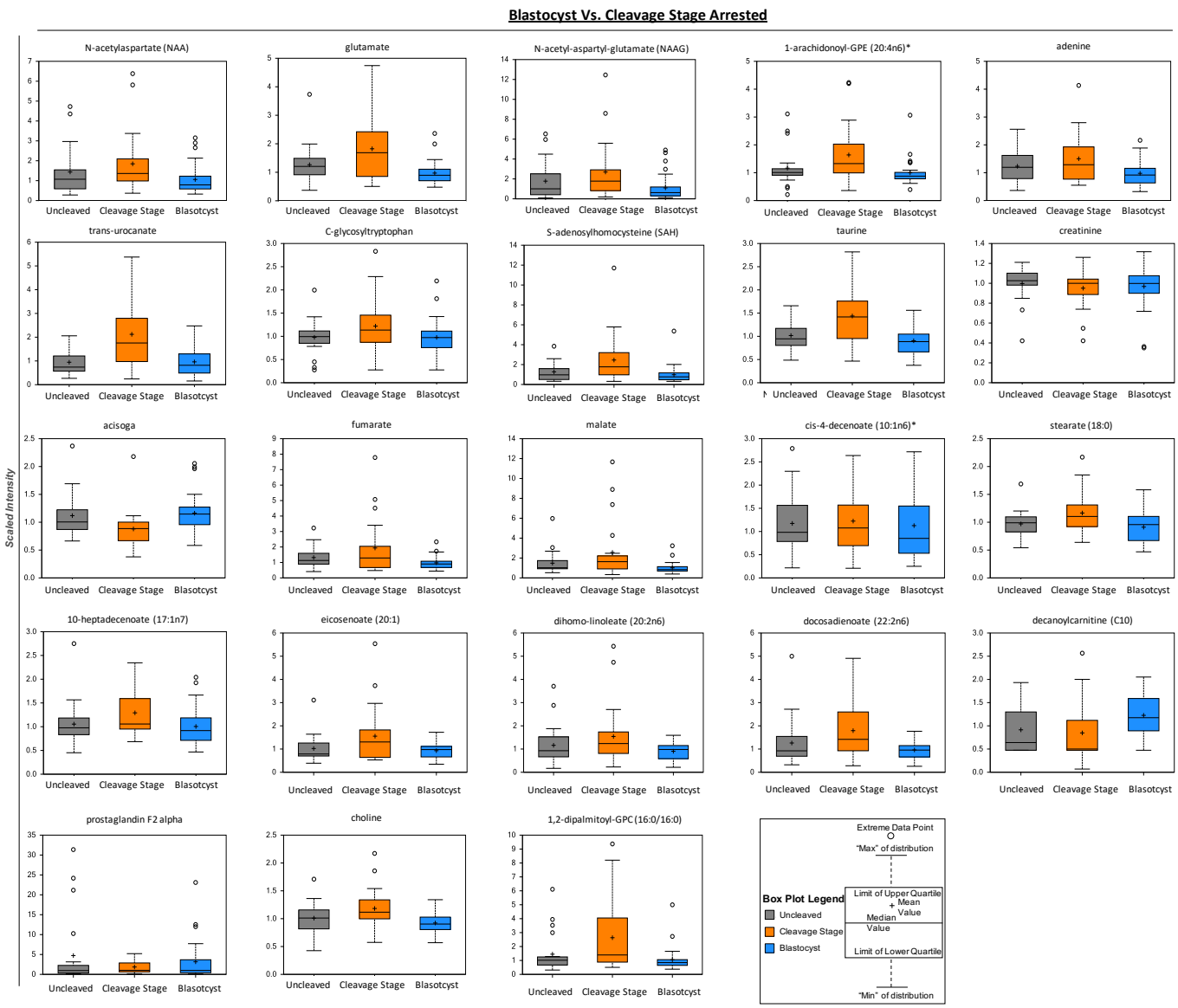


**Figure 2. 2. Box plots of metabolites that were significantly different between FF samples belonging to the blastocyst versus cleavage stage arrested embryo group.**

The y-axis reflects the scaled intensity of each metabolite in uncleaved (gray) cleavage stage arrested (orange) and blastocysts (blue). The original data generated by the area under curve of the MS peaks was used for median-scaling, determining the minimum and maximum of data distribution, and identification of outliers. Note that with the exception of acisoga, an end product of polyamine metabolism, and the fatty acid lipid molecule, decanoylcarnitine (C10), most of the metabolites were downregulated in blastocysts compared to cleavage stage arrested embryos.

1095 *Correlation between glucocorticoid levels in FF and embryo developmental potential*

1096 Since the merged metabolomics dataset identified differences in several key
1097 pathways that grouped according not only to the developmental outcome, but also based
1098 on individual female rhesus macaques, we unmerged the assessments and determined that
1099 corticosteroid signaling was highly significant in each independent metabolomics
1100 evaluation. More specifically, we observed that the levels of the glucocorticoid
1101 metabolites, cortisol and cortisone, in FF were strongly associated with the developmental
1102 potential of the resident oocyte. Cortisone is biologically inactive because it has low
1103 affinity for GR, whereas cortisol binds the GR at high affinity to activate downstream
1104 signaling events. While higher FF cortisol levels were detected within follicles associated
1105 with an oocyte that formed a blastocyst (**Fig. 2. 3a**), higher cortisone levels were detected
1106 within follicles with oocytes that remained uncleaved or arrested in development post-
1107 fertilization. (**Fig. 2. 3b**). **Figure 2. 3c** represents a pairwise comparison of the FF ratio of
1108 cortisol: cortisone and shows that the ratio of these glucocorticoids in the FF associated
1109 with an oocyte that formed a blastocyst was significantly higher than the oocyte that did
1110 not form a blastocyst ($p=0.0283$). Based on these findings, we reasoned that the
1111 cortisol:cortisone ratio in FF is an important determinant of oocyte competency and that
1112 the intrafollicular levels of cortisol and cortisone during the periovulatory interval should
1113 be further investigated. Thus, we obtained FF from rhesus macaque females undergoing a
1114 COS that did not receive hCG (0 hr) or FF collected 36 hr after an ovulatory stimulus by
1115 hCG administration for LC-MS. As shown in **Figure 2. 4a**, cortisone levels significantly
1116 declined, whereas cortisol levels significantly increased with hCG administration,
1117 supporting a role for glucocorticoid signaling in the periovulatory process.

1118

1119

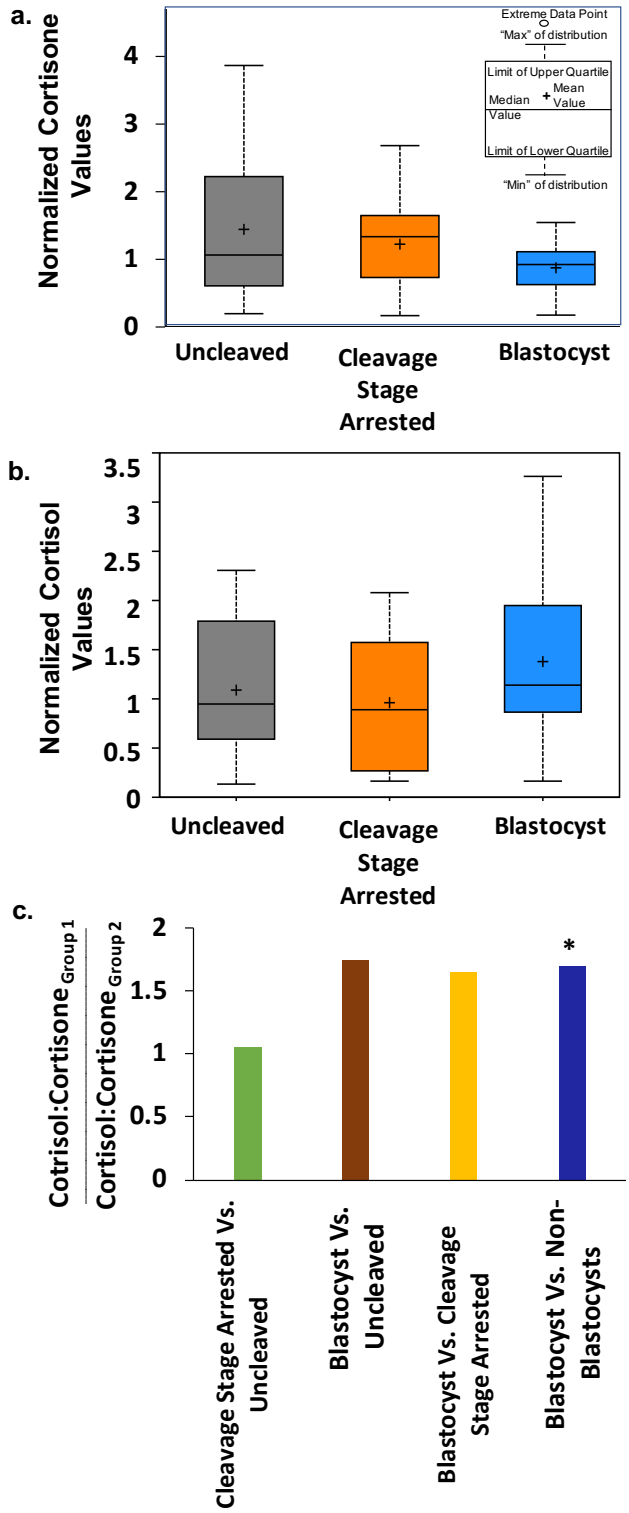


**Figure 2. 3. Glucocorticoid levels in FF are indicative of oocyte competency.** Box plots depicting the normalized values of **(a)** cortisone and **(b)** cortisol in the FF of each corresponding embryo group. **(c)** The ratio of cortisol to cortisone in the FF shown by a pairwise comparison between the embryo groups. Note that the cortisol to cortisone ratio is significantly higher in the FF of the blastocyst versus non-blastocyst groups (*p=0.0283).

1120 *Enzymatic interconversion of glucocorticoids in the periovulatory follicle*

1121 The active and inactive forms of glucocorticoids are interconvertible through the
1122 action of two enzymes, HSD11B1 and HSD11B2[91]. HSD11B1 converts cortisone to
1123 cortisol, which binds to and activates GR, whereas HSD11B2 coverts cortisol to cortisone,
1124 a compound that has low to minimal affinity for GR[92,93]. We previously demonstrated by
1125 microarray analysis in female rhesus macaques undergoing a COv protocol that HSD11B1
1126 and HSD11B2 mRNA levels in the periovulatory follicle significantly increase and
1127 decrease, respectively, after hCG administration[96]. In order to determine the cellular
1128 localization of the two enzymes in the follicle during the periovulatory interval, IHC was
1129 performed on ovaries removed from animals undergoing a Cov protocol prior to (0 hr) or
1130 12 hr, 24 hr, and 36 hr after hCG administration. As shown in **Figure 2. 4b**, HSD11B1 was
1131 expressed in the oocyte and CCs of ovarian follicles both pre- and post-hCG
1132 administration, and there was an apparent increase in mGCs over time with the highest
1133 level of expression detected at 36 hr post-hCG administration. While the theca cells were
1134 devoid of HSD11B1 expression pre-hCG administration, post-hCG administration
1135 HSD11B1 expression in theca cells was evident, particularly at 24 hr and 36 hr post-hCG
1136 administration. In contrast, positive HSD11B2 immunostaining (**Fig. 2. 4c**) was observed
1137 in the oocyte and CCs before hCG administration (0 hr), but diminished after hCG
1138 administration. HSD11B2 immunolabeling was not detected in theca cells at all time
1139 points. Thus, an increase in HSD11B1, with a corresponding decrease in HSD11B2
1140 expression, in the follicle correlated with the increased cortisol:cortisone ratio observed in
1141 FF following an ovulatory stimulus.

1142

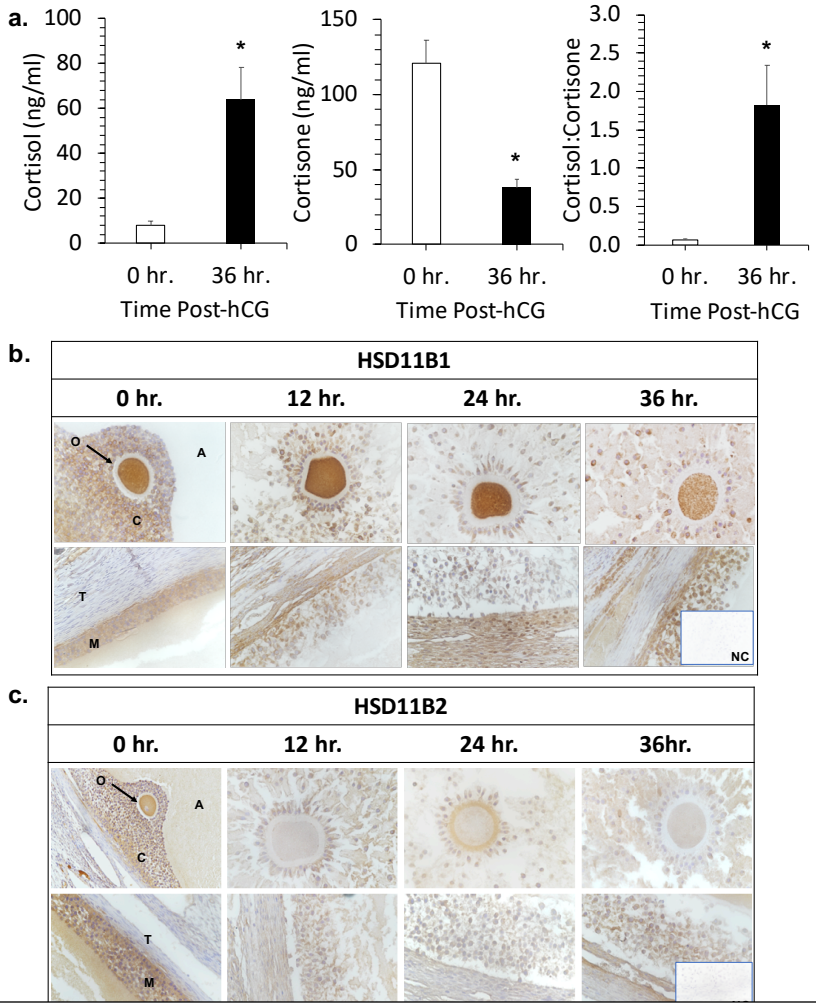


**Figure 2. 4. Glucocorticoids and the enzymes that metabolize glucocorticoids are present in the rhesus macaque periovulatory follicle.**

**(a)** LC-MS/MS analysis of cortisol and cortisone concentrations in the FF obtained from rhesus macaque follicles between pre- (0 hr) and 36 hr post-hCG administration. A statistically significant increase in cortisol (*p=0.0137) and decrease in cortisone (*p=0.0110), with a corresponding increase in the cortisol to cortisone ratio (*p=0.0256), was observed following hCG injection. Error bars = mean ± SEM, n= 5 follicles. **(b)** Representative photomicrographs for IHC of HSD11B1 and **(c)** HSD11B2 immunolocalization in the rhesus macaque periovulatory follicle pre- (0 hr) as well as 12 hr, 24 hr and 36 hr post-hCG administration. Note the overall increase in HSD11B1, as well as a concomitant decrease in HSD11B2 expression, in the ovarian follicle prior to hCG administration and with increasing time after the ovulatory stimulus. O=oocyte, C=cumulus cells, A=antrum, T=theca cells, M=mural granulosa cells and NC=negative control. The 0 hr panel in HSD11B2 IHC staining (2c) was captured at 10x magnification. Other IHC images in 2.4 b. and 2.4 c. were captured at 20x magnification.

1143

1144 *Expression and localization of GR in oocytes and ovarian follicles*

1145 Our next objective was to determine which cell types are potentially responsive to
1146 glucocorticoid action by immunolocalizing GR in the rhesus macaque periovulatory
1147 follicle. Ovarian tissues obtained from female rhesus macaques undergoing a Cov protocol
1148 at the same time points pre- and post-hCG injection as described above were examined by
1149 IHC. GR immunostaining was observed in the oocyte, CCs, mGCs, as well as the theca
1150 cells lining the follicle wall (**Fig. 2. 5a**). There was a reduction in oocyte-specific GR
1151 staining at 12 hr post-hCG and the highest intensity of GR staining was detected in all cell
1152 types at 36 hr post-hCG administration. Since GR was evident in the oocyte, we further
1153 assessed its expression within immature and mature oocytes by IF. GV oocytes were
1154 collected from non-luteinized, pre-ovulatory follicles (0 hr COS) and GR
1155 immunolocalization was observed in both the cytoplasm and nucleus of immature oocytes
1156 (**Fig. 2. 5b**). However, 36 hr post-hCG administration, GR expression was only observed
1157 in the nucleus of GV oocytes and CCs that remained attached from the luteinizing follicles.
1158 Unexpectedly, GR also localized to the metaphase plate of mature MII oocytes. The GV
1159 oocytes from non-luteinized follicles that reinitiated meiosis by IVM did not exhibit
1160 nuclear localization of GR.

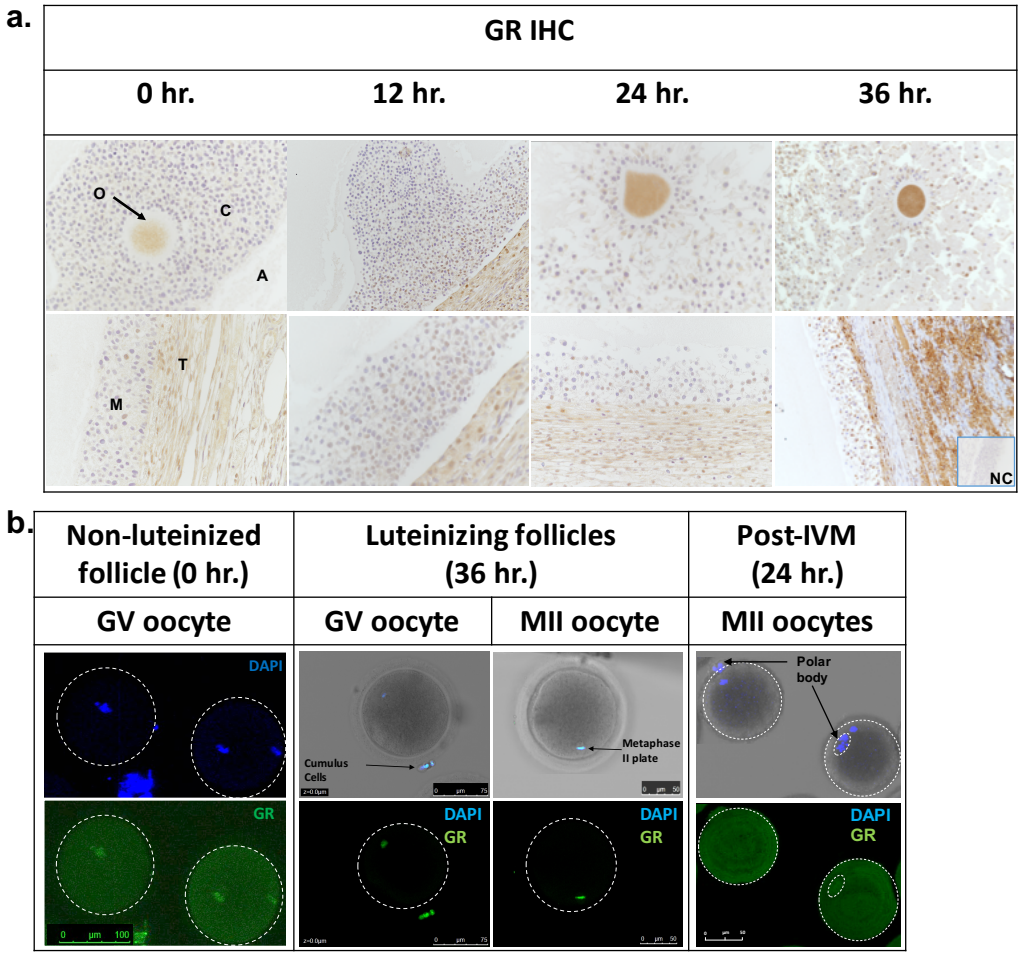


1161

**Figure 2. 5. GR localizes to oocytes and somatic cells in the rhesus macaque periovulatory follicle.**

**(a)** Representative photomicrographs of GR IHC was performed on rhesus macaque periovulatory follicles pre- (0 hr) and 12 hr, 24 hr and 36 hr post-hCG administration. Positive immunolabeling (brown) was detected in the oocyte, CCs, mGCs, as well as the theca cells lining the follicle wall. There was an apparent reduction in oocyte-specific GR staining at 12 hr post-hCG and the highest intensity of GR staining was detected in all cell types at 36 hr post-hCG administration. O=oocyte, C=cumulus cells, A=antrum, T=theca cells, M=mural granulosa cells, and NC=negative control. The IHC images were captured at 20x magnification. **(b)** Representative photomicrographs of GR IF in rhesus macaque oocytes obtained from follicles before (0 hr) and 36 hr after hCG administration demonstrated GR localization (green) in both the cytoplasm and nucleus of non-luteinized GV oocytes, but only in the nucleus of luteinizing GV oocytes and CCs that remained attached. Note that GR also localized to the metaphase plate of mature MII oocytes and that GV oocytes from non-luteinized follicles that reinitiated meiosis by IVM exhibited only cytoplasmic

1162 *Functional assessment of GR action*

1163 After determining the expression patterns of GR, HSD11B1, and HSD11B2 in the
1164 primate periovulatory follicle, we next sought to ascertain the functional role of GR and
1165 the glucocorticoid signaling pathway in rhesus macaque oocyte function, maturation,
1166 fertilization, and pre-implantation embryo development. Thus, a MAO designed to target
1167 the 5'UTR of GR was microinjected into oocytes using a non-targeting MAO as a negative
1168 control. Initially, GV, MI, and MII oocytes aspirated 36 hr after hCG administration were
1169 injected with either STD MAO (N=8) or the GR MAO (N=15) and GR knockdown
1170 assessed by IF. Within 24 hr of microinjection, up to 80% of the GR MAO injected oocytes
1171 did not contain any discernable GR expression (**Supplementary Fig. S2. 6a**).This was not
1172 observed in STD MAO injected oocytes, demonstrating that the knockdown of GR in
1173 oocytes using a MAO approach was robust and specific.

1174 Once we confirmed efficient GR knockdown in oocytes, GR involvement in
1175 fertilization and the initial cleavage divisions leading up to blastocyst formation was also
1176 assessed in oocytes collected from a 36 hr post-hCG COS cycle. Comparison of oocytes
1177 injected with GR MAO (N= 43; 38 MI/MIIs and 5 GVs) or STD MAO (N=38 33 MI/MIIs
1178 and 5 GVs) showed no significant differences in maturation, fertilization, cleavage or
1179 blastocyst formation rates (**Supplementary Fig. S2. 6b**). To determine if blocking GR
1180 expression closer to the time that re-initiation of meiosis occurs *in vivo* would have an
1181 impact on oocyte maturation, fertilization, or embryonic development, oocytes were
1182 collected 6 hr after hCG administration during a COS protocol. As expected, mostly GV
1183 oocytes were obtained at this time point, but a small number of maturing MI oocytes were
1184 also collected. These oocytes were injected with STD MAO (N=30; 27 GVs and 2 Mis) or

1185 GR MAO (N=28; 27 GVs and 1MI) and cultured in the absence or presence of cortisol.
1186 However, no significant differences in the completion of meiosis, fertilization, or
1187 percentage of cleaved embryos were detected between treatment groups, which suggested
1188 that GR was not directly involved in the resumption of oocyte meiosis *in vitro* or
1189 subsequent development (**Supplementary Fig. S2. 6c**).
1190
1191 *GR knockdown in oocytes has indirect effects on GC expansion*
1192 Although there was no effect of GR knockdown on oocyte function, it was noted
1193 that the CCs obtained as part of the COCs exhibited a different morphology based on
1194 whether they were incubated with oocytes microinjected with the GR MAO versus those
1195 injected with STD MAO. At 6 hr post-hCG administration, CCs have not yet undergone
1196 expansion and remain closely associated with one another relative to the expanded CCs
1197 retrieved 36 hr after hCG administration. In the presence of the GR MAO injected oocytes,
1198 the CCs did not expand even after 30 hr in culture and remained tightly associated with
1199 one another similar to the CCs obtained immediately after follicular aspiration (**Fig. 2. 6a**).
1200 In contrast, the CCs cultured with the STD MAO injected oocytes expanded so that
1201 individual cells, rather than cell clumps, were observed. To confirm that GR knockdown
1202 in the oocyte was having an effect on the processes important for CC expansion, we
1203 performed a similar GR MAO or STD MAO microinjection experiment whereby each
1204 injected oocyte was cultured with its corresponding CCs in IVM media for 24 hours. CC
1205 cultures were stained with HABP, a protein that binds to secreted HA, which serves as a
1206 definitive marker for CC expansion[118]. While HA localized to the extracellular space in
1207 between the CCs of STD MAO injected oocytes, the CCs cultured with the GR MAO

1208 injected oocytes were negative for HA staining and appeared similar to the pre-IVM
1209 CCs/mGCs (**Fig. 2. 6b**). This suggests that GR knockdown in oocytes has indirect effects
1210 on COC function by preventing the expansion of CCs via paracrine signaling during oocyte
1211 maturation and the resumption of meiosis.
1212

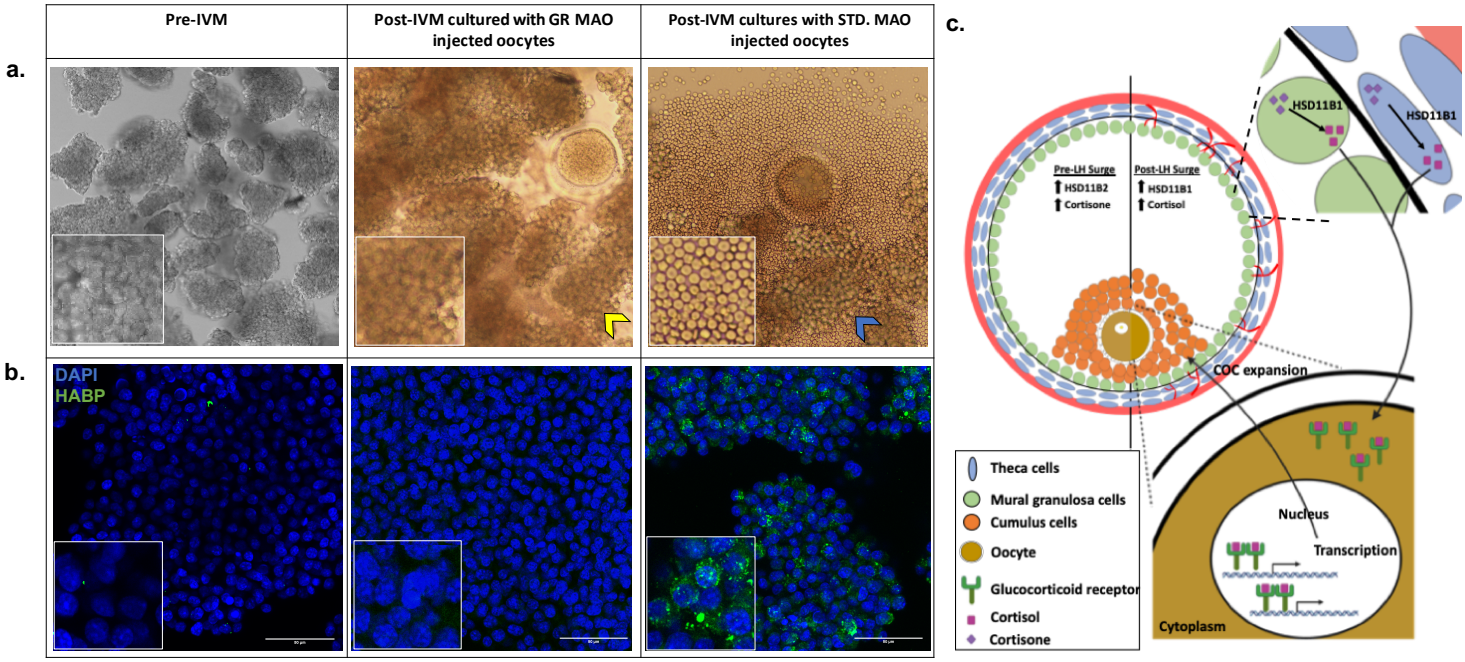


1213

**Figure 2. 6. GR is essential for cross-communication between the oocyte and the surrounding CCs.**

(a) Stereomicroscope image of CC morphology immediately after aspiration and prior to IVM (left) and in the presence of a GR MAO-injected oocyte (middle) versus an STD MAO-injected oocyte (right) after IVM. Note the clumped CCs (image insets) in the pre-IVM and GR MAO co-cultures (yellow arrowhead) compared to the single CCs visible following expansion (blue arrowhead) **(b)** IF detection of HA using HABP confirmed a lack of expansion in pre-IVM CCs and those incubated with GR MAO-injected oocytes as evidenced by the little to no HABP (green) immunostaining in CCs also stained with DAPI (blue). In contrast, robust HABP expression was observed in the CCs co-cultured with STD MAO-injected oocytes. **(c)** Proposed model for GR dependent bidirectional communication between the oocyte and somatic cells. The relative levels of 11β-HSD1/2 enzymes in the mGCs/CCs (green) and the theca cells (blue) convert cortisone to cortisol post-LH surge. This cortisol binds to the GR in the oocyte. Nuclear translocation of cortisol bound GR, activation of transcription, and further unknown downstream events leads to COC expansion that takes place during meiotic maturation of the oocyte.

1214

1215 **Discussion**

1216 Circulating and intrafollicular derived factors are critical for ovulatory follicle
1217 development in humans, non-human primates (NHPs), and rodents[26,33,34,61,198,200,223-225] and
1218 thus, the FF and its constituents are likely a reflection of the resident oocyte's capacity for
1219 fertilization and development. Indeed, we observed in this study that the volume of FF is a
1220 significant indicator of whether a fertilized oocyte will cleave and successfully form a
1221 blastocyst, which supports previous reports of a positive correlation between FF volume
1222 and IVF outcome[226,227]. However, previous genomics, proteomics and metabolomics
1223 studies reported mixed results in correlating follicular contents with pre-implantation
1224 embryo development[24-32,210,228]. In the metabolomics studies performed to date, techniques
1225 that were only able to discern a limited number of known metabolites were primarily
1226 utilized and/or a pool of FF from a heterogenous population of multiple follicles was
1227 analyzed. By pooling the FF, it is not possible to directly correlate identified factors with
1228 the oocyte's potential to undergo fertilization, cleavage, and blastocyst formation. Here,
1229 we performed an unbiased metabolomics analysis of FF samples from individual rhesus
1230 macaque periovulatory follicles to evaluate metabolites that represent the sum of all
1231 genomic, transcriptomic, and proteomic processes occurring in the follicle. Our approach
1232 also gave us the ability to directly correlate the metabolomics profile of each ovarian
1233 follicle to the developmental outcome of the corresponding resident oocyte post-IVF
1234 through the blastocyst stage. To the best of our knowledge, this study is the first to perform
1235 a comprehensive assessment of the metabolome in the FF of a large number of individual
1236 developing follicles using a unique and translationally relevant NHP model.

1237 Over the past several years, nuclear magnetic resonance (NMR) and tandem mass
1238 spectrometry (MS/MS) were used to characterize the FF metabolome. MS/MS, which was
1239 used in this study, is more sensitive than NMR based approaches[229] and the addition of
1240 different chromatographic methods has increased the number of metabolites that can be
1241 detected in a sample. Nonetheless, NMR identified glucose, choline, and creatine in FF as
1242 possible biomarkers of mature oocytes, while glucose, citrate and valine appeared
1243 important for early embryogenesis[210]. However, there was no significant association
1244 between these molecules and any particular stage of pre-implantation development. A
1245 meta-analysis of progesterone in FF indicated that it might be a useful biomarker for
1246 successful fertilization, but it also failed to explain the competency of a fertilized oocyte to
1247 form a blastocyst[230]. Unlike these factors, lower amino acid turnover in the spent media of
1248 4- to 8-cell embryos was shown to be significantly correlated with development to the
1249 blastocyst stage, whereas a higher amino acid turnover rate was more likely to result in
1250 embryo arrest[204,205]. It was proposed that the high turnover of amino acids is an indicator
1251 of the metabolic stress involved in repairing the damage to DNA, RNA or proteins during
1252 development[231]. From our analysis, we were able to confirm this finding by showing that
1253 the majority of the FF samples with higher amino acid quantities belonged to the arrested
1254 embryos, rather than the uncleaved or blastocyst groups. Moreover, the assessment of
1255 individual amino acids revealed an abundance of glutamate metabolism in the FF of
1256 oocytes that formed blastocysts. Glutamate is a main component of the fluid in the human
1257 fallopian tube[232] and our results concur with other reports suggesting that supplemental
1258 glutamate in bovine embryo culture media promotes blastocyst formation[233]. Besides
1259 amino acid differences, we also observed an enrichment of metabolites associated with the

1260 TCA cycle in the blastocyst group, which supports previous findings that glucose
1261 metabolism and pyruvate uptake may serve as markers for embryo viability[204,234,235].
1262 Overall, the majority of statistically significant metabolites were downregulated in the FF
1263 of embryos that formed a blastocyst, providing support for the "quiet embryo hypothesis"
1264 that states that endogenous energy resources are more important over nutrient
1265 supplementation in embryo survival[236].

1266 One of the most significant findings from our metabolomics analysis was the
1267 identification of the corticosteroid pathway and, in particular, the ratio of cortisol to
1268 cortisone in promoting oocyte fertilization and embryo development. While it was
1269 previously reported that cortisol and cortisone, as well as the HSD11B1 and HSD11B2
1270 enzymes responsible for their interconversion, are present in bovine and human
1271 ovaries[95,102,237-239], there are no studies indicating an association between FF glucocorticoid
1272 levels and oocyte competency. We note that the presence of significant levels of cortisol in
1273 the FF of rhesus macaque periovulatory follicles has been previously reported and that both
1274 HSD11B1 and HSD11B2 mRNA are expressed in mGCs[95]. In response to hCG
1275 administration, it was also shown that HSD11B1 mRNA expression increased, while
1276 HSD11B2 mRNA expression decreased in rhesus macaque periovulatory follicles as early
1277 as 12 hr post-hCG injection and was retained up to 36 hr[96]. However, neither of these
1278 studies examined which follicular cell type(s) might be responsible for these changes in
1279 enzyme expression and whether it correlated with the levels of cortisol and cortisone in the
1280 FF. Here, we show that the HSD11B1 and/or HSD11B2 localize to all sub-compartments
1281 of follicle, including the oocyte, GCs, CCs, and theca cells, and that HSD11B1 expression
1282 increased with a corresponding decrease in HSD11B2 expression post-hCG administration.

1283 Thus, the changes in the FF cortisol to cortisone ratio in the follicle appears to be directly
1284 linked to the relative expression levels of both enzymes.

1285 With the exception of NHPs, the expression of the GR was observed in the ovary
1286 of several species[94,102,103,240]. Most recently, GR was shown to be expressed in both murine
1287 and porcine oocytes and CCs, but there were species-specific differences noted in oocyte
1288 sensitivity to glucocorticoids that was mediated by GR in pigs and GR-independent in
1289 mice[105,241]. Our study is the first to show the presence and localization of GR within the
1290 oocyte and surrounding somatic cells of naturally selected primate follicles. We also
1291 demonstrate that GR expression is retained in oocytes *in vitro* and appears to change its
1292 intracellular location from the cytoplasm to the nucleus during maturation. GR is a member
1293 of the nuclear receptor superfamily of ligand-dependent transcription factors and
1294 translocates from the cytoplasm to the nucleus after ligand binding. Once in the nucleus,
1295 GR binds to glucocorticoid response elements (GREs) in DNA to control transcription and
1296 activate downstream signaling[242]. We observed a similar cytoplasmic to nuclear
1297 translocation of GR in rhesus macaque oocytes 36 hr after hCG administration and,
1298 unexpectedly, GR also localized to the metaphase plate of MII oocytes that matured *in*
1299 *vivo*. In contrast, IVM MII oocytes retained GR expression in the cytoplasm. It is well-
1300 established that the oocytes matured via IVM have increased likelihood of aneuploidy[243,244]
1301 and lower IVF success rates than those that are matured *in vivo*[245-247], accounting for its
1302 limited use (1-2%) in human IVF cycles (cdc.gov/art). Our results suggest that a lack of
1303 GR nuclear translocation and activation in oocytes matured *in vitro* might also disrupt
1304 downstream signaling events that contribute to lower IVF success.

1305 To complement our expression studies and further interrogate GR function in
1306 primate oocytes, we performed GR knockdown to determine if glucocorticoid signaling is
1307 necessary for the establishment or maintenance of oocyte competency. Reduced GR
1308 expression had no impact on oocyte maturation, fertilization, or subsequent development.
1309 It was observed, however, that the expansion of CCs did not occur when they were co-
1310 incubated with GR MAO-injected oocytes compared to the expansion that was observed
1311 when CCs were co-incubated with STD MAO-injected oocytes. During cumulus-oocyte
1312 expansion, HA is released by the CCs into the extracellular space surrounding the oocyte
1313 to form a 3-dimensional network of macromolecules that facilitates gradual CC dispersion
1314 and extracellular matrix reorganization[61,248]. Using HABP, we observed HA localization
1315 to the extracellular space between CCs that had been co-cultured with STD MAO injected
1316 oocytes, but not those mGCs and CCs cultured in the presence of the GR MAO injected
1317 oocytes. Our findings suggest that HA production by the CCs was inhibited by oocyte GR
1318 deficiency and that GR mediated signaling in the oocyte indirectly regulates cumulus
1319 expansion. Thus, by binding to and activating GR, glucocorticoids within the periovulatory
1320 follicle are likely involved in regulating the cross communication between the oocyte and
1321 somatic cells that is essential for cumulus-oocyte function (**Fig. 2. 6c).**

1322 Given conflicting findings on whether cortisol improves IVF treatment over the
1323 past three decades[249-251] and that cortisol concentrations significantly vary in women after
1324 a 36 hr stimulation, additional studies are needed to determine the precise relationship
1325 between FF cortisol and oocyte competency. Based on the results presented here, we would
1326 suggest that focus be placed on assessing the entire follicular microenvironment, consisting
1327 of the CCs, mGCs and the FF, to unveil potential paracrine signaling and oocyte-somatic

1328 cell crosstalk that is important for ovarian function. Apart from cortisol, there were other
1329 metabolites identified in FF whose concentration indicated an association with oocyte
1330 competency, but their biological function is currently unknown and we plan to follow-up
1331 to determine the importance of these molecules. Since metabolomics profiling is expensive
1332 and time-consuming, we also suggest that fertilization and embryo developmental
1333 outcomes be validated by assays that are feasible in a clinical setting such as a quick and
1334 relatively inexpensive ELISA of particular metabolites in the FF at the time of oocyte
1335 aspiration. Once these assays are established, then subsequent studies can include the
1336 monitoring of embryo development and assessment of live birth, with the ultimate goal of
1337 improving IVF efficiency.
1338

1339 **Acknowledgements**

1340 We thank the ONPRC ART Core for their services in oocyte and sperm collection, the
1341 Division of Comparative Medicine for their animal care and research support, the Surgical
1342 Services Unit for their follicular aspiration expertise, the Endocrine Technologies Core for
1343 performing the cytokine and steroid analysis assays, the Bioinformatics and Biostatistics
1344 Core for providing help with statistical analysis, and the Integrated Pathology Core for
1345 confocal microscopy, all under the auspices of the NIH/OD ONPRC core grant (P51
1346 OD011092). This work was supported by the NIH/NICHD (R01 HD020869 to JDH) and
1347 the Abby and Howard Milstein Innovation Award from the Howard and Georgeanna Jones
1348 Foundation for Reproductive Medicine to JDH and SLC.
1349
1350

1351 **Author Contributions**

1352 SR, SLC, and JDH designed the study, performed experiments, analyzed data, and wrote
1353 the manuscript. KEB and JR performed oocyte microinjections. NR assisted with oocyte
1354 collections and MJM helped perform the IHC experiments. JK helped with the
1355 metabolomics analysis. All authors were involved in editing the manuscript.

1356

1357

1358

1359 **Table 2. 1.** List of metabolites that are significantly different between the embryo groups.
1360 Color coding: pink=downregulated, green=upregulated.

| Number | Super Pathway | Sub Pathway | Cleavage-Stage Non-Fertilized |
|---|---|---|---|
| 1 | Amino acid | Histidine metabolism | 1.85 |
| 2 | | Tryptophan Metabolism | 1.33 |
| 3 | Peptide | Dipeptide | 1.35 |
| 4 | Lipid | Long Chain Saturated Fatty Acid | 1.11 |
| 5 | | Long Chain Polyunsaturated Fatty Acid (n3 and n6) | 1.43 |
| 6 | | Fatty Acid Metabolism (also BCAA Metabolism) | 1.39 |
| 7 | | Phosphatidylethanolamine (PE) | 1.41 |
| 8 | | Phosphatidylethanolamine (PE) | 1.37 |
| 9 | | Phosphatidylinositol (PI) | 1.26 |
| 10 | | Phosphatidylinositol (PI) | 1.24 |
| 11 | | Sphingomyelins | 1.31 |
| 12 | | Sphingomyelins | 1.28 |
| 13 | | Androgenic Steroids | 1.73 |
| 14 | Nucleotide | Purine Metabolism, (Hypo)Xanthine/Inosine | 1.63 |
| 15 | | Pyrimidine Metabolism, Orotate containing | 0.71 |
| 16 | | Pyrimidine Metabolism, Uracil containing | 2.24 |
| 17 | | Purine and Pyrimidine Metabolism | 2.08 |
| 18 | Co-factors and vitamins | Ascorbate and Aldarate Metabolism | 1.27 |
| 19 | Xenobiotics | Food Component/Plant | 2.47 |
| 20 | Unnamed compounds | Unnamed compounds | 1.4 |
| 21 | | Unnamed compounds | 1.81 |
| **Number** | **Super Pathway** | **Sub Pathway** | **Blastocyst Non-Fertilized** |
| 1 | Dipeptide | Guanidino and Acetamido Metabolism | 0.78 |
| 2 | Lipid | Long Chain Saturated Fatty Acid | 0.83 |
| 3 | | Fatty Acid, Dicarboxylate | 0.63 |
| 4 | | Androgenic Steroids | 1.76 |
| 5 | Xenobiotics | Chemical | 1.36 |
| 6 | Unnamed compounds | Unnamed compounds | 1.36 |
| 7 | | Unnamed compounds | 1.93 |
| 8 | | Unnamed compounds | 1.35 |
| 9 | | Unnamed compounds | 0.66 |
| **Number** | **Super Pathway** | **Sub Pathway** | **Blastocyst Cleavage-Stage** |
| 1 | Amino acid | Alanine and Aspartate Metabolism | 0.69 |
| 2 | | Glutamate Metabolism | 0.71 |
| 3 | | Glutamate Metabolism | 0.55 |
| 4 | | Histidine metabolism | 0.57 |
| 5 | | Tryptophan metabolism | 0.76 |
| 6 | | Methionine, Cysteine, SAM and Taurine | 0.56 |
| 7 | | Methionine, Cysteine, SAM and Taurine | 0.77 |
| 8 | | Creatine Metabolism | 0.87 |
| 9 | | Polyamine Metabolism | 1.22 |
| 10 | peptide | Dipeptide | 0.78 |
| 11 | Energy | TCA cycle | 0.66 |
| 12 | | TCA cycle | 0.63 |
| 13 | Lipid | Medium Chain Fatty Acid | 0.68 |
| 14 | | Long Chain Saturated Fatty Acid | 0.88 |
| 15 | | Long Chain Monounsaturated Fatty Acid | 0.85 |
| 16 | | Long Chain Monounsaturated Fatty Acid | 0.7 |
| 17 | | Long Chain Polyunsaturated Fatty Acid (n3 and n6) | 0.73 |
| 18 | | Long Chain Polyunsaturated Fatty Acid (n3 and n6) | 0.66 |
| 19 | | Fatty Acid Metabolism (also BCAA Metabolism) | 0.76 |
| 20 | | Fatty Acid Metabolism (Acyl Carnitine, Medium Chain) | 1.5 |
| 21 | | Eicosanoid | 0.47 |
| 22 | | Phospholipid Metabolism | 0.84 |
| 23 | | Phosphatidylcholine (PC) | 0.65 |
| 24 | | Phosphatidylethanolamine (PE) | 0.77 |
| 25 | | Lysophospholipid | 0.73 |
| 26 | | Spingomyelins | 0.8 |
| 27 | Nucleotide | Purine Metabolism, Adenine containing | 0.65 |
| 28 | | Purine and Pyrimidine Metabolism | 0.44 |
| 29 | Co-factors and Vitamins | Ascorbate and Aldarate Metabolism | 0.82 |
| 30 | Xenobiotics | Food Component/Plant | 0.61 |

1361

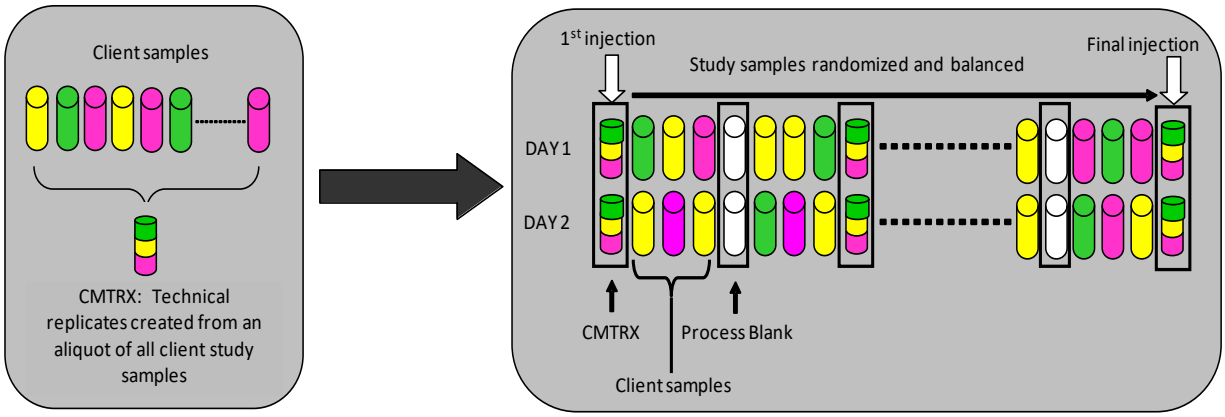


**Supplementary Figure S2. 1.** Schematic representation of the pipeline used for metabolomics analysis.

The process includes the preparation of technical replicates, quality control, randomization, and final injection for tandem MS analysis.

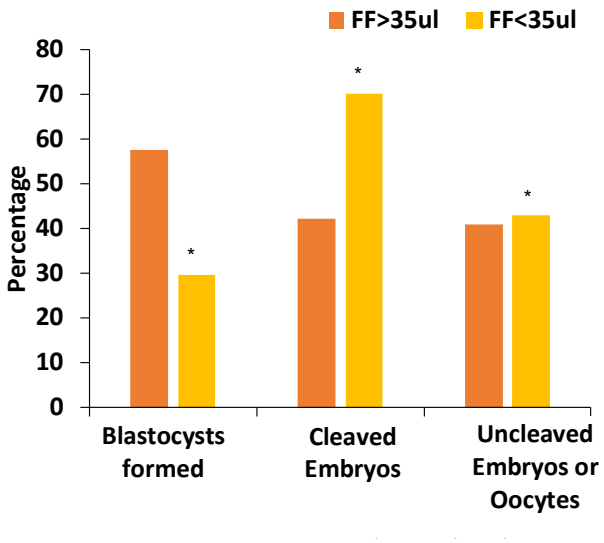


**Supplementary Figure S2. 2. The periovulatory FF volume predicts oocyte competency.**

A bar chart demonstrating the effects of periovulatory FF volume on the different post-IVF embryo outcomes. A significant correlation was found by chi-square test ($\chi^2$) between embryo groups, whereby a FF volume > 35 µl (orange bars) was associated with a higher likelihood of blastocyst formation, whereas a FF volume of < 35 µl (yellow bars) was associated with a greater probability of embryonic arrest before blastulation ($\chi^2$=15.921, p<0.001).

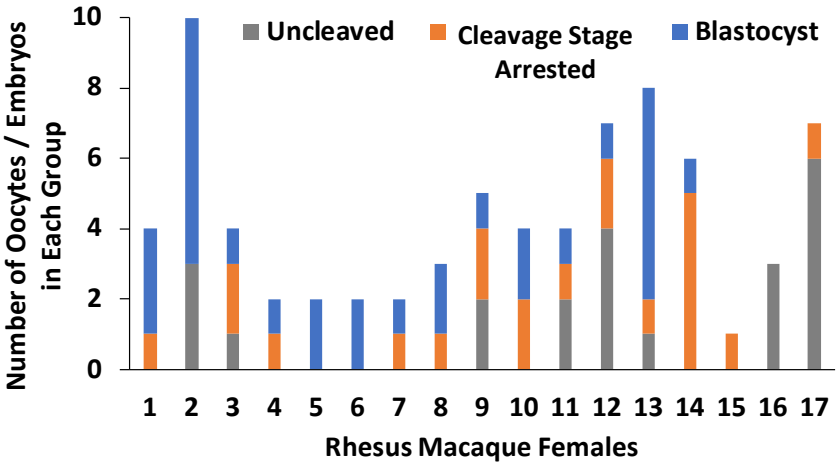


1365

**Supplementary Figure S2. 3. Distribution of the female rhesus macaques from which all 74 FF samples were obtained.**

Each rhesus macaque female (N=17) is represented as a number on the x-axis and the number of corresponding oocytes and/or embryos in the uncleaved (gray), cleavage stage arrested embryos (orange), and blastocyst (blue) groups is shown on the y-axis.

1366

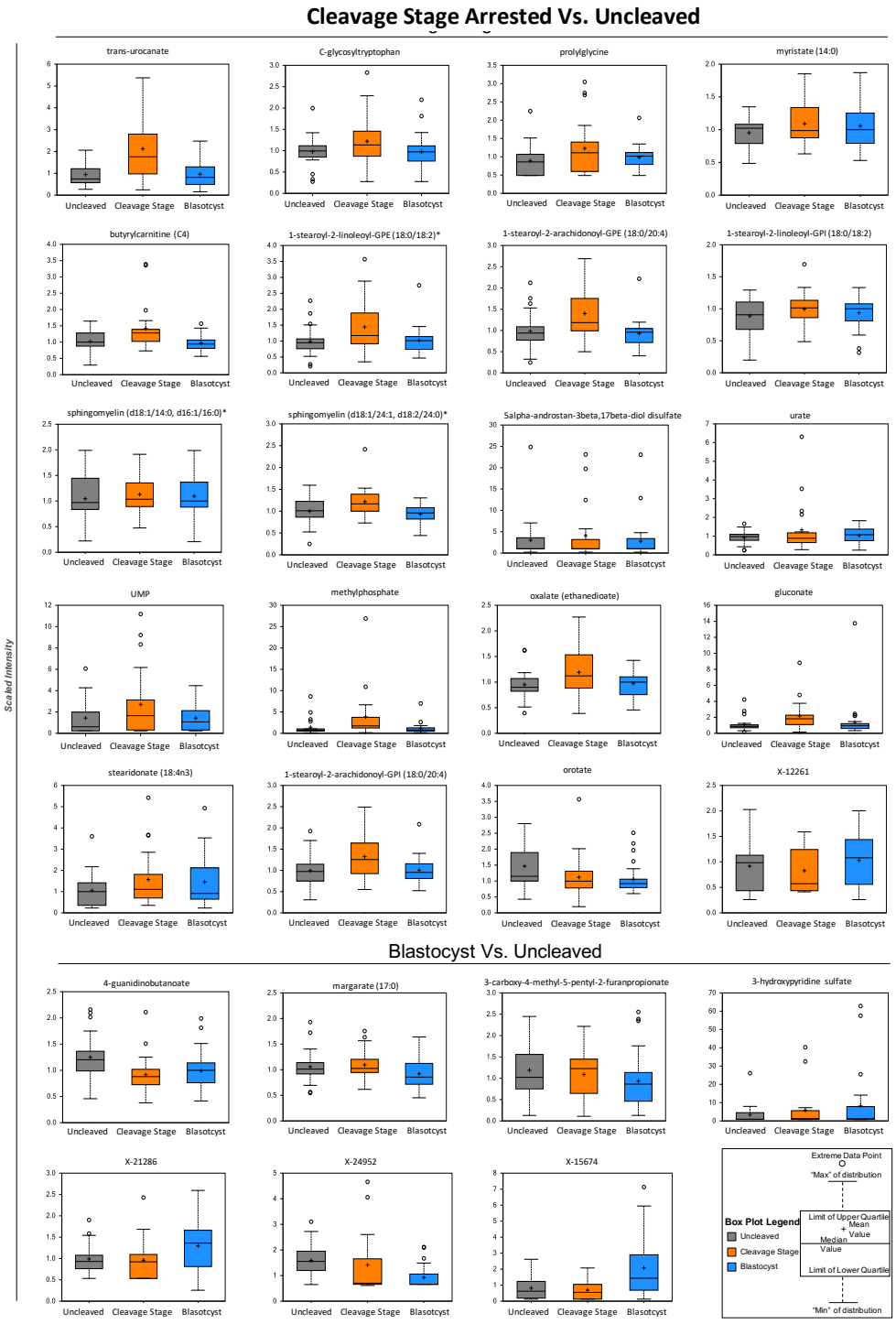


1367

**Supplementary Figure S2. 4. Box plots of the statistically significant ($p<0.05$) metabolites between the FF samples belonging to the cleavage stage versus uncleaved and blastocyst versus uncleaved embryo groups.**

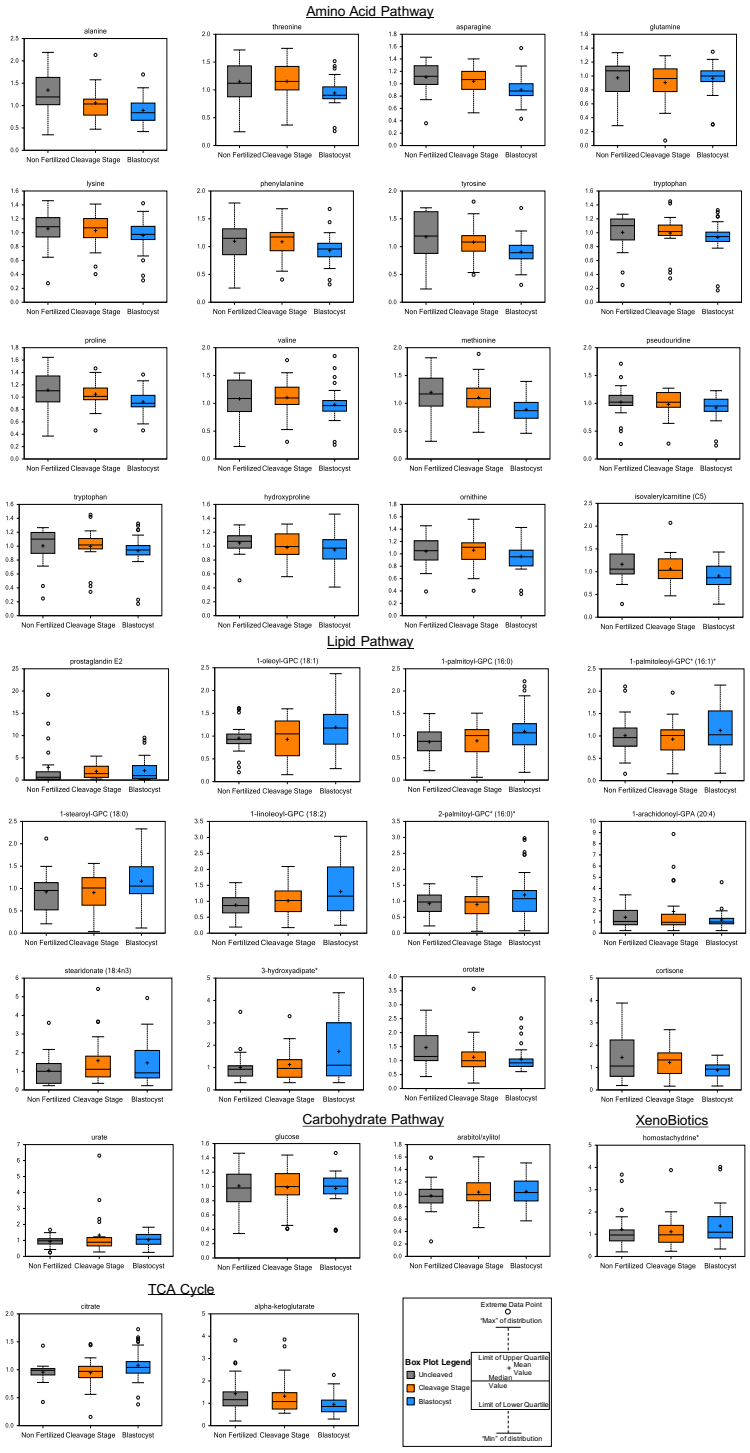


1368

**Supplementary Figure S2. 5. Box plots of metabolites that exhibited a trend between the uncleaved, cleavage stage arrested, and blastocyst embryo groups, but were not statistically significant.**

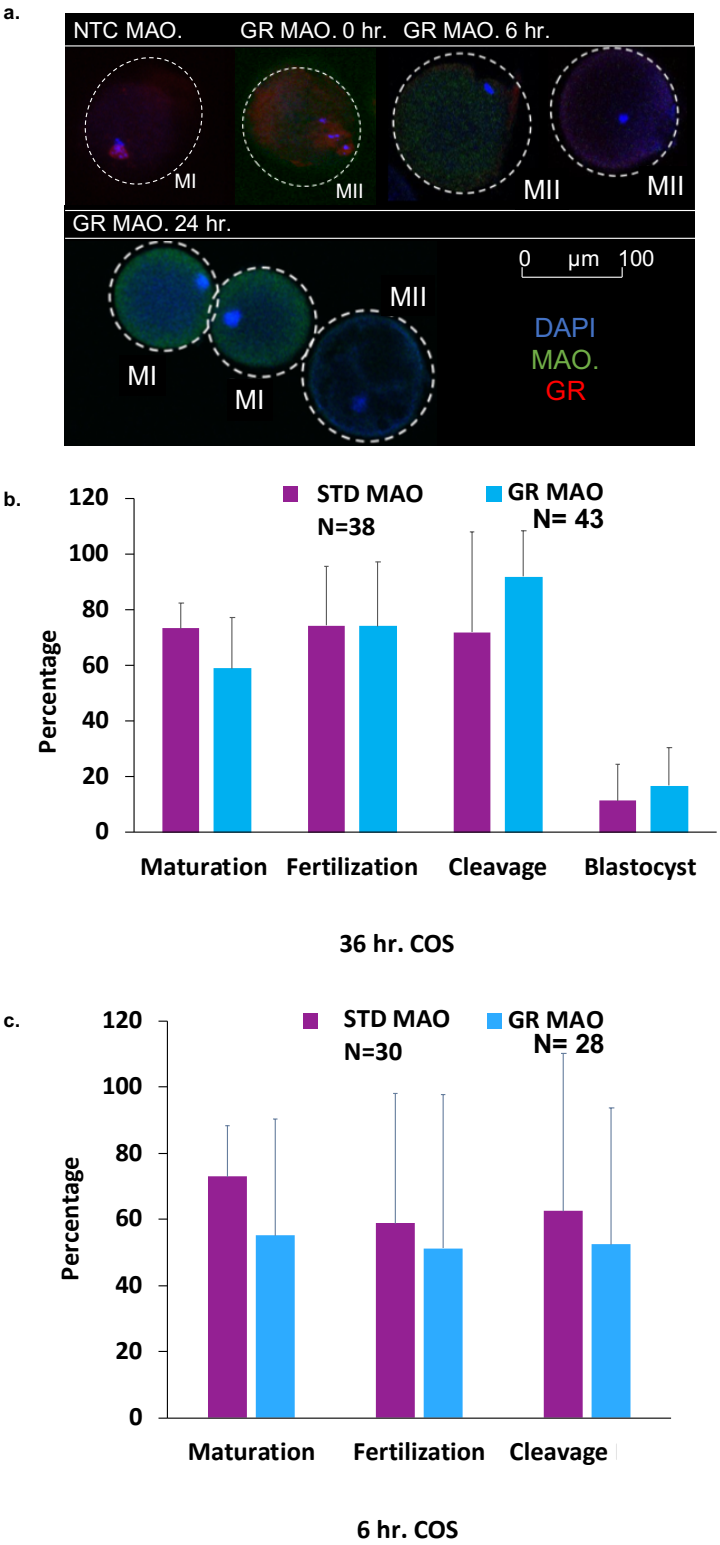


**Supplementary Figure S2. 6. GR knockdown in rhesus macaque oocytes has no effect on preimplantation development.**

(a) GR MAO knockdown was optimized in rhesus macaque oocytes obtained from a 36 hr COS cycle and reduced expression confirmed between 0 hr and 24 hr post-microinjection using the STD MAO as a control. Both MAOs were tagged with 3'-carboxyflorescein (green) for visualization of successful microinjection and oocytes stained for DAPI (blue) and immunolabeled for GR (red). Note the decrease in the expression of GR in MI/MII oocytes at 6 hr and 24 hr after injection compared to 0 hr and the STD MAO control. GR expression was knocked down in immature rhesus macaque oocytes from a **(b)** 36 hr COS and **(c)** a 6 hr COS. Oocytes were fertilized 30 hr post-hCG administration, and allowed to undergo pre-implantation development post-IVF. The maturation, fertilization, cleavage, and/or blastocyst formation rates were calculated between STD MAO (purple) and GR MAO (blue) injected oocytes and no differences were detected. N=number of oocytes microinjected with each MAO.

1371 **Chapter 3:**

1372 **Short-Term Western-Style Diet Negatively Impacts Reproductive Outcomes in**

1373 **Primates**

1374

1375 Sweta Ravisankar[1,2], Alison Y. Ting[2,3], Melinda J. Murphy[2], Nash Redmayne-Titley[2],

1376 Dorothy Wang[2], Carrie A. McArthur[4], Diana L. Takahashi[4], Paul Kievit[4], Shawn L.

1377 Chavez[2,5,6], Jon D. Hennebold[2,6]

1378

1379 [1]Department of Cell, Developmental & Cancer Biology; Graduate Program in Molecular

1380 & Cellular Biosciences, Oregon Health & Science University School of Medicine,

1381 Portland, Oregon

1382 [2]Division of Reproductive & Developmental Sciences, Oregon National Primate Research

1383 Center, Beaverton, Oregon

1384 [3]21st Century Medicine, Inc., Fontana, CA

1385 [4]Division of Cardiometabolic Health, Oregon National Primate Research Center,

1386 Beaverton, Oregon

1387 [5]Department of Molecular & Medical Genetics; Oregon Health & Science University

1388 School of Medicine; Portland, Oregon

1389 [6]Department of Obstetrics & Gynecology; Oregon Health & Science University School of

1390 Medicine; Portland, Oregon

1391

1392 **Authorship note:** SLC and JDH contributed equally to this work.

1393 **Conflict of interest:** The authors have declared that no conflict of interest exists.

1394

**Abstract**

A maternal high-fat Western-style diet (WSD) is associated with poor reproductive outcomes, but whether this is from the diet itself or underlying metabolic dysfunction is unknown. Here, we performed a longitudinal study using regularly cycling female rhesus macaques (N=10) that underwent two consecutive *in vitro* fertilization (IVF) cycles, one while consuming a low-fat chow diet and another 6-8 months after consuming a high-fat, high carbohydrate WSD. Metabolic data was collected from the females prior to each IVF cycle. Follicular fluid (FF) and oocytes were assessed for cytokine/steroid levels and IVF potential, respectively. Although transition to a WSD led to considerable weight gain, no significant effects on metabolism were observed. A decrease in both IL-1RA concentration and cortisol:cortisone ratio was observed in FF post-WSD intake. Despite an increased probability of isolating mature oocytes, a 44% reduction in blastocyst number was observed following IVF with WSD consumption and time-lapse imaging revealed delayed mitotic timing and multipolar divisions. RNA-sequencing of individual blastocysts also demonstrated dysregulation of genes and pathways involved in mitochondrial function and cell differentiation post-WSD consumption. Thus, short-term maternal WSD consumption promotes a proinflammatory intrafollicular microenvironment that is associated with impaired preimplantation development in the absence of large-scale metabolic changes.

1414 **Introduction**

1415 Obesity is often associated with various physiological, metabolic, and
1416 psychological diseases and disorders, including hypertension, diabetes, arthritis, and
1417 depression, in both men and women[252-257]. There is also a known correlation between
1418 maternal/paternal obesity and infertility or sub-fertility in humans as well as
1419 rodents[184,188,258]. Indeed, overweight/obese women are more likely to experience
1420 reproductive issues such as menstrual irregularities[259], decreased chances of conception,
1421 and defects in placentation during pregnancy than normal-weight women [260,261]. However,
1422 whether the manifestations of maternal obesity are due to abnormal ovarian follicular
1423 development, interruption of the hypothalamic-pituitary-ovarian (HPO) axis that regulates
1424 ovulation, and/or changes in endometrial receptivity is unclear[259,262].

1425 In obese women undergoing infertility treatment, findings of unresponsiveness or
1426 a delayed response to controlled ovarian stimulation (COS) by administration of exogenous
1427 gonadotropins[184,263-265], as well as poor *in vitro* fertilization (IVF) outcomes [266-268], suggests
1428 that it is the ovarian follicular microenvironment that is altered with obesity. This
1429 conclusion is consistent with other IVF studies, whereby increased pregnancy failure rates
1430 in obese women returned to normal if donor oocytes were used[269]. Additional evidence is
1431 provided by rodent studies showing that a highly obesogenic diet caused adverse effects
1432 on murine oocyte quality and metabolism, producing mature metaphase II (MII) oocytes
1433 with chromosomal abnormalities[188,270]. Upon fertilization of these oocytes, increased
1434 embryo degradation and delayed developmental progression distinct from meiotic
1435 aneuploidy was also observed, which indicated further effects on preimplantation
1436 development[188]. Transfer of maternal high-fat diet blastocysts into a non-obese uterine

1437 environment still resulted in brain development defects, fetal growth retardation and
1438 embryonic loss[188]. Thus, findings of abnormal post-implantation fetal development in these
1439 rodent studies was likely due to deficiencies in oocyte or maternal factors rather than the
1440 uterine microenvironment[188,271]. The identity of these factors and at which stage of
1441 preimplantation development the defects occurred, however, remains to be defined.

1442 Besides the precise contributors to embryo loss in obesity, it is also unclear,
1443 especially in women, if the negative effect on reproductive processes is due to the diet itself
1444 or the subsequent development of metabolic dysfunction. Moreover, it is difficult to
1445 distinguish these possibilities with human studies due to obvious ethical and technical
1446 limitations as well as the considerable challenge in controlling for environmental and
1447 dietary factors that could have an influence on reproductive outcome. Additionally, mice
1448 are generally sacrificed to obtain oocytes or embryos, which precludes longitudinal
1449 analyses. Here, we conducted a longitudinal study using a cohort of female rhesus
1450 macaques that allowed us to assess the ovarian follicular microenvironment and IVF
1451 outcomes under a highly controlled switch from a Standard Chow Diet (SCD) to a WSD.
1452 Each rhesus macaque female served as its own experimental control such that short-term
1453 diet-induced effects on primate ovarian follicle, oocyte, and preimplantation embryo
1454 development could be assessed directly without the complicating influences of metabolic
1455 dysfunction. Given similarities in reproductive physiology, hormonal stimulation during
1456 controlled ovulation, typical oocyte yields, and blastocyst formation rates shared between
1457 women and female rhesus macaques, our findings are translationally relevant to obese
1458 women undergoing infertility treatment in IVF clinics[197,272].

1459

1460 **Results**

1461 *The effects of maternal short-term WSD intake on metabolic parameters*

1462 Ten regularly cycling female rhesus macaques of young maternal age (5 to 6 yrs
1463 old) and between 5 and 7 kg body weight were selected for this longitudinal study (**Fig. 3.**
1464 **1a**). Each female consumed a SCD (15% fat, 59% carbohydrate, 26% protein) since birth
1465 and underwent an initial COS cycle (COS #1). The females were then switched to a high-
1466 fat WSD (36% fat, 46% carbohydrate, 18% protein) for 6-8 months and underwent a
1467 second COS cycle (COS #2). Weight, body fat percentage, circulating glucose and insulin
1468 levels, and insulin resistance (homeostatic model assessment of insulin resistance; HOMA-
1469 IR) were measured in the animals while consuming a SCD and 1-3 months post-COS #1,
1470 4 months after transitioning to a WSD, and one month post-COS #2 approximately 6-8
1471 months after beginning the WSD. Because one female did not undergo COS #2 (detailed
1472 below), the average weight for the remaining nine female rhesus macaques was assessed
1473 during the three time periods. Weight gain was statistically significant as early as 4 months
1474 post-WSD consumption as well as 6-8 months later (**Fig. 3. 1b**; $p<0.05$). When the average
1475 weight of each female was analyzed separately, two animals appeared to be resistant to
1476 weight gain (**Fig. 3. 1c**), which is typical of non-human primate diet studies[273]. However,
1477 no significant differences in the other metabolic parameters were observed over the same
1478 time course, including percent body fat (**Fig. 3. 2a**), HOMA-IR (**Fig. 3. 2b**), as well as
1479 glucose (**Fig. 3. 2c**) and insulin (**Fig. 3. 2d**) levels. Thus, while the females exhibited
1480 significant weight gain from short-term WSD consumption, they had not yet developed
1481 overall metabolic dysfunction.

1482

1483

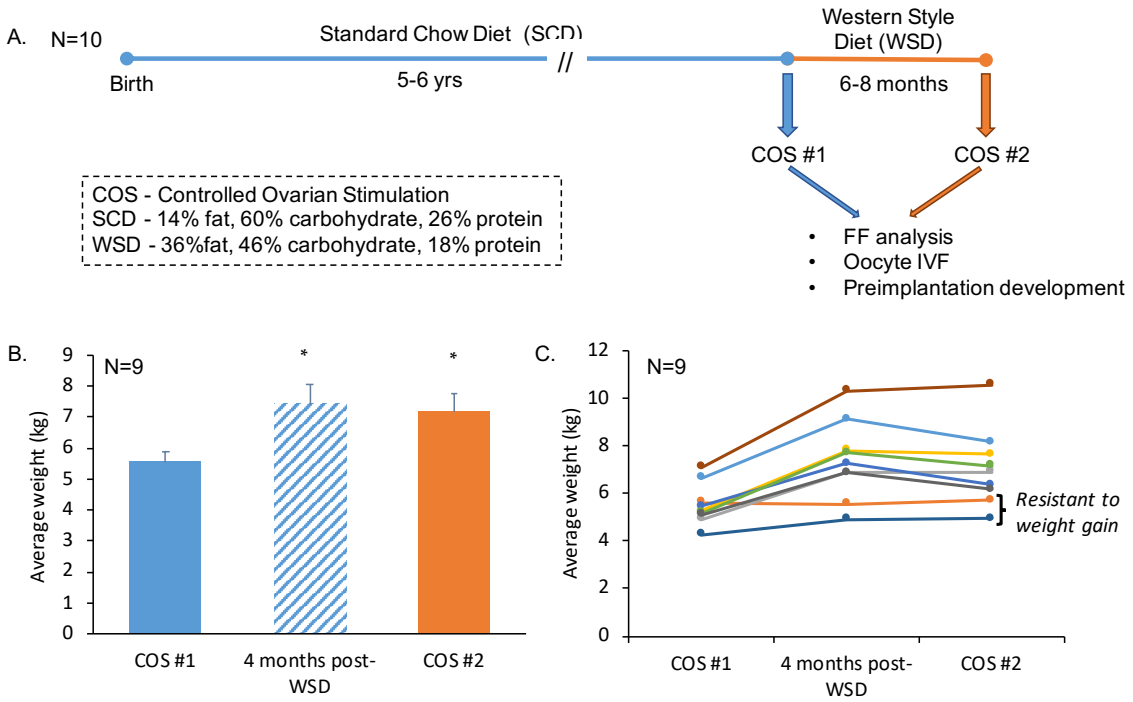


1484

1485

**Figure 3. 1. Longitudinal study to determine the effects of short-term maternal WSD intake on reproductive outcomes.**

**(A)** Experimental design: a cohort of female rhesus macaques (N=10) consuming SCD since birth underwent a baseline ovarian stimulation protocol (COS #1), which was then followed by 6-8 Months of high fat WSD consumption and a second stimulation protocol (COS #2). FF and oocytes were collected from each COS to assess the intrafollicular environment and oocyte post-IVF development, respectively. **(B)** A significant difference (*=$p<0.05$; $\pm$ SEM) was observed in the average weight of the female rhesus macaques measured post-COS #1 while consuming SCD compared to 4 months post-WSD consumption and post-COS #2 (6-8 months post-WSD consumption). **(C)** Individual weight gain comparisons revealed the resistance to weight gain displayed by two females. One female who was non-respondent to COS#2, but still gained weight after being switched to a WSD, was excluded from the analysis for (B) and (C).

1486

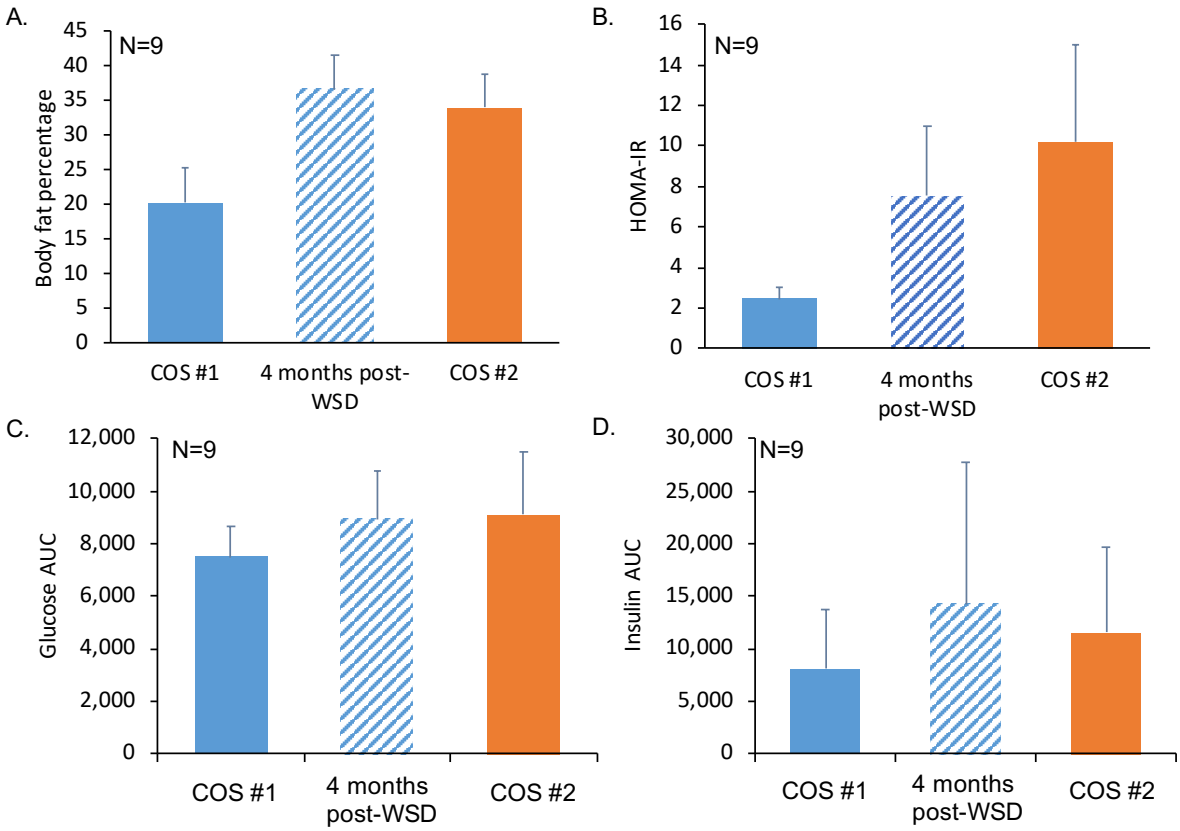


**Figure 3. 2. Short-term WSD consumption by rhesus macaques does not cause overt metabolic dysfunction.**

Metabolic parameters, including **(A)** body fat percentage, **(B)** HOMA-IR, **(C)** glucose AUC, and **(D)** insulin AUC were measured post-COS #1 while consuming SCD, 4 months post-WSD consumption, and post-COS #2 (6-8 months post-WSD consumption). None of these parameters showed any significant change pre- and post-WSD intake. Data (means + SEM) was collected from all the females that underwent both COS cycles (N=9).

1487

1488 *Responsiveness to gonadotropin stimulation before and after WSD consumption*

1489 All 10 rhesus macaque females responded positively to exogenous gonadotropin
1490 administration during COS #1 based on increases in circulating E2 levels[84] that were
1491 observed over the course of the stimulation protocol. However, 2 out of the 10 females
1492 failed to respond to hormonal stimulation after consuming the WSD (COS #2). The two
1493 non-responders were different from the two rhesus macaques detailed above that were
1494 resistant to weight gain. Of the two non-respondent females, E2 levels never increased
1495 beyond the required threshold (above 200 pg/ml on day 3 or day 4 of the COS protocol as
1496 described in methods) in one female and the other female demonstrated a rise in E2 levels
1497 that were barely above baseline. Therefore, COS #2 was terminated for the first female
1498 mid-cycle, but the follicular aspiration for COS #2 on the second female proceeded. We
1499 note that these results are in accordance with previous human studies, whereby
1500 unresponsiveness or a delayed response to exogenous gonadotropin administration was
1501 reported in obese women undergoing IVF[184,263-265].

1502

1503 *Impact of short-term WSD consumption on intrafollicular steroid and cytokine levels*

1504 Our next objective was to assess the intrafollicular milieu of ovarian follicles in the
1505 rhesus macaque females at the time of oocyte aspiration. This was accomplished by
1506 obtaining FF samples from each female both pre- and post-WSD consumption and
1507 analyzing the concentrations of cytokines and steroids by cytokine array and liquid
1508 chromatography-tandem mass spectrometry (LC-MS/MS), respectively. Of the 29
1509 cytokines analyzed (**Supplementary Table 3. 1)**, a significant decrease in the
1510 concentration of interleukin (IL) -1 receptor antagonist (IL-1RA) was observed in FF post-

1511 WSD consumption (**Figure 3. 3a**; p<0.01). A significant reduction (p<0.05) in the level of
1512 IL-2 was also detected with WSD intake (data not shown). From the seven steroids assessed
1513 (**Supplementary Table 3. 2**), there was an increase in average cortisone concentration,
1514 with a corresponding decrease in the average cortisol concentration, in the FF post-WSD
1515 consumption, resulting in a significantly decreased cortisol to cortisone ratio (**Figure 3.**
1516 **3b**; p<0.05). Because both IL-1RA and cortisol have anti-inflammatory properties[274-276],
1517 these results suggest that the WSD consumption led to an increased inflammatory state in
1518 primate ovarian follicles.
1519
1520

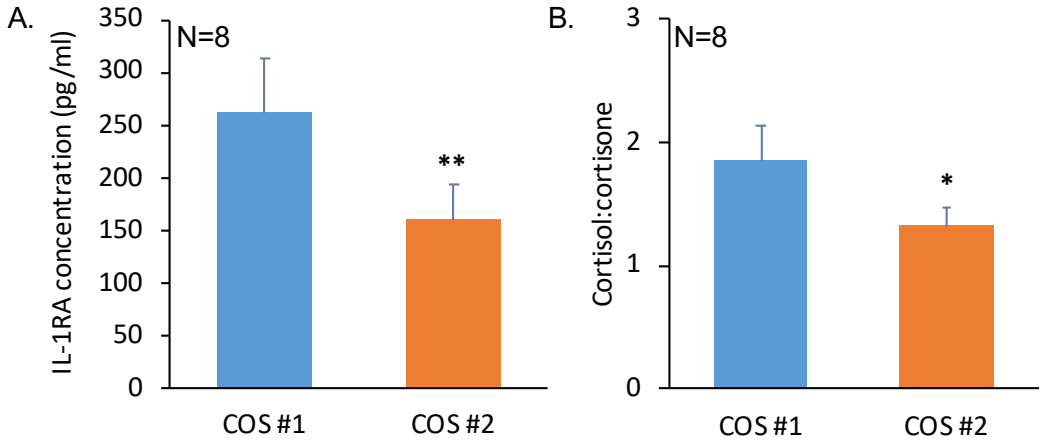


**Figure 3. 3. The cytokine and steroid milieu in rhesus macaque ovarian follicles affected by short-term WSD intake.**
Cytokines and steroids were measured in the FF post-COS #1 while consuming SCD and post COS #2 (6-8 months post-WSD consumption) by Luminex 29-plex platform and LC/MS, respectively. There was a significant decrease in the concentration of **(A)** IL-1RA (**=p<0.01) and the **(B)** ratio of cortisol:cortisone (*=p<0.05) from only 6-8 months of WSD consumption. The error bars on each measurement indicates the calculated standard errors. Only females that responded to the COS from which a sufficient volume of FF was collected were included in this analysis (N=8).

1521 *Correlation between short-term WSD consumption and oocyte maturity*

1522 To further assess the effects of WSD consumption on the intrafollicular
1523 microenvironment, oocytes were obtained from the rhesus macaque females both pre- and
1524 post-WSD consumption. A total of 527 oocytes were collected from the 10 females during
1525 COS #1, with an average of 53 oocytes per female, while 399 oocytes were obtained from
1526 9 of the females during COS #2, with an average of 44 oocytes per animal. Aspirated
1527 oocytes were classified as either a mature MII oocyte, maturing metaphase I (MI) oocyte,
1528 immature germinal vesicle (GV) oocyte, or degenerated oocyte. The odds of isolating a
1529 GV oocyte for a female on the WSD was 0.611 times the odds of when the female was
1530 consuming SCD (95% confidence interval; CI: 0.402-0.929 times; $p<0.05$). In contrast, the
1531 odds of obtaining MII oocytes was higher, but not statistically significant post-WSD
1532 consumption. Thus, aspirated oocytes were less likely to be at the GV stage and more likely
1533 to be in the MII stage of development when the female was consuming the WSD.

1534

1535 *Preimplantation embryo fate following SCD versus WSD consumption*

1536 The isolated oocytes were fertilized and the post-IVF developmental outcomes
1537 were compared between COS #1 and COS #2. While the average percentage of fertilized
1538 oocytes post-SCD versus post-WSD (68% and 73%, respectively) was not statistically
1539 different, we did observe a significant decrease in the average number of blastocysts
1540 formed per female (**Fig. 3. 4**; $p<0.05$). In total, we obtained 138 blastocysts from the
1541 females on the SCD and only 77 blastocysts after converting animals to the WSD, resulting
1542 in a 44% reduction in the number of blastocysts formed. Statistical testing determined that
1543 the odds of forming a blastocyst for a female post-WSD consumption was 0.673 times that

1544 when the female was receiving a SCD (95% CI: 0.485-0.935 times). We also note that the
1545 ability of the resident oocyte to form a blastocyst following IVF was negatively correlated
1546 with a reduced cortisol to cortisone ratio in the FF post-WSD intake (R=-0.66; p<0.05) as
1547 described above.

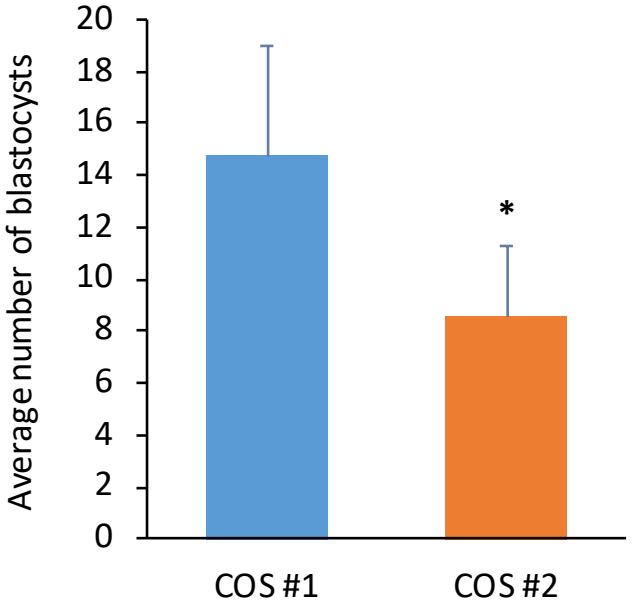


**Figure 3. 4. Short-term WSD consumption is associated with a reduced blastocyst formation.**
The total number of blastocysts formed post-WSD consumption decreased by 44% relative to that formed post-SCD intake and a statistically significant difference (*=p<0.05)was detected when the average number of blastocysts formed per female rhesus macaque was analyzed. The error bars on each measurement indicates the calculated standard errors. Data was collected from all the females that underwent both COS cycles (N=9).

1548

1549 *WSD intake is associated with delayed mitotic timing and multipolar divisions in embryos*

1550 To determine if there were morphological or other characteristics that might explain
1551 the lower number of blastocysts formed in embryos following WSD consumption, the
1552 development of fertilized SCD versus WSD oocytes up to the blastocyst stage was
1553 monitored by time-lapse imaging. A total of 174 time-lapse videos from either pre- or post-
1554 WSD intake were analyzed and the timing of initial mitotic divisions were measured based
1555 on their predictive value of blastocyst formation in human embryos[277,278]. Of the first three

1556 mitoses, the duration of the first mitotic division and time interval between the second and
1557 third mitotic division was 0.15±0.03 and 3.25±0.07 hr longer in post-WSD than post-SCD
1558 intake, respectively (**Fig. 3. 5a**; $p<0.05$). A higher incidence of cellular fragmentation was
1559 also observed in the embryos obtained from females following WSD consumption, but this
1560 was not statistically significant. Moreover, while normal bipolar divisions more often
1561 occurred in SCD embryos (**Fig. 3. 5b**, **Supplementary Movie 3. 1**), a higher frequency of
1562 multipolar divisions was observed in WSD embryos at the zygote stage or later in
1563 development (**Fig. 3. 5c**, **Supplementary Movie 3. 2**). Delayed mitotic timing and
1564 multipolar divisions were even detected in embryos from the females that were resistant to
1565 weight gain. Although the occurrence of multipolar divisions in post-WSD was not
1566 significantly associated with WSD intake, the odds of observing a multipolar division in
1567 an embryo post-WSD consumption was 1.617 times the odds of an abnormal division
1568 occurring in an embryo from a female receiving a SCD (95% CI: 0.577 – 4.687). Thus, the
1569 WSD embryos were more likely to result in their arrest at the cleavage-stage compared to
1570 SCD-derived embryos.
1571
1572

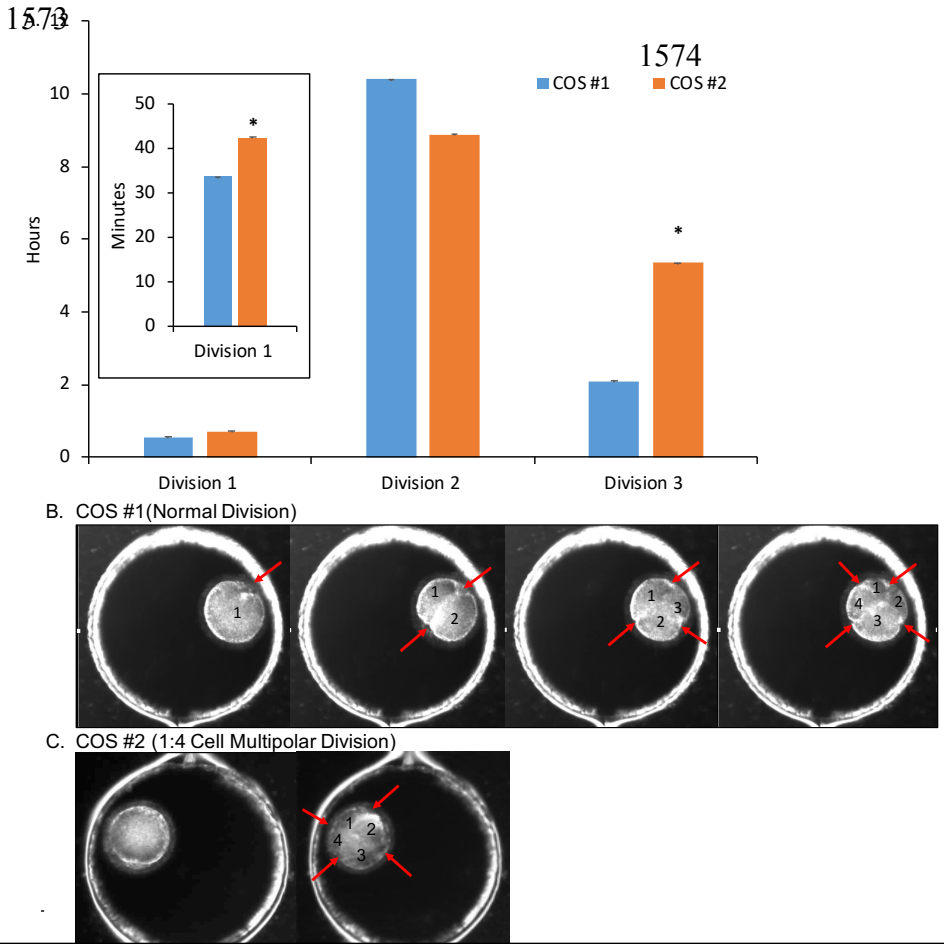


**Figure 3. 5. Abnormal mitotic timing and multipolar divisions were observed in WSD preimplantation embryos.**

The time intervals between the appearance of the 1st cleavage furrow to the end of the 1st cytokinesis, the beginning of the 2nd mitotic division, and the start of the 3rd mitotic division were measured and preimplantation development monitored until the embryo arrested or formed a blastocyst in COS#1 versus COS#2. **(A)** These measurements were averaged (error bars = ± std. dev.) amongst 5 independent reviewers and the 1st and 3rd division were significantly longer (*=p<0.05) in the embryos obtained post-WSD consumption relative to post-SCD intake. **(B)** Individual image frames from TLM videos of a representative SCD embryo showing normal bipolar divisions up to the 4-cell stage. **(C)** Similar imaging of a representative WSD embryo revealed a 1:4 cell multipolar division at the zygote stage. The cleavage furrows are denoted by red arrows in (B) and (C). The corresponding full-length TLM movies of these two embryos can be viewed in **Supplementary Movie 1** (post-SCD) and **Supplementary Movie 2** (post-WSD), respectively.

1575 *Differential gene expression in blastocysts following SCD versus WSD consumption*

1576 Of the 215 total blastocysts obtained from the rhesus macaque females either pre-
1577 or post-WSD intake, we chose 33 blastocysts (N=15 for SCD; N=18 for WSD) distributed
1578 amongst all of the animals (**Supplementary Table 3. 3**). After sequence alignment and
1579 quality assessment of the RNA-seq data, we determined that one sample from the SCD
1580 group and another one from the WSD group had lower gene counts than expected and
1581 appeared as outliers when compared to the other embryos represented by Euclidean
1582 distance clustering (**Supplementary Fig. 3. 1**). Therefore, these two samples were
1583 removed from further examination and the remaining 31 blastocysts (N=14 for SCD; N=17
1584 for WSD) were carried forward for differential gene expression analysis. We identified
1585 13,167 genes, 1057 (8%) of which were differentially regulated between the blastocysts
1586 obtained from the two treatment groups. An almost equal percentage of the genes were
1587 significantly upregulated (513 genes; ~49%) or downregulated (544 genes; ~51%) in
1588 blastocysts formed post-WSD consumption versus those following SCD intake (**Fig. 3. 6a**;
1589 $p<0.05$). Principal component analysis (PCA) revealed a subset of blastocysts from COS
1590 #1 (N=6) and COS #2 (N=7) were separated distinctly from each other (**Fig. 3. 6b**). All the
1591 other blastocyst samples that did not segregate within the two subsets did not cluster based
1592 on females or the diet.

1593

1594 *WSD consumption impacts biological processes crucial to preimplantation development*

1595 Gene ontology (GO) and pathway analyses were performed to identify the
1596 biological processes and molecular functions most associated with WSD-induced gene
1597 upregulation and downregulation. The upregulated genes were enriched in functions such

1598 as RNA binding, protein channel activity, tRNA-specific ribonuclease activity, and
1599 transmembrane amino-acid betaine and carnitine transporter activity (**Fig. 3. 6c**). The
1600 biological processes that the upregulated genes belonged to were mostly involved in
1601 mitochondrial functions which suggested that the blastocysts had a compromised
1602 mitochondrial translation machinery post-WSD intake. Upon pathway analysis for the
1603 downregulated genes, protein binding, cell adhesion molecule binding, transforming
1604 growth factor-β (TGF-β) receptor activity, and enzyme binding were the molecular
1605 functions determined to be highly associated with the WSD in blastocysts (**Fig. 3. 6d**). We
1606 note that these pathways are involved in critical biological processes during embryogenesis
1607 such as activation or stimulation of cell migration, differentiation, growth factor signaling,
1608 and tissue development.

1609 Among the 513 genes that were significantly upregulated in WSD compared to
1610 SCD blastocysts, the top genes ranked according to fold change (X) were PRAME family
1611 member 18 (PRAMEF18; 20X), notochord homeobox (NOTO; 15X), GEM like GTPase
1612 2 (REM2; 13X), acyl-CoA synthetase medium chain family member 4 (ACSM4; 12X),
1613 and killer cell lectin like receptor G2 (KLRG2; 11X) as shown in **Figure 3. 6e**. In addition
1614 to the top upregulated genes, pathways related to mitochondrial translation elongation,
1615 translation termination and mitochondrial transport (PTCD3, TIMM17A, TOMM22,
1616 TOMM40, TOMM 20, MRPL46, MRPL45, MRPL38, MRPL37, MRPS35, MRPS16,
1617 MRPS25,SLC25A19, SLC25A10, SLC25A20, and SLC25A2) were also upregulated in
1618 WSD blastocysts. In contrast, the most drastically downregulated gene in WSD blastocysts
1619 was the somatostatin receptor-5 (SSTR5), with a 88X lower expression in the blastocysts
1620 post-WSD compared to the SCD. This was followed by a decrease in the expression of toll

1621 like receptor-7 (TLR7; 37X), zinc finger protein 750 (ZNF750; 28X), DISC1 scaffold
1622 protein (DISC1; 21X), and fibronectin leucine rich transmembrane protein 3 (FLRT3; 19X)
1623 in WSD versus SCD blastocysts (**Fig. 3. 6c**). Other than these genes / pathways the BMP
1624 pathway and mesodermal commitment pathway (HAND1, FOXA2, TRIM71, BMPR2,
1625 BMPR1A, BMP2, and FGFR1), focal adhesion pathway (IGF1, COL4A2, COL4A1,
1626 PAK1, and ACTN1), and endoderm differentiation pathway (CTNNB1, FOXA2, TRIM71,
1627 and BMPR1A) were significantly reduced in blastocysts post-WSD intake.
1628
1629

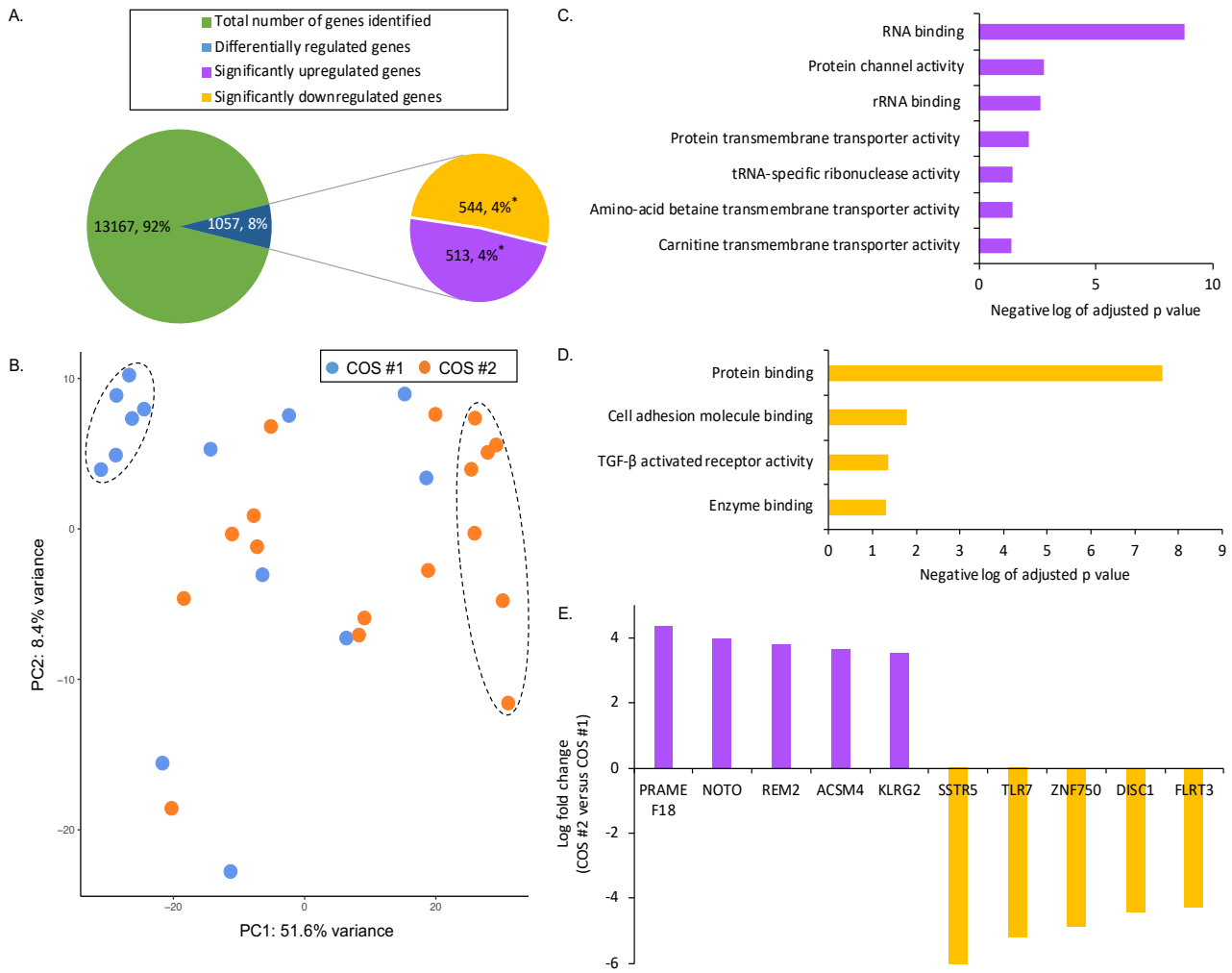


**Figure 3. 6. RNA-sequencing analysis of blastocysts reveals short-term WSD consumption leads to changes in gene expression.**

**(A)** A total of 13,269 genes were identified from the RNA-seq analysis of 32 blastocysts (N=14 for SCD; N=18 for WSD), out of which 628 genes (5%) were differentially expressed (DE). Out of the differentially regulated genes, 357 (3% of the total number of genes and 52% of the DE genes) were significantly downregulated and 328 genes (2% of the total number of genes and 48% of the DE genes) were significantly upregulated in the WSD blastocysts versus the blastocysts following SCD intake (*=p<0.05). **(B)** Principal component analysis (PCA) revealed two distinct populations of blastocyst samples enclosed in dotted lines representative of the blastocysts obtained from COS #1 and COS #2. The top gene ontology (GO) terms for molecular functions of the **(C)** significantly upregulated and **(D)** significantly downregulated genes are represented. The x-axis is the negative log of the adjusted p-value. **(E)** Out of the list of significantly differentially regulated genes, upregulated (16-32 fold) and downregulated (16-64 fold) genes in WSD blastocysts are represented. The x-axis represents the gene names and the y-axis represents the $\log_2$ fold change in gene expression. For (C), (D), and (E), the purple bars indicate the upregulated genes and the yellow bars indicate the downregulated genes.

1630

1631 **Discussion**

1632 Maternal obesity and its negative impact on IVF treatments has been reported in
1633 both humans and rodents[188,279,280], but it was unclear if these effects were due to the diet
1634 itself or the subsequent development of metabolic dysfunction. To our knowledge, we
1635 present the first longitudinal study to assess the consequences of a short-term WSD
1636 consumption on the ovarian microenvironment and preimplantation development in the
1637 translationally relevant rhesus macaque model. With the exception of two females that
1638 were resistant to weight gain, we observed an overall increase in body weight as early as 4
1639 months post-WSD intake and by 6-8 months, the females began to become less responsive
1640 or non-responsive to ovarian stimulation. This is in concordance with previously reported
1641 studies indicating that obese women undergoing assisted reproduction for infertility
1642 treatment not only often require extended periods of gonadotropin stimulation, but also
1643 increased amounts of gonadotropin than normal-weight women[184,264,265]. Therefore, obese
1644 women experience a higher incidence of IVF cycle cancellation[263] and weight loss has been
1645 reported to improve the detrimental effects of obesity on reproductive potential in these
1646 patients[184,259]. Despite the increase in body weight, we did not observe significant changes
1647 in body fat percentage, glucose levels, or insulin resistance, which is somewhat contrary to
1648 previous rodent studies[259]. There are a number of factors that could explain this
1649 discrepancy, including the duration of WSD consumption[186,281,282], differences in the
1650 percentage of calories from fat [283], and that a certain percentage of the non-human primate
1651 population is resistant to the metabolic effects of the high-fat diet [281]. Nevertheless, because
1652 we observed a dramatic transformation in ovarian physiology and embryo development

1653 from the WSD without overall metabolic dysfunction, we expect that our findings will help
1654 inform human studies on diet consumption and maternal obesity that are difficult to control.
1655 The first indication of a disturbance in the intrafollicular milieu from the WSD was
1656 a decrease in IL-1RA concentration in the FF of ovarian follicles. As an antagonist to the
1657 IL-1 receptor, IL-1RA inhibits downstream signaling of the proinflammatory cytokine, IL-
1658 1, upon receptor binding[274]. This suggests that the maternal high-fat WSD promotes
1659 heightened inflammatory activity in the follicle that in turn, may induce aberrant
1660 developmental programming in the offspring produced from the developing oocyte as
1661 previously described[284]. Further support is provided by observations of a decrease in the
1662 ratio of cortisol to cortisone in the FF since cortisol is a potent anti-inflammatory hormone
1663 and the active form of the glucocorticoid pair. Indeed, high concentrations of cortisol or
1664 elevated cortisol to cortisone ratios in the FF of periovulatory follicles was shown to
1665 positively or negatively correlate with human IVF outcomes in previous studies[249,251,285].
1666 Moreover, from multiple studies across species, FF and its constituents have shown to
1667 influence oocyte competency; i.e., the ovum's ability to undergo meiotic maturation,
1668 fertilization, and preimplantation development[26,33,34,61,198,200,223-225]. Thus, we suggest that
1669 the loss of anti-inflammatory factors within the intrafollicular microenvironment produced
1670 as a result of a WSD limits the potential of the resident oocyte to yield a blastocyst
1671 following IVF. WSD consumption also resulted in reduced FF IL-2 levels and IL-2 is well
1672 recognized as being produced primarily by activated $CD4^+$ T cells in secondary lymphoid
1673 organs, where it promotes T cell proliferation and inflammatory processes[286]. Although IL-
1674 2 was reported to have variable effects on steroidogenesis in mGCs and luteal cells[287-289],
1675 it was detected in the FF of women after gonadotropin stimulation[290]. Increased synthesis

1676 of IL-2 by mGCs obtained from women with ovarian hyperstimulation syndrome has also
1677 been reported[291], but the significance of IL-2 in the ovarian follicle remains unknown.
1678 Despite the decreased odds of aspirating an immature GV oocyte and a higher
1679 probability of obtaining a MII oocyte with WSD consumption, a reduced blastocyst yield
1680 was observed in post-WSD embryos. The isolation of predominantly mature oocytes was
1681 somewhat unexpected, since we previously reported that long-term (~3 yrs) WSD
1682 consumption in rhesus macaque females led to the retrieval of 33-43% degenerated oocytes
1683 when the naturally selected dominant follicle was obtained prior to ovulation[218].
1684 Nevertheless, reduced blastocyst formation rates were also detected in fertilized oocytes
1685 from the female that underwent COS #2 but exhibited no significant weight gain and
1686 suggests a decline in oocyte competency post-WSD even in those oocytes that successfully
1687 matured. While aneuploidy was not directly assessed, it also indicates that a certain
1688 percentage of WSD oocytes and embryos were likely chromosomally abnormal as
1689 previously shown in a high-fat diet rodent model[188]. Given that aneuploid embryos often
1690 arrest and/or are developmentally delayed, this could also be a cause for the reduced
1691 blastocyst formation post-WSD consumption[292]. Time-lapse imaging demonstrated that the
1692 duration of the first mitotic division and time interval between the second and third mitotic
1693 division was significantly longer in embryos post-WSD than post-SCD intake. It also
1694 revealed a greater incidence of multipolar divisions in WSD embryos, which are associated
1695 with aneuploidy, cause embryo arrest, or often result in implantation failure if
1696 transferred[293-296].
1697 When gene expression patterns were analyzed in the blastocysts that did
1698 successfully form after SCD versus WSD consumption, we observed a surprisingly high

1699 number of genes that were differentially regulated between the two treatment groups. The
1700 genes upregulated in WSD blastocysts belonged to diverse biological processes, including
1701 retinoic acid metabolism, GTP binding and GTPase activity, maternal imprinting, and
1702 pluripotency maintenance[297-299]. An upregulation of genes involved in mitochondrial
1703 activity was also detected in the blastocysts post-WSD intake. These findings are supported
1704 by previous studies reporting that maternal high fat diet increased mitochondrial membrane
1705 hyperpolarization and mitochondria DNA copy number to compensate for the abnormal
1706 mitochondrial functions in murine oocytes and zygotes[188,300], which could lead to apoptosis
1707 in subsequent preimplantation development[301]. On the other hand, the genes that were
1708 significantly downregulated in WSD compared to SCD blastocysts were associated with
1709 processes important for early embryogenesis such as the cytokine/steroid response[302], cell
1710 proliferation[303], lineage specification[304], and differentiation of the placental-derived
1711 trophectoderm-[305] or other extra embryonic lineages[306], as well as development of the
1712 mesoderm layer[307]. Since all of these molecular pathways are critical for the peri-
1713 implantation period, we suspect that the WSD blastocysts may have lower implantation
1714 rates, possibly resulting in early embryo loss, and exhibiting placental dysfunction as
1715 shown from previous studies of rhesus macaque females on a long-term WSD and obese
1716 women undergoing IVF treatment[184,308-310].

1717 In order to potentially improve embryo transfer success and pregnancy outcomes
1718 in obese patients, we suggest that a more in-depth assessment of the biological processes
1719 and signaling pathways revealed by our RNA-seq analysis be conducted on WSD embryos.
1720 Moreover, determining whether a similar pro-inflammatory follicular microenvironment,
1721 embryonic arrest, and differential gene expression is observed when the females are on a

1722 WSD for a longer period of time and develop metabolic dysfunction should also be
1723 determined. We note that there are already published findings of adverse effects from long-
1724 term WSD consumption on rhesus macaque ovarian and uterine structure and
1725 function[190,311], but not yet on oocyte fertilization and preimplantation development during
1726 COS cycles and this is a current research focus of our group. The results of these studies
1727 will help determine the precise impact of WSD on infertility and its confounding effects
1728 on IVF success[184,312]. With the ultimate goal of reducing embryo loss while increasing live
1729 birth rates, the findings from this study serve to advance our understanding of how maternal
1730 diet modulation affects embryogenesis and subsequent development in both obese and
1731 normal weight women.
1732

1733 **Materials and Methods**

1734 *Cohort of rhesus macaque females and diet modulation*

1735 A cohort of 10 regularly cycling female rhesus macaques of young reproductive
1736 age (5-7 yrs) and average body weight (5-7 kg) were chosen for this study. The females
1737 resided in the ONPRC Obese Resource, which provided animal care and research support.
1738 Each female initially underwent COS #1 after consuming a SCD (15% fat, 59%
1739 carbohydrate, 26% protein) since birth. Their diet was switched to a high fat WSD (36%
1740 fat, 46% carbohydrate, 18% protein) for 6-8 months before undergoing COS #2.
1741

1742 *Intravenous Glucose Tolerance Testing (ivGTT) and body fat percentage*

1743 Animals were fasted overnight and sedated with Telazol (5 mg/kg IM Tiletamine
1744 HCl/Zolazepam HCl, Fort Dodge Animal Health, Fort Dodge, Iowa, USA). If needed,

1745 additional anesthesia was accomplished with Ketamine (3–10 mg/kg IM, Abbott
1746 Laboratories, North Chicago, Illinois, USA). Once sedated, animals received an IV glucose
1747 bolus (50% dextrose solution) at a dose of 0.6 g/kg via the saphenous vein. Baseline blood
1748 samples were obtained prior to the infusion and at 1, 3, 5, 10, 20, 40 and 60 min after
1749 infusion. Glucose was measured immediately using FreeStyle Lite Glucose Monitor
1750 (Abbott Laboratories, North Chicago, Illinois, USA), and the remainder of the blood was
1751 kept in heparinized tubes on ice for insulin measurement. After centrifugation, samples
1752 were stored at –80°C until assayed. Insulin measurements were performed by the
1753 Endocrine Technologies Core (ETC) at the ONPRC using a chemiluminescence-based
1754 automatic clinical platform (Roche Diagnostics Cobas e411, Indianapolis, IN, USA).

1755 Percent body fat for each animal was measured using dual-energy X-ray
1756 absorptiometry (DEXA; Hologic QDR Discovery A; Hologic, Inc., Bedford, MA, USA).
1757 Total body scans were performed on the same day of the ivGTTs to minimize the number
1758 of sedations for each animal. Animals were positioned prone on the bed of the scanner and
1759 QDR software (Hologic, Inc., Bedford, MA, USA) was used to calculate percent body fat.
1760 All the metabolic parameter measurements were performed at three time points: 1-3
1761 months after COS #1 when the females were consuming SCD, 4 months post-WSD
1762 consumption, and one month after COS #2 (6-8 months post-WSD consumption).

1763

1764 *Oocyte aspiration and processing*

1765 Both COS cycles were performed as previously described[180]. Briefly, exogenous
1766 gonadotropins were administered to stimulate the development of multiple ovarian
1767 follicles. A positive COS response was measured by serum E2 levels rising above 200

1768 pg/ml on day 3 or day 4 of the COS protocol. Female rhesus macaques were anesthetized
1769 for laparoscopic follicular aspirations 36 hr after the administration of human chorionic
1770 gonadotropin (hCG) to induce events necessary for the re-initiation of meiosis. Two
1771 individual follicle aspirates per ovary were collected manually with a with a low dead space
1772 3ml syringe with a 22-gauge X 1.5 inch needle (Ulticare) for each aspirate. Individual
1773 follicle aspirates were centrifuged at room temperature for 30 seconds at 1000g to separate
1774 the FF from the cumulus-oocyte complex (COC) and the GCs. The COCs were then
1775 examined for presence of oocytes under a stereomicroscope by dilution with Tyrode's
1776 albumin lactate pyruvate (TALP) HEPES buffer. They were then denuded by gentle
1777 micropipeting in TALP buffer containing 0.3% bovine serum albumin (BSA; Sigma-
1778 Aldrich, St. Louis, MO). Each oocyte from an individual aspirate was placed in a separate
1779 100 μL TALP complete drops pre-equilibrated IVF dish covered by mineral oil (Sage™,
1780 Trumbull, CT). The FF and CCs were frozen down separately for further analysis. The rest
1781 of the follicular aspirates were collected in bulk using vacuum suction in TALP-HEPES
1782 buffer with 0.3% BSA and 1% Heparin sodium salt solution at 37$^{o}$C to obtain the remaining
1783 COCs. Oocytes from the bulk aspirates were denuded by gentle micropipeting in TALP-
1784 HEPES buffer containing 0.3% BSA and 3% hyaluronidase (Sigma-Aldrich). These
1785 oocytes were grouped according to their developmental stage and placed in 100 μL TALP
1786 complete drops in a pre-equilibrated IVF dish covered by mineral oil (Sage™, Trumbull,
1787 CT).
1788
1789
1790

1791 *IVF and embryo culture*

1792 Fresh semen from 3 adult male rhesus monkeys of average paternal age (9.4 $\pm$ 1.5
1793 yrs old) and proven fertility was used for IVF throughout this project. The semen was
1794 collected the same day as oocyte retrieval for conventional IVF. In brief, seminal
1795 plasma was removed as previously described[216] and used for IVF at a final concentration
1796 of $2x10^6$ sperm /ml in TALP-complete medium. IVF was performed the evening of
1797 the collection. Sperm was treated with cyclic adenosine monophosphate (cAMP; 5 mg/ml)
1798 and caffeine (2 mg/ml) 15 min before fertilization to induce hyperactivation and increase
1799 fertilization potential. In each well containing oocytes, 1µl of the activated sperm was
1800 added. IVF dishes were incubated at 5% $CO_2$ and 37ºC overnight for fertilization.

1801 After IVF for 14-16 hr, oocytes were stripped of excess sperm by micropipeting
1802 and visually assessed for fertilization, i.e. two pronuclei and/or two polar bodies.
1803 Confirmed zygotes were individually transferred to custom Eeva™ 12-well polystyrene
1804 petri dishes (Progyny, Inc., San Francisco, CA; formerly Auxogyn, Inc.) for TLM and
1805 cultured in 100 µL of one-step commercial medium supplemented with 10% serum protein
1806 (LifeGlobal, Guildford, CT) under mineral oil (Sage™, Trumbull, CT) at 37°C with 6%
1807 $CO_2$, 5% $O_2$. The remaining zygotes were transferred to a pre-equilibrated 10-well IVF
1808 dish and cultured in the same medium as the TLM dish. Embryo development was
1809 individually tracked through day 8 post-IVF. Medium was changed at day 3 post-IVF and
1810 the embryos were left to continue developing to the blastocyst stage up until day 8. Arrested
1811 (pre-blastocyst stage) embryos and blastocyst development outcomes were recorded.
1812 Percentage of fertilized oocytes was calculated as the number of zygotes post-IVF/number

1813 of mature MII oocytes X 100. Percentage of blastocysts formed was calculated as the
1814 number of blastocysts formed/number of cleaved embryos X 100.
1815
1816 *Time-lapse monitoring (TLM)*
1817 Individual confirmed zygotes transferred to a TLM dish (N=12) were monitored
1818 with an Eeva™ darkfield 2.2.1 time-lapse microscope system (Progyny, Inc., San
1819 Francisco, CA) as previously described[313]. The Eeva™ time-lapse monitoring (TLM)
1820 systems were comprised of an inverted microscope with a 10X Olympus objective, auto-
1821 focus, and 5-megapixel CMOS digital camera placed inside a tri-gas incubator (Panasonic
1822 Healthcare, Japan). The embryos were imaged every 5 min. with a 0.6 sec. exposure time
1823 until developmental arrest or up to 8 days if they progressed to the blastocyst stage. Each
1824 image was time stamped with a frame number and all images compiled into an AVI movie
1825 using FIJI software. The time intervals between the appearance of the 1$^{st}$ cleavage furrow
1826 to the end of the 1$^{st}$ cytokinesis, the beginning of the 2$^{nd}$ mitotic division, and the start of
1827 the 3$^{rd}$ mitotic division identified by cleavage furrows were manually recorded and
1828 represented as an average. Other morphological features such as cellular fragmentation and
1829 asymmetrical/multipolar division were also examined and recorded for each embryo. A
1830 total of 174 TLM videos post- SCD and post-WSD intake were analyzed by 5 independent
1831 observers.
1832
1833 *Cytokine and steroid analysis of FF*
1834 The FF from two individual aspirates collected from each female rhesus macaque
1835 were pooled together for each COS. These pooled FF samples were analyzed for

1836 concentrations of 29 cytokines and 7 steroids. Analyses of steroid hormone levels was
1837 performed in the ETC at ONPRC by LC-MS/MS on a Shimadzu Nexera-LCMS-8050
1838 using a previously described method[218]. Accuracies for the steroid hormone assays ranged
1839 from 87.9%-103.0% and intra-assay coefficients of variation (CVs) were <4%. All samples
1840 were analyzed in a single assay. Cytokine levels were determined using a rhesus macaque
1841 29-plex cytokine panel (ThermoFisher Scientific, Waltham, MA) following the
1842 manufacturer's instructions. Concentrations of each cytokine were calculated from a
1843 standard control curve. Samples were analyzed on a Milliplex Analyzer (EMD Millipore,
1844 Billerica, MA) bead sorter with Xponent Software version 3.1 ( Luminex, Austin, TX).
1845 Data were calculated using Milliplex Analyst software version 5.1 (EMD Millipore,
1846 Billerica, MA). Intra-assay CVs for all analytes were <15%. The list of all the cytokines
1847 and steroids and their CVs and accuracies can be viewed in **Supplementary Table 3. 1**
1848 **and 3. 2**, respectively.
1849
1850 *RNA-sequencing*
1851 Blastocysts were collected from COS #1 (n=138) and COS #2 (n=77) and incubated
1852 in EmbryoMax Acidic Tyrode's Solution (EMD Millipore, Burlington MA) for ~30
1853 seconds for removal of the zona pellucida. These zona free blastocysts were then
1854 transferred to the extraction buffer of the ARCURUS PicoPure RNA Isolation Kit
1855 (ThermoFisher Scientific KIT0204, Waltham, MA) and frozen at -80$^{o}$C until RNA
1856 isolation. From all of the blastocysts, 34 were chosen for RNA-seq analysis to equalize the
1857 number of embryos from both diet groups. To minimize variability between treatment
1858 groups due to abnormal cytokinesis, only blastocysts that exhibited bipolar divisions with

1859 or without cellular fragmentation were sequenced as shown in **Supplementary Table 3. 3**.
1860 RNA was extracted from the blastocysts and cDNA prepared using the SMART-Seq v4
1861 Ultra Low Input RNA Kit for sequencing (TakaraBio, Shiga, Japan) and the amplified
1862 cDNA was purified using the Agencourt AMPure XP Kit (Beckman Coulter, Brea, CA),
1863 both according to manufacturer's instructions. cDNA was then sheared to approximately
1864 250 base pairs in length using a Covaris M220 sonicator. Sheared cDNA was resuspended
1865 in Tru-seq Resuspension Buffer and libraries prepared using a Tru-Seq Nano kit (Illumina,
1866 San Diego, CA) according to the manufacturer's instructions, except that 16 cycles of
1867 amplification were performed to account for the low input samples. Fragment size was
1868 measured using a Fragment Analyzer 5200 and samples quantified with qPCR and pooled
1869 at equimolar concentration. Multiplexed samples were sequenced across seven lanes of a
1870 single-read, 75 cycle run on an Illumina HiSeq 4000 sequencer. The sequencing data was
1871 demultiplexed using Illumina's bcl2fastq software and sample quality assessed with
1872 FastQC (v 0.11.8), followed by trimming of low-quality bases and adapter sequences with
1873 Trimmomatic (v 0.39). Trimmed sequences were aligned via STAR (version 2.7.0) to the
1874 most recent rhesus macaque reference genome from Ensembl (Mmul_10) and gene counts
1875 obtained by specifying the "quantMode GeneCounts" parameter of STAR, along with the
1876 Mmul_10.99 Ensembl annotation gtf file. Two outliers (one from the SCD group and
1877 another one from the WSD group) had lower gene counts than expected, which was likely
1878 due to DNA contamination, and were removed from further analyses. Differential
1879 expression between groups was performed with edgeR (version 0.28.0) using the
1880 "QLFTest" option. The Enrichr and G-profiler online tools were used for molecular
1881 pathway and gene ontology assessment.

1882
1883 *Statistical analysis*

1884 One-way ANOVA and a post-hoc t-test comparison with Bonferroni adjustment
1885 was performed to assess any significant differences in body weight, body fat percentage,
1886 HOMA-IR, glucose AUC and insulin AUC. Paired t-test was performed to assess any
1887 significant differences cytokine or steroid levels in the FF, and the number of blastocysts
1888 formed pre- and post-WSD consumption. The logistic mixed effects regression models
1889 with random intercept was used to account for intra-female correlation to the odds ratio of
1890 obtaining oocytes of different stages of maturity and the significant differences in the
1891 percentage of fertilization, cleavage, and blastocyst formation and the incidence of cellular
1892 fragmentation and/or multipolar divisions between the two groups. RNA-seq data p-values
1893 were adjusted for multiple comparisons with the Benjamini-Hochberg method.

1894

1895 *Study approval*

1896 All protocols involving animals were approved by the ONPRC Institutional Animal
1897 Care and Use Committee and conducted in accordance with the National Institutes of
1898 Health Guidelines for the Care and Use of Laboratory Animals. The housing and general
1899 care of rhesus macaques (*Macaca mulatta*) was previously described[144].

1900

1901 **Acknowledgements**

1902 We thank the ONPRC ART Core for their services in oocyte and sperm collection, the
1903 Division of Comparative Medicine and the Obese Resource for their animal care and
1904 research support, the Surgical Services Unit for their follicular aspiration expertise, the
1905 Endocrine Technologies Core for performing the cytokine and steroid analysis assays, and

1906 the Bioinformatics and Biostatistics Core for providing help with statistical analysis, all
1907 under the auspices of the NIH/OD ONPRC core grant (P51 OD011092). This work was
1908 also supported by the NIH/NCTRI Project II (P50 HD071836; Project II) to co-Pis: JDH
1909 and SLC.

1910

1911 **Author Contributions**

1912 SR, SLC, and JDH designed the study, performed experiments, analyzed data, and wrote
1913 the manuscript. AYT performed the oocyte collection and monitored the preimplantation
1914 development for COS #1. CAM, DLT, and PK performed animal care and metabolic
1915 studies. MJM helped with coordinating and scheduling for COS cycles. SR, MJM, NR,
1916 DW, and SLC were each an independent observer for TLM analysis. All authors were
1917 involved in editing the manuscript.

1918

1919

1920 **Supplementary table S3. 1.** Assay metrics for the cytokine analysis (Luminex 29-plex)

| **Target Cytokine** | **Intra-Assay CV (%)** |
|---|---|
| FGF-Basic | 2.64 |
| IL-1B | 3.13 |
| G-CSF | 3.57 |
| IL-10 | 3.86 |
| IL-6 | 3.00 |
| IL-12 | 4.62 |
| RANTES | 11.27 |
| Eotaxin | 14.23 |
| IL-17 | 8.86 |
| MIP-1a | 2.79 |
| GM-CSF | 5.72 |
| MIP-1B | 3.98 |
| MCP-1 | 4.86 |
| IL-15 | 10.05 |
| EGF | 3.81 |
| IL-5 | 9.48 |
| HGF | 3.59 |
| VEGF | 11.06 |
| IFN-γ | 2.88 |
| MDC | 4.63 |
| I-TAC | 10.21 |
| MIF | 0.93 |
| IL-1RA | 4.78 |
| TNF-α | 7.22 |
| IL-2 | 8.23 |
| IP-10 | 4.59 |
| MIG | 0.00 |
| IL-4 | 4.44 |
| IL-8 | 2.94 |

1921
1922

1923 **Supplementary table S3. 2.** Assay metrics for the steroid analysis (LC/MS)

| **Steroid Hormone** | **Accuracy (%)** | **Intra-assay CV (%)** |
|---|---|---|
| Cortisol | 93.9 | 1.5 |
| Cortisone | 94.0 | 2.1 |
| Testosterone | 94.4 | 4.0 |
| Estradiol | 101.1 | 2.8 |
| Estrone | 99.2 | 2.4 |
| Progesterone | 87.9 | 1.8 |
| Androstenedione | 103.0 | 3.5 |

1924
1925

1926 **Supplementary table S3. 3.** Distribution of blastocyst samples for RNA-sequencing

1927 from COS #1 and COS #2

| Sample Name | Comments |
|---|---|
| COS_1_1 | Fragmented, non-multipolar |
| COS_1_2 | Fragmented, non-multipolar |
| COS_1_3 | Fragmented, non-multipolar |
| COS_1_4 | Fragmented, non-multipolar |
| COS_1_5 | Fragmented, non-multipolar |
| COS_1_6 | Fragmented, non-multipolar |
| COS_1_7 | Fragmented, non-multipolar |
| COS_1_8 | Non-fragmented, non-multipolar |
| COS_1_9 | Non-fragmented, non-multipolar |
| COS_1_10 | Non-fragmented, non-multipolar |
| COS_1_11 | Non-fragmented, non-multipolar |
| COS_1_12 | Non-fragmented, non-multipolar |
| COS_1_13 | Non-fragmented, non-multipolar |
| COS_1_14 | Non-fragmented, non-multipolar |
| COS_1_15 | Non-fragmented, non-multipolar |
| COS_2_1 | Fragmented, non-multipolar |
| COS_2_2 | Fragmented, non-multipolar |
| COS_2_3 | Fragmented, non-multipolar |
| COS_2_4 | Fragmented, non-multipolar |
| COS_2_5 | Fragmented, non-multipolar |
| COS_2_6 | Fragmented, non-multipolar |
| COS_2_7 | Fragmented, non-multipolar |
| COS_2_18 | Fragmented, non-multipolar |
| COS_2_8 | Fragmented, non-multipolar |
| COS_2_9 | Non-fragmented, non-multipolar |
| COS_2_10 | Non-fragmented, non-multipolar |
| COS_2_11 | Non-fragmented, non-multipolar |
| COS_2_12 | Non-fragmented, non-multipolar |
| COS_2_13 | Non-fragmented, non-multipolar |
| COS_2_14 | Non-fragmented, non-multipolar |
| COS_2_15 | Non-fragmented, non-multipolar |
| COS_2_16 | Non-fragmented, non-multipolar |
| COS_2_17 | Non-fragmented, non-multipolar |

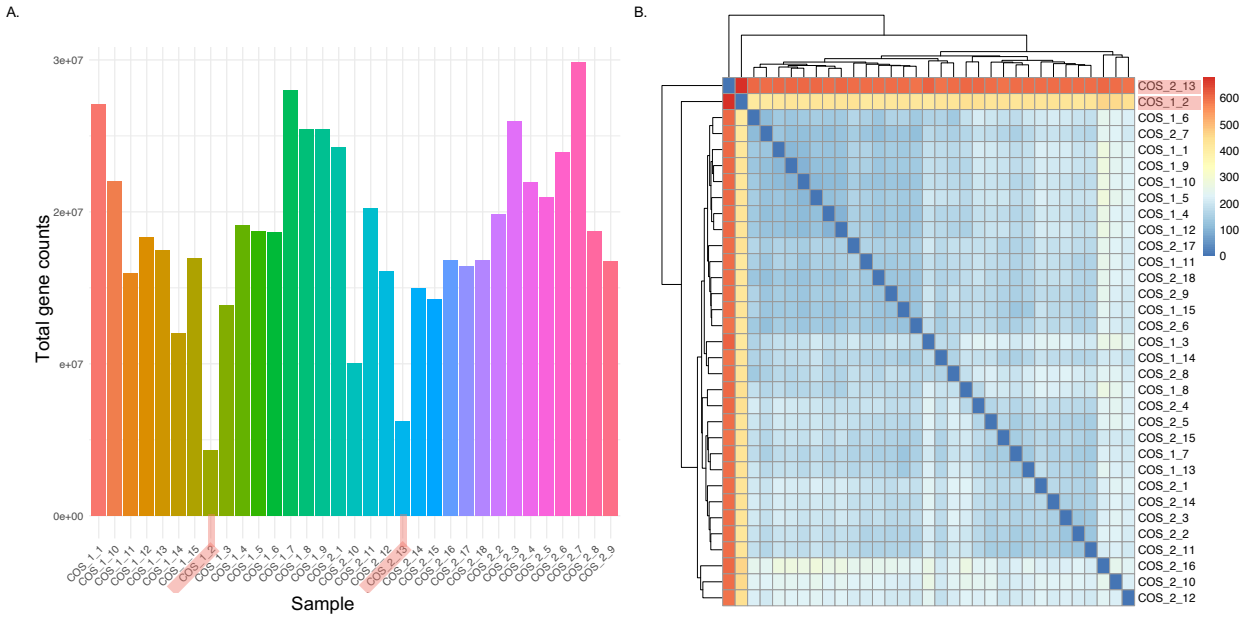


**Supplementary Figure S3. 1. Quality control assessment of the RNA-sequencing data from blastocysts.**

**(a)** Bar graph showing the total gene counts per sample after alignment. Note the two samples, one from each COS, with a reduced number of total genes highlighted in pink. **(b)** A Euclidean distance clustering map demonstrated that these two outliers clustered together and were different from the other samples in the analysis and likely contaminated with DNA.

1931 **Chapter 4:**

1932 **Long-Term Hyperandrogenemia and/or Western-Style Diet Impairs Rhesus**

1933 **Macaque Preimplantation Embryo Development**

1934 Sweta Ravisankar[1,2], Melinda J. Murphy[2], Nash Redmayne-Titley[2], Brett Davis[3],

1935 Cadence A. True[2,4], Jon D. Hennebold[2,5*], Shawn L. Chavez[2,5,6*]

1936

1937

1938 [1]Department of Cell, Developmental & Cancer Biology; Graduate Program in Molecular

1939 & Cellular Biosciences; Oregon Health & Science University School of Medicine;

1940 Portland, Oregon

1941 [2]Division of Reproductive & Developmental Sciences; Oregon National Primate Research

1942 Center; Beaverton, Oregon

1943 [3]Knight Cardiovascular Institute; Oregon Health & Science University, Portland, Oregon

1944 [4]Division of Cardiometabolic Health, Oregon National Primate Research Center;

1945 Beaverton, Oregon

1946 [5]Department of Obstetrics & Gynecology; Oregon Health & Science University School of

1947 Medicine; Portland, Oregon

1948 [6]Department of Molecular & Medical Genetics; Oregon Health & Science University

1949 School of Medicine; Portland, Oregon

1950

1951 *Corresponding authors: henneboj@ohsu.edu and chavesh@ohsu.edu

**Abstract**

Both hyperandrogenemia and obesity are common in polycystic ovary syndrome (PCOS), which is a leading cause of infertility among women worldwide. It is currently unclear, however, the effects hyperandrogenemia and/or diet/obesity have on development of the disease and its progression. Thus, we established a nonhuman primate model of prepubertal rhesus macaque females (~2.5 years of age) received a standard low-fat chow diet (control; C) or were treated with testosterone alone (T), a Western-style diet (WSD), or received the combination of T+WSD. Treatments continued over 5-6 yrs until 7-8 yrs of age wherein the animals underwent controlled ovarian stimulations to stimulate the growth of multiple follicles from which follicular fluid (FF) and oocytes were collected. Although the T+WSD females exhibited a trend (p=0.06) in higher insulin resistance compared to the control group, there were no significant differences in metabolic parameters between treatments. Significantly higher concentrations of the chemokine, CXCL10, was detected in the FF from T animals, while no significant changes in intrafollicular steroid levels were observed between groups. Oocytes underwent *in vitro* fertilization (IVF) to assess the effect of T and/or WSD treatments on oocyte maturation, fertilization, and preimplantation embryo development. A WSD with or without T significantly reduced blastocyst formation rates compared to the C and T only groups, despite yielding a higher number of mature metaphase II oocytes. Immunostaining of cleavage-stage embryos revealed micronuclei formation and the presence of DNA in cellular fragments indicative of aneuploidy in WSD and T+WSD groups, but single-cell DNA-seq and chromosomal copy number variation (CNV) analysis did not show CNV differences between groups. However, RNA-Sequencing analysis of the blastocysts

1975 indicated differential expression of genes that could impair critical preimplantation and
1976 peri-implantation processes in the T,WSD and T+WSD groups compared to the C group.
1977 Our results demonstrate that long-term consumption of a WSD reduces the capacity of
1978 fertilized oocytes to develop into blastocysts and that the addition of T has synergistic
1979 effects on preimplantation embryo development and IVF outcomes.
1980

1981 **Introduction**

1982 Elevated levels of circulating testosterone (T) and other androgens
1983 (hyperandrogenism), as well as obesity and obesity/diet-induced metabolic dysfunction, in
1984 women are associated with increased rates of infertility[314,315] and polycystic ovary
1985 syndrome (PCOS)[316-318]. PCOS affects about 5-10% of reproductive age females[192], with
1986 patients exhibiting a range of clinical symptoms based on the presence of at least two out
1987 of three features that include hyperandrogenism, oligoovulation (infrequent or irregular
1988 ovulation), and polycystic ovaries[194]. Women with PCOS exhibit a 3-4 fold increase in
1989 circulating androgens[319] and typically have metabolic issues such as insulin resistance and
1990 obesity[318,320,321]. PCOS directly affects ovarian function, leading to the noted
1991 oligoovulation or anovulation[319-321]. Qualitative and quantitative changes in intrafollicular
1992 steroid[322-328] and growth factor/cytokine[329,330] levels are frequently noted in both PCOS
1993 animal models and women with PCOS. Thus, alteration of the ovarian intrafollicular
1994 milieu[326,330-332] is likely associated with the abnormal follicle development and reduced
1995 oocyte competency detected in these studies.

1996 Although metabolic and endocrine dysfunction, as well as genetic predisposition,
1997 were reported to contribute to the etiology of PCOS[320,321,333,334], it is presently unclear how
1998 each contributes to the observed alterations in ovarian physiology. Elevated T levels in
1999 PCOS are thought to directly promote small antral follicle development and survival,
2000 giving rise to the polycystic phenotype[319,335,336]. However, obesity and metabolic
2001 dysfunction associated with PCOS have also been implicated in directly contributing to the
2002 ovarian phenotype. Reduced oocyte quality, chromosomal abnormalities, and diminished
2003 capacity of oocytes to fertilize and develop into blastocysts were also observed after

2004 consumption of an obesogenic high-fat diet[259,337,338]. Of the metabolic parameters, insulin
2005 resistance observed in PCOS animal models and patients is hypothesized to be the major
2006 contributor to reduced oocyte competency[333,334,339]. It is unclear, however, how diet or diet-
2007 associated changes in metabolic function and hyperandrogenemia each contribute to
2008 aberrant ovarian physiology and thus, female subfertility or infertility.

2009 To define the individual contributions of diet and hyperandrogenemia alone or in
2010 combination on altered ovarian function, studies were initiated wherein rhesus macaque
2011 females received a standard low-fat chow diet (controls; C) or a high-fat Western-style diet
2012 (WSD) in the absence or presence of T implants[311]. All treatments, including C, WSD, T,
2013 T+WSD, were initiated just prior to the onset of puberty to coincide with the stage at which
2014 PCOS symptoms typically emerge in women. T implants resulted in an increase circulating
2015 T levels by 3 to 5-fold[340], which is well below the concentration detected in males. Body
2016 weight and fat mass gain were significantly increased, as was insulin resistance, in the
2017 T+WSD group at 2-3 years after the initiation of treatments[186]. At 3 years post-treatment,
2018 animals in the T and the T+WSD groups exhibited a PCOS like morphology[190,309,311] as
2019 determined by the presence of small antral follicles (SAF) in the periphery of the ovary[311].
2020 Other effects on ovarian function included significantly reduced circulating progesterone
2021 (P4) levels during the luteal phase in the T+WSD group. Relative to controls, the animals
2022 also had reduced blood flow and blood volume in the corpus luteum, demonstrating that T
2023 and WSD diminish luteal vascular function[311]. The treatments also had an effect on the
2024 uterine environment, whereby endometrial blood vessel formation was impaired in the T
2025 and WSD groups and uterine decidualization in T±WSD treatment groups were reduced[311].
2026 Fertility trials conducted beginning at 3 yrs of treatment revealed that WSD treatment

2027 caused a delay in the time to pregnancy, while the T+WSD treatment was associated with
2028 reduced pregnancies[309].

2029 After 3.5 years of treatment, the females underwent a controlled ovulation (COv)
2030 cycle and a significantly increased the number of degenerated oocytes were aspirated from
2031 the naturally selected follicle in T, WSD, and T+WSD groups[218]. Treatment specific
2032 changes in follicular fluid (FF) steroids (cortisol) and cytokines/growth factors (CC
2033 chemokine ligand -2 and -11; fibroblast growth factor 2) were also observed. Moreover,
2034 metaphase II (MII) oocytes obtained from the WSD group often underwent abnormal
2035 multipolar divisions after *in vitro* fertilization (IVF)[218]. Although these findings indicate
2036 that there are direct T and/or WSD effects on the single ovulatory follicle and the
2037 competency of the resident oocyte, it was not possible to obtain sufficient numbers of
2038 oocytes to assess effects on maturation, fertilization, and embryonic development. In this
2039 study, ovarian stimulation cycles were utilized to generate multiple follicles from which
2040 the impact of long-term (5 to 6 years) hyperandrogenemia, WSD consumption, or the
2041 combination of WSD and hyperandrogenemia on the oocyte pre- and post-IVF could be
2042 quantified. The COS protocol used in this study is analogous to that used in women
2043 undergoing infertility treatments[84], which along with the shared reproductive physiology
2044 between rhesus macaques and humans[197,272], provides insight into how hyperandrogenemia
2045 and WSD consumption, by themselves and in combination, impact infertility treatment
2046 outcomes. Our results demonstrate that WSD intake reduces oocyte competency and
2047 impacts subsequent preimplantation embryo development, which is further worsened by
2048 hyperandrogenemia.
2049

2050 **Materials and Methods**

2051 *Animal treatment groups and metabolic measurements*

2052 All protocols involving animals were approved by the Oregon National Primate
2053 Research Center (ONPRC) Institutional Animal Care and Use Committee and conducted
2054 in accordance with the National Institutes of Health Guidelines for the Care and Use of
2055 Laboratory Animals. The housing and general care of rhesus macaques (*Macaca mulatta*)
2056 was previously described[144]. At the onset of the study, a cohort of 40 female rhesus
2057 macaques were equally divided into 4 treatment groups (N=10/group) at ~2.5 yrs of age
2058 just prior to puberty, including control (C), testosterone (T), Western-style diet (WSD),
2059 and T+WSD, as described previously[218]. Control animals consumed a standard chow diet
2060 (SCD: 15% fat, 59% carbohydrate, 26% protein) and received cholesterol implants.
2061 Females in the T group received T implants to increase and maintain their circulating blood
2062 T levels up to 3-5 times the normal circulating T concentration. The WSD group was fed
2063 an obesogenic high-fat diet (36% fat, 46% carbohydrate, 18% protein). All 10 C underwent
2064 COS protocols, but only 7 T, 6 WSD, and 3 T+WSD animals were available to undergo a
2065 COS protocol after 5 to 6 yrs of treatment due to health issues that prevented further
2066 reproductive testing.

2067 Weight, body mass index (BMI), body fat percentage, and HOMA-IR were
2068 measured after 5 yrs of their respective treatments as previously described[186]. In brief, body
2069 fat percentage for each animal was measured using dual-energy X-ray absorptiometry
2070 (DEXA; Hologic QDR Discovery A; Hologic, Inc.). Fasting insulin and glucose levels
2071 were obtained to determine HOMA-IR values (fasting insulin x fasting glucose/405) as

2072 previously described[186]. Animal weight and crown-rump (CR) length was measured and
2073 used to calculate BMI (BMI= weight/CR*CR).
2074
2075 *Controlled ovarian stimulations (COS) and follicle aspiration*
2076 COS protocols were performed as previously published[84]. Briefly, exogenous
2077 gonadotropins were administered to stimulate the development of multiple ovarian
2078 follicles. Female rhesus macaques were anesthetized for laparoscopic follicular aspirations
2079 36 hours (hr) after a bolus of human chorionic gonadotropin (hCG) was administered to
2080 induce events necessary for the re-initiation of meiosis. Two individual follicle aspirates
2081 per ovary (N=4 per animal) were collected manually with a low dead space 3ml syringe
2082 with a 22-gauge X 1.5inch needle (Ulticare, UltaMed Inc., Excelsior, MN). Individual
2083 follicle aspirates were centrifuged to separate the follicular fluid (FF) from the COCs and
2084 the granulosa cells (GCs). The FF and GCs were stored at -80°C until analysis and the
2085 oocytes from the individual aspirates were denuded from the surrounding cumulus cells
2086 (CCs) in the COC by pipetting. The remaining follicles were aspirated in bulk using a
2087 needle connected to a vacuum system. Bulk aspirated COCs were collected in Tyrode's
2088 albumin lactate in pyruvate (TALP)-HEPES medium with 0.3% bovine serum albumin
2089 (BSA; Sigma-Aldrich, St. Louis, MO) and 1% Heparin sodium salt solution at 37$^{o}$C.
2090 Oocytes from the bulk aspirates were denuded by gentle micropipeting in TALP-HEPES
2091 medium containing 0.3% BSA and 3% hyaluronidase (Sigma-Aldrich). Each oocyte's
2092 developmental stage was recorded and categorized as either immature germinal vesicle
2093 (GV), metaphase I (MI), metaphase MII (MII), or degenerated. Individual oocytes were

2094 placed in pre-equilibrated 100 μL TALP complete drops in a 10 well IVF dish (LifeGlobal,
2095 Guildford, CT).
2096
2097 *FF cytokine and steroid analyses*
2098 FF samples obtained from the individual follicular aspirates of each female were
2099 pooled and used for the analysis of 29 cytokines and 7 steroids by the Endocrine
2100 Technologies Core (ETC) at ONPRC. The number of samples analyzed for steroid analysis
2101 included: N=10 C, N=5 T, N=6 WSD, and N=3 T+WSD. For cytokine analysis, there were
2102 N=9 C, N=4 T, N=4 WSD, and no T+WSD samples because only 1 female from that group
2103 had sufficient volume for testing. Steroid hormone analysis was performed by liquid
2104 chromatography-tandem mass spectrometry (LC-MS/MS) on a Shimadzu Nexera-LCMS-
2105 8050 using a previously described method[218]. Accuracies for the steroid hormone assays
2106 ranged from 87.3%-108.5% and intra-assay coefficient of variation (CV) were <11%.
2107 Cytokine levels were determined in the ETC using a monkey 29-plex cytokine panel
2108 (Thermo Fisher, Waltham, MA) following the manufacturer's instructions. Concentrations
2109 of each cytokine were calculated from a standard control curve. Samples were analyzed on
2110 a Milliplex Analyzer (EMD Millipore, Billerica, MA) with XPonent Software version 3.1
2111 (Luminex, Austin, TX). Data were calculated using Milliplex Analyst software version 5.1
2112 (EMD Millipore, Billerica, MA). All samples were analyzed on a single run and the intra-
2113 assay CVs for all analytes were <20%. The list of the cytokines and steroids analyzed with
2114 their CVs and accuracies are included **Supplementary Table S4. 1 and S4. 2 respectively.**
2115

2116 *IVF and preimplantation embryo development*

2117 Fresh semen from four adult male rhesus monkeys (aged 10-13 yrs old) that were
2118 proven breeders was used for IVF throughout this project. The semen was obtained on the
2119 same day as IVF, and the sperm were prepared as previously described[216] for use at a final
2120 concentration of $2x10^6$ sperm/ml in TALP-Complete medium. IVF was performed the
2121 evening of the collection as previously described[216]. In brief, the sperm sample was treated
2122 with cyclic adenosine monophosphate (cAMP; 5 mg/ml) and caffeine (2 mg/ml) 15 min
2123 before fertilization to induce hyperactivation. Activated sperm (1µl) were added to each
2124 well. The IVF dishes were incubated at 5% $CO_2$ at 37ºC for 14-16 hr. Any remaining sperm
2125 were removed from fertilized oocytes (i.e. presence of two pronuclei and/or two polar
2126 bodies) by pipetting. Zygotes (N=12) were randomly selected and transferred to custom
2127 Eeva™ 12-well polystyrene petri dishes (Progyny, Inc., San Francisco, CA) containing
2128 100 µl of preequilibrated culture medium (IVF Bioscience, UK, BO-IVC) under mineral
2129 oil (Sage™, Trumbull, CT) for time-lapse monitoring (TLM) at 37°C with 6% $CO_2$, 5%
2130 $O_2$. The remaining zygotes were transferred to a 10-well IVF dish (LifeGlobal, Guildford,
2131 CT) and cultured in the same media as the TLM dish. Media was changed at day 3 post-
2132 IVF and the embryos were allowed to develop up to day 8. The maturation, fertilization,
2133 cleavage and percentage of blastocysts formed were calculated as follows: percentage of
2134 mature oocytes = (number of mature metaphase MII (MII) oocytes/total number of
2135 oocytes) *100, percentage of fertilized oocytes = (number of zygotes formed post-
2136 IVF/number of mature MII oocytes) *100, and percentage of blastocysts formed= (number
2137 of blastocysts formed/number of cleaved embryos) *100.

2138

2139 *Time-lapse imaging and assessment of initial mitotic divisions*

2140 Monitoring embryo division kinetics using the Eeva™ darkfield 2.2.1 time-lapse
2141 microscope system was performed as previously described[313]. Embryos were imaged every
2142 5 min. with a 0.6 second (sec) exposure time up to 8 days until they developed into
2143 blastocysts. Each image was time stamped with a frame number and all images compiled
2144 into an AVI movie using FIJI software version 2.0.0 (NIH, Bethesda, MD). The time
2145 intervals between the appearance of the 1$^{st}$ cleavage furrow to the end of the 1$^{st}$ cytokinesis,
2146 the beginning of the 2$^{nd}$ mitotic division, and the start of the 3$^{rd}$ mitotic division for 296
2147 embryos were manually determined by four independent observers and represented as an
2148 average. Cellular fragmentation and asymmetrical/multipolar division were also recorded
2149 for each embryo.

2150

2151 *Fluorescence-based detection of nuclear integrity in cleavage-stage embryos*

2152 Cleavage-stage embryos that underwent cellular fragmentation and/or multipolar
2153 divisions indicative of chromosomal abnormalities during TLM[341,342] were collected at the
2154 6-11 cell stage for immunostaining since they would likely arrest prior to the blastocyst
2155 stage . Removal of the zona pellucida (ZP) was accomplished by incubating the embryos
2156 in EmbryoMax Acidic Tyrode's Solution (EMD Millipore, Burlington MA) for ~30 sec.
2157 The embryos were washed in 0.1% BSA (Sigma-Aldrich) plus 0.1% Tween 20 (Sigma-
2158 Aldrich, St. Louis, MO; PBS-T) and fixed by incubation in cold 4% PFA in PBS for 20
2159 min. at room temperature (RT). Embryos were washed with PBS-T for 30 min at RT to
2160 remove any fixative and permeabilized in 1% Triton-X (Calbiochem; Burlington, MA).
2161 Non-specific binding sites were blocked by incubation in 4% donkey serum (Jackson
2162 ImmunoResearch Laboratories, Inc.; West Grove, PA) for 30 min at RT. Embryos were

2163 incubated with a primary antibody (Abcam, Cambridge, MA, catalog# ab16048, rabbit
2164 monoclonal, RRID: AB_443298, 1:100 in PBS-T) recognizing LAMIN-B1 (LMNB1;
2165 nuclear envelope marker) as previously reported[341]. LMNB1 antibody binding was
2166 detected by incubating samples with a donkey anti-rabbit secondary antibody conjugated
2167 with Alexa Fluor 488 (Thermo Fisher, Waltham, MA, A-21206, RRID: AB_2535792,
2168 1:100) for 2 hr at RT. All antibodies were diluted in PBS-T + 1% donkey serum. DNA was
2169 stained with 1 µg/ml DAPI (Thermo Fisher, Waltham, MA, D1306, RRID: AB_2629482,
2170 1:1000) for 10 min. In between each step, the embryos were washed with PBS-T three
2171 times for 5 min. each. Embryos were transferred to glass bottom petri-dishes (Mattek;
2172 Ashland, MA) and LMNB1 immunolocalization was visualized on a Leica SP5 AOBS
2173 spectral confocal system using the 10x and 20 x objective. Z-stacks 1-5 µM apart were
2174 imaged sequentially to avoid spectral overlap between channels.
2175
2176 *Multiplex DNA-sequencing and copy number variation (CNV) analyses*
2177 Another cohort of cleavage-stage embryos undergoing TLM were collected at the
2178 3-9 cell stage on day 2 to 3 of preimplantation development for DNA-seq analysis. The ZP
2179 was removed as described above and the embryos were disassembled into single
2180 blastomeres and cellular fragments if present by incubating in Quinn's advantage $Ca^{2+}$ and
2181 $Mg^{2+}$-free medium with HEPES plus 10% human albumin (CooperSurgical) and 0.05%
2182 trypsin-EDTA (Thermo Fisher Scientific, Waltham, MA) if necessary with gentle pipetting
2183 as previously reported[341]. Each sample was washed with $Ca^{2+}$ and $Mg^{2+}$-free PBS and
2184 collected individually for transfer to a sterile Ultraflux™ PCR tube (VWR, Radnor, PA).
2185 Single blastomeres or fragments (N=88) belonging to 16 cleavage-stage embryos from the
2186 C (N=40 blastomeres; 7 embryos), T (N=21 blastomeres; 3 embryos), WSD (N=19

2187 blastomeres; 4 embryos), T+WSD (N=8 blastomeres; 2 embryos) groups were processed
2188 for DNA isolation, amplification, and library construction (Takara Bio-SMARTer®
2189 PicoPLEX® DNA-seq Kit, Shiga, Japan) as per the manufacturer's instructions. Libraries
2190 were quantified using the Qubit high sensitivity (HS) DNA assay (Life Technologies) and
2191 validated for sequencing by PCR amplification of the adapter sequence. Only libraries with
2192 DNA quantities greater than the no-template controls were included in sequencing. 50 ng
2193 of DNA was prepared from each blastomere or euploid fibroblast, which served as a
2194 positive control for CNV analysis, and 25 ng from cellular fragments as previously
2195 described[341]. DNA from pooled libraries was purified and concentrated using a MagBead
2196 kit (Zymo Research, Irvine, CA) and re-quantified by the Qubit HS DNA kit. Pooled
2197 multiplexed libraries were loaded at 1.6 pM and sequenced on the NextSeq 500 platform
2198 using a 75 cycle single-end protocol (Illumina, San Diego, CA).

2199 Quality of sequencing reads was assessed with FastqC (v 0.11.8), and low-quality
2200 bases and adapters were trimmed with Trimmomatic (v 0.39). Trimmed reads were
2201 deduplicated with fastqx collapser from FASTX Toolkit (v 0.0.14). Mapping to the rhesus
2202 reference genome (Mmul_8) was performed with bwa mem (v 0.7.17) with the "-M"
2203 parameter specified to mark shorter split hits as secondary. CNV was determined by
2204 integrating a bioinformatics pipeline called VNOWC and the previously published
2205 pipeline, CHI[343,341]. The VNOWC pipeline generates variable-sized windows with a
2206 constant number of expected reads per window and uses Circular Binary Segmentation
2207 (CBS) to identify putative copy number changes between windows across each
2208 chromosome[344]. To correct for GC bias across the genome, we also implemented the CHI
2209 pipeline, which uses the Hidden Markov Model (HMM)[345] based on parameters determined

2210 previously[346]. We used 4000 reads per window size as this was shown to yield accurate
2211 CNV calling[341].
2212
2213 *RNA-Sequencing of blastocysts*
2214 Blastocysts were collected from all the 4 treatment groups and incubated in
2215 EmbryoMax Acidic Tyrode's Solution (EMD Millipore, Burlington MA) for ~30 seconds
2216 for removal of the zona pellucida. These zona free blastocysts were then washed with PBS
2217 and frozen at -80ºC until RNA isolation. To analyze the effects of treatment without adding
2218 any confounding preimplantation morphologies, 38 blastocysts that did not exhibit
2219 fragmentation or multipolar divisions were chosen for RNA-Seq analysis (N=12 C, N=12
2220 T, N=10 WSD, and N=4 T+WSD). RNA was extracted from the blastocysts using the
2221 ARCTURUS PicoPure RNA Isolation Kit (ThermoFisher Scientific KIT0204, Waltham,
2222 MA), cDNA prepared using the SMART-Seq v4 Ultra Low Input RNA Kit for sequencing
2223 (TakaraBio, Shiga, Japan) and the amplified cDNA was purified using the Agencourt
2224 AMPure XP Kit (Beckman Coulter, Brea, CA), all according to manufacturer's
2225 instructions. cDNA was then sheared to approximately 250 base pairs in length using a
2226 Covaris M220 sonicator. Sheared cDNA was resuspended in Tru-Seq Resuspension
2227 Buffer and libraries prepared using a Tru-Seq Nano kit (Illumina, San Diego, CA)
2228 according to the manufacturer's instructions, except that 16 cycles of amplification were
2229 performed to account for the low input samples. Fragment size was measured using a
2230 Fragment Analyzer 5200 and samples quantified with qPCR and pooled at equimolar
2231 concentration. Multiplexed samples were sequenced across seven lanes of a single-read,
2232 75 cycle run on an Illumina HiSeq 4000 sequencer. The sequencing data was demultiplexed

2233 using Illumina's bcl2fastq software and sample quality assessed with FastQC (v 0.11.8),
2234 followed by trimming of low-quality bases and adapter sequences with Trimmomatic (v
2235 0.39). Trimmed sequences were aligned via STAR (version 2.7.0) to the most recent rhesus
2236 macaque reference genome from Ensembl (Mmul_10) and gene counts obtained by
2237 specifying the "--quantMode GeneCounts" parameter of STAR, along with the
2238 Mmul_10.99 Ensembl annotation gtf file. Out of the total number of blastocyst samples
2239 that underwent RNAseq, those that had more than 10 million total gene counts were
2240 retained for differential analysis (N=25 ; N= 5 C, N=10 T, N=8 WSD, and N=2 T+WSD).
2241 Differential expression between groups was performed with edgeR (version 0.28.0) using
2242 the "QLFTest" option. The Enrichr and G-profiler online tools were used for molecular
2243 pathway and gene ontology assessment.
2244
2245 *Statistical analysis*
2246 An ANOVA Type III test was performed for assessing the significance of the
2247 metabolic parameters among the treatment groups. In addition, one-way ANOVA and a
2248 post-hoc t-test comparison with Bonferroni adjustment was performed to test for
2249 significance of HOMA-IR. Significance differences in FF levels of steroids and cytokines
2250 were assessed by one-way ANOVA and a post-hoc t-test comparison with Bonferroni
2251 adjustment. Statistical analyses of oocyte number, percentage of mature oocytes,
2252 fertilization rate, and percentage of cleaved embryos among the treatment groups was
2253 conducted using a chi-square test followed by post-hoc pair-wise comparisons. Poisson
2254 regression was used to model the number of blastocysts. More specifically, a generalization
2255 of Poisson regression, Negative Binomial regression was used to accommodate over-

2256 dispersion followed by the three degree-of-freedom chi-square test for blastocyst numbers
2257 and formation rates. For the TLM analysis, a linear mixed effects model was used followed
2258 by the three degree-of-freedom chi-square test for differences in the initial three mitotic
2259 division timings between the treatment groups.
2260
2261 **Results**
2262 *Chronic exposure to T+WSD produces a trend in increased insulin resistance*
2263 The metabolic profile of the female rhesus macaques in each of the four treatment
2264 groups was determined prior to undergoing a COS protocol. At this point, the females had
2265 been on their treatment regimen for 5 yrs and their weight **(Fig. 4. 1a)**, BMI **(Fig. 4. 1b)**,
2266 total percent body fat (**Fig. 4. 1c**), and HOMA-IR **(Fig. 4. 1d**) were measured and assessed
2267 for significant differences between groups. Despite previously reported gains in body
2268 weight and fat mass in the T+WSD group at 2-3 years of treatment[186], no significant
2269 differences in body condition and metabolic parameters were observed between the
2270 treatment groups, which may be due to the *ad libitum* diet conditions over-time even in the
2271 controls. A higher trend in insulin resistance was detected in the T+WSD group when
2272 compared to the other treatments, but this was not statistically significant (p=0.06).
2273
2274 *The FF chemokine milieu is altered by T treatment*

To determine if the treatments affected the ovarian follicular milieu, FF samples obtained at the time of oocyte retrieval were examined for cytokine and steroid levels. Out of the 7 steroids analyzed (**Supplementary Table S4. 2**), none significantly differed between the four treatment groups. However, of the 29 cytokines analyzed (**Supplementary Table S4. 1**), a nearly 10-fold increase ($p<0.05$) in FF levels of the chemokine C-X-C motif ligand 10 (CXCL10) was observed in the T group relative to C and WSD groups (**Fig. 4. 2,** $p<0.05$). In fact, while all FF samples from the T group had measurable levels of CXCL10, the CXCL10 concentration was below the detectable limits

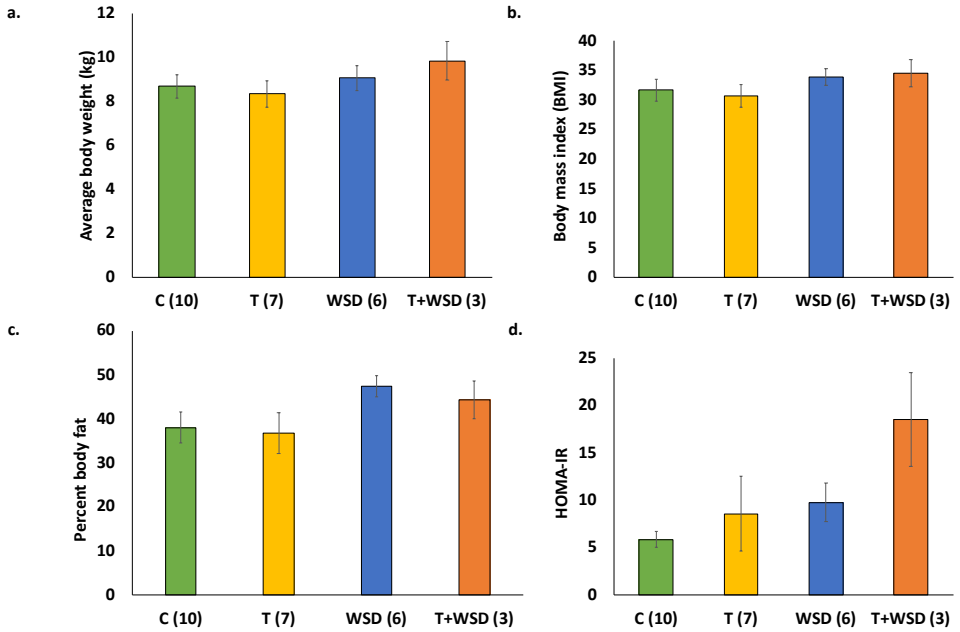


**Figure 4. 1. Weight, body mass index (BMI), percent body fat, and insulin resistance in female rhesus macaques receiving a standard chow diet (control, C; N=10), testosterone (T; N=7), a western-style diet (WSD; N=6), or a combination of T+WSD (N=3) for 5 yrs.** Treatments were initiated prior to the onset of puberty at ~2.5 yrs. The physical and metabolic parameters (mean±SEM) analyzed include **(a)** weight, **(b)** BMI, **(c)** percent body fat, and **(d)** insulin resistance (HOMA-IR) as determined by HOMA. There was no significant difference in the physical and metabolic parameters among the treatment groups, although HOMA-IR trended higher in the T+WSD females compared to the C group females ($p=0.06$).

2283 in all WSD samples and all but one sample in the C group. Because of limitations in the
2284 minimal volume required for analysis, cytokine levels were not determined in the T+WSD
2285 samples due to insufficient FF quantity, which we demonstrated is indicative of reduced
2286 oocyte competency (Ravisankar *et al*. submitted – Chapter 2).

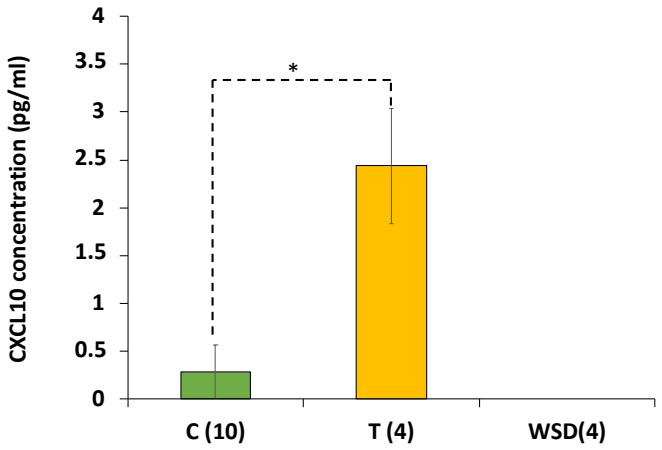


2287

**Figure 4. 2. Effect of T and WSD treatment on the FF cytokine milieu.**
Follicular fluid samples were collected from all the treatment groups and analyzed for 29 cytokines (**Supplementary Table S1**) using a luminex-29 plex platform. The cytokine C-X-C motif chemokine 10 (CXCL10) was not detectable in the FFs from the WSD group and in all but one FF sample in the C group. The mean concentration (± S.E.M.) was significantly higher in FF from T treated animals when compared to FF from the C group. Only 1 female from the T+WSD group had sufficient volume for the cytokine analysis and, therefore, was not included in the analysis. The number of FF samples that were analyzed for each group are in parentheses on the x-axis. Statistical significance was calculated by one-way ANOVA followed by a post-hoc comparison with Bonferroni adjustment (*=$p<0.05$).

2288

2289

2290 *WSD is associated with poor preimplantation development outcomes*

2291 To understand the effect of hyperandrogenemia alone or in combination with
2292 consumption of a WSD, oocyte maturation as well as post-IVF development of each
2293 embryo was assessed. The average number of mature MII oocytes per female, though not
2294 statistically significant, varied amongst the treatment groups with the highest being in T
2295 and T+WSD groups (C=26, T=32, WSD=21, T+WSD=33). In spite of the larger number
2296 of mature oocytes obtained, embryos from the WSD and T+WSD groups yielded the fewest
2297 blastocysts per female following IVF (**Fig. 4. 3a**, $p<0.05$). The blastocyst formation rate,
2298 or the percentage of blastocysts that formed from the total number of cleaved embryos, was
2299 lowest in the T+WSD group relative to the control and WSD animals, and significantly
2300 lower than the T group (**Fig. 4. 3b**, $p<0.05$). Interestingly, the T group produced the highest
2301 number of blastocysts per female, although this was not significantly different.

2302

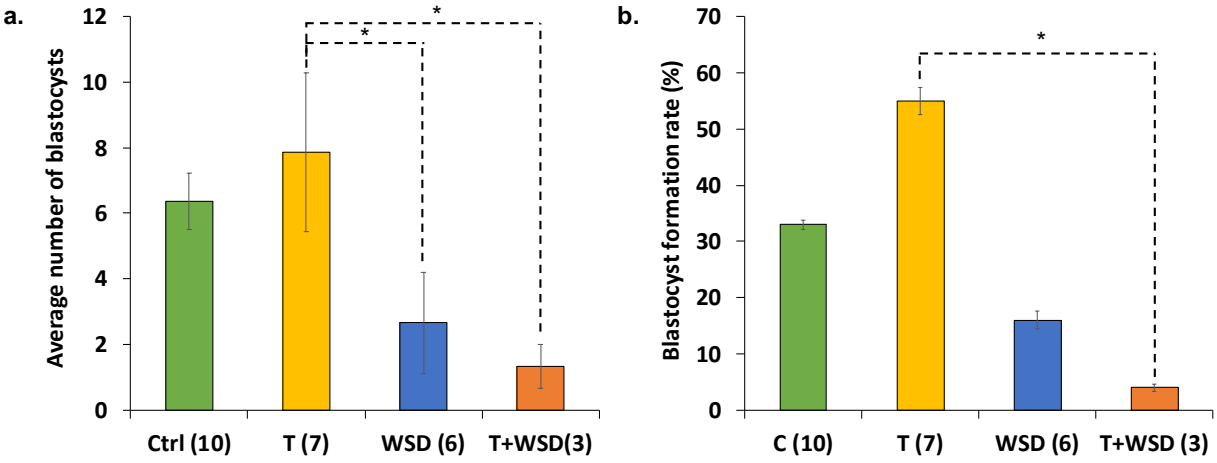


**Figure 4. 3. Preimplantation developmental outcomes after long-term WSD consumption and/or hyperandrogenemia exposure.**

**(a)** The average number of blastocysts (± S.E.M.) formed per female were reduced significantly in WSD and T+WSD groups. There was a trend for the T group to yield a greater number of blastocysts per animal relative to the T+WSD (p=0.065) or the WSD group (p=0.12). **(b)** The mean percentage of blastocysts formed (± S.E.M.) in the T+WSD group had the lowest percentage of blastocysts formed and was significantly different form the T group. The numbers in parentheses along the x-axes in (a) and (b) indicate the number of females that underwent the COS protocol in each treatment group. Poisson regression, followed by the three degree-of-freedom chi-square test for calculating the statistical significance of the blastocyst numbers and percentage of blastocysts formed among the treatment groups.

2303

2304

2305 *Nuclear integrity is compromised in T, WSD, and T+WSD embryos*

2306 The time intervals of the first three mitotic divisions predictive of blastocyst
2307 formation[277,278] were measured in 12 confirmed zygotes per animal in each treatment group
2308 by TLM. However, mitotic timing and morphological features such as multipolar divisions
2309 or cellular fragmentation were not statistically different between the four groups.
2310 Randomly selected cleavage-stage embryos from each of the four groups (2C, 3T, 4WSD,
2311 and 4T+WSD) were immunolabelled with the nuclear envelope marker, LMNB1, and
2312 stained with DAPI to visualize DNA. While some micronuclei were noted, which is typical
2313 of rhesus preimplantation development[341], embryos from the C group predominantly
2314 exhibited an intact nuclear envelope around the primary nucleus of each blastomere. (**Fig.
2315 4. 4a**). In contrast, blastomeres of cleavage-stage embryos from the T, WSD, and the
2316 T+WSD groups lacked well-defined primary nuclei and possessed not only micronuclei,
2317 but also DNA without nuclear envelope, chromosome-containing cellular fragments, and
2318 nuclear fragmentation (**Fig. 4. 4b-4d**). Although these nuclear abnormalities are suggestive
2319 of aneuploidy[341], CNV was not significantly different between embryos (N=16) collected
2320 from each of the four treatment groups (**Supplementary Fig. S1**).

2321

2322

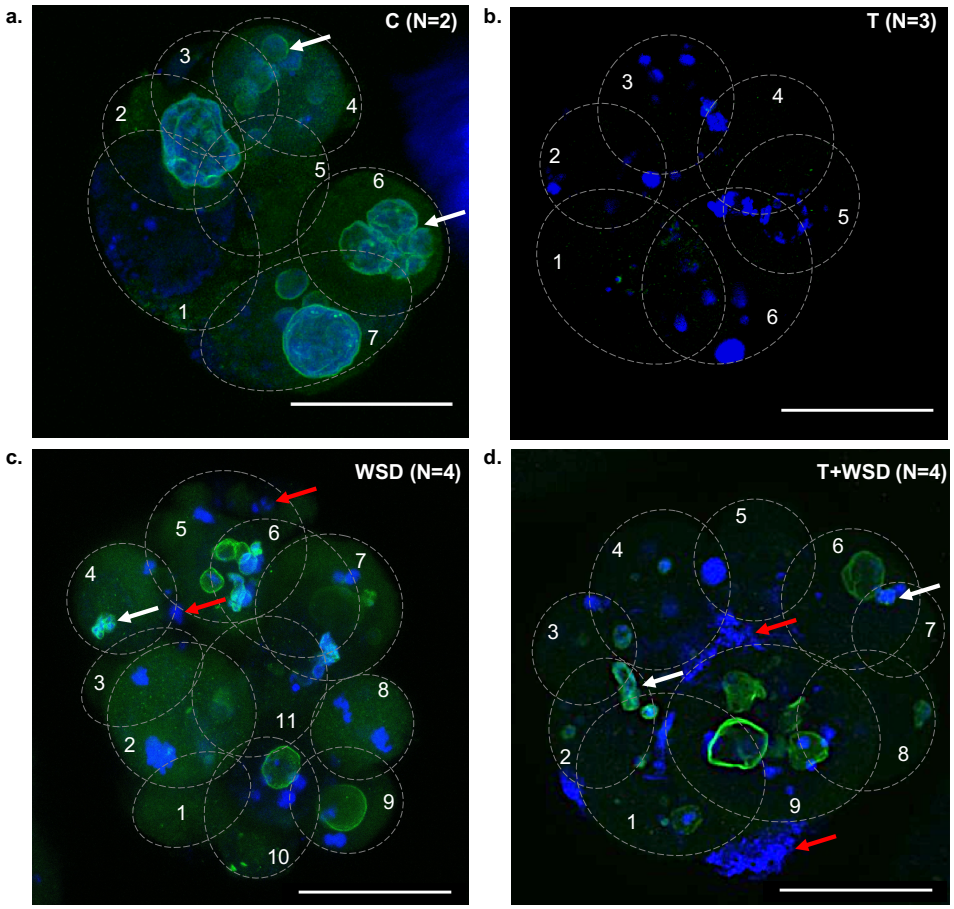


**Figure 4. 4. Fluorescence based analysis of cleavage stage embryo nuclear integrity.** Cleavage stage embryos (6-11 cells) from each group were collected when multipolar division was visualized on the TLM scope. These were stained for the nuclear envelope marker LMNB1 (green) and DNA (DAPI; blue). **(a)** The nucleus in each blastomere was enclosed by a nuclear envelope and few micronuclei were present (white arrow) in cleavage stage embryos from the control group (C; N=2). **(b)** In cleavage stage embryos from the T group (N=3), the nuclear envelope did not colocalize with DNA in the individual blastomeres. In the embryos from the WSD **(c)** and T +WSD **(d)** groups (N=4 for both), micronuclei (white arrow) and DNA fragments (red arrow) were commonly observed, which was more extensive in the T+WSD group (d). To aid in the visualization of each blastomere each cell is numbered and outlined with a gray dashed line. The white arrows indicate micronuclei formation and the red arrows indicate presence of DNA in fragments that lack a nuclear envelope (i.e., LMNB1 negative). The scale bar in all the images represents 50 µm.

2323

2324 *RNA-Seq of the blastocysts revealed common and unique treatment effects, with greatest*
2325 *effect in the T+WSD blastocysts*

2326 Out of the 38 blastocyst samples that were RNA-Sequenced, 25 samples (N= 5 C,
2327 N=10 T, N=8 WSD, and N=2 T+WSD) with sufficient number of total gene counts were
2328 retained for differential analysis (**Supplementary Fig. S4. 2**). More than 20,000
2329 differentially expressed genes were identified in the T, WSD and T+WSD blastocysts
2330 when compared to the C blastocysts, out of which we found the significantly differentially
2331 regulated genes ($p<0.05$; N= 645 T, N= 581 WSD, and N= 134 T+WSD). A set of common
2332 genes (N=18) were significantly upregulated (N=8) and downregulated (N=10) in T, WSD
2333 and T+WSD blastocysts **(Fig. 4. 5a and 4. 5b)**. The biological pathways that these common
2334 up or downregulated genes belonged to were enriched in cell cycle and DNA replication
2335 related processes (**Fig. 4. 5c**). Further, amongst these genes, the combined T+WSD
2336 treatment had the maximum effect for upregulated or downregulated gene expression (**Fig.**
2337 **4. 5d**). The genes expression was 2-4 fold upregulated and 2-14 fold downregulated in the
2338 T+WSD blastocysts when compared to T and WSD blastocysts (**Supplementary Table**
2339 **S4. 3**). Other than the 18 genes that were commonly upregulated or downregulated,
2340 majority of the genes were unique to and significantly expressed either, T, WSD or
2341 T+WSD blastocyst compared to the C blastocysts. The genes that were the most
2342 upregulated and downregulated in the treatment groups are given in **Supplementary Table**
2343 **S4. 4**. Amongst these top differentially expressed genes, the log fold change (X) was
2344 observed to be the highest in the WSD blastocysts (13.8 X downregulated to 9.6 X
2345 upregulated) followed by the T+WSD blastocysts (11.37 X downregulated to 10.79 X

2346 upregulated) . The T blastocyst gene expression has (11 X downregulated to 7 X
2347 upregulated).

2348 Gene ontology (GO) and pathway analyses were performed to identify the
2349 molecular functions most associated with T, WSD and T+WSD-induced gene upregulation
2350 and downregulation. The significantly expressed genes in the T blastocysts (adjusted p
2351 value<0.05) showed upregulation of functions associated to mitosis, cell cycle and DNA
2352 replication whereas the downregulated functions included heparin and glycosaminoglycan
2353 binding (**Supplementary Fig. S4. 3**). On the other hand, the WSD blastocyst genes were
2354 upregulated in single-stranded DNA binding, DNA replication origin binding, nucleotide
2355 binding, and ATP binding while functions associated with signaling receptor binding,
2356 growth factor binding, protein binding, heparin binding, glycosaminoglycan binding, and
2357 protein dimerization were downregulated. The combined T+WSD treatment effects on
2358 blastocyst gene expression resulted in upregulation of functions, once again associated with
2359 DNA replication origin binding, single-stranded DNA binding, and nuclear pore structural
2360 constituent, and downregulation of TNF-related apoptosis-inducing ligand (TRAIL)
2361 binding function.

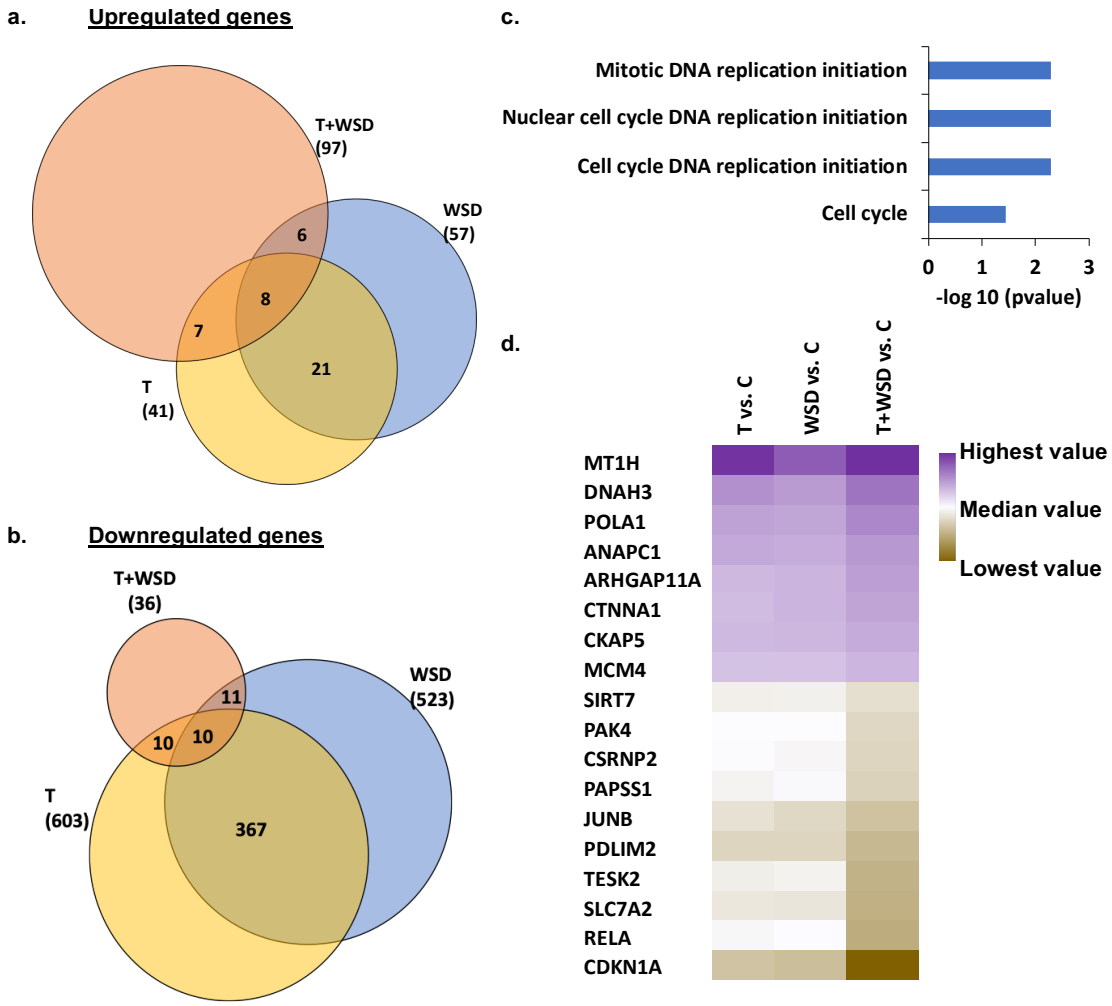


**Figure 4. 5. Common set of genes differentially regulated genes in the blastocysts identified by RNA-Sequencing.**

Out of the total number of genes that were significantly expressed (adjusted $p<0.05$), there were a few genes that were common between the T, WSD, and T+WSD blastocysts. The pie charts represent the number of genes that were **(a)** upregulated and **(b)** downregulated in their expression unique to each group as well as common between the different groups. **(c)** The top gene ontology (GO) terms for the 18 genes differentially regulated (adjusted $p<0.05$) in the blastocysts in T, WSD and, T+WSD groups compared to the C blastocysts are represented. The x-axis is the negative log of the p-value. **(d)** The heat map of the adjusted p values of these common genes is depicted. The 8 common upregulated (purple) and the 10 common downregulated (brown) genes show maximum effect in the T+WSD blastocysts when compared to the only T and only WSD blastocysts.

2362

2363 **Discussion**

2364 Using our established nonhuman primate model to distinguish the individual and
2365 combined effects of hyperandrogenemia and diet/obesity on ovarian function and fertility,
2366 we show that there was only a trend for greater insulin resistance in the T+WSD females
2367 compared to controls after 5 yrs of treatment in the present study. Unexpectedly, no
2368 significant differences in the other metabolic parameters, particularly body weight and fat
2369 mass, were detected between groups. The difference between the 2 to 3 year measurements
2370 and those conducted here may be due to the age of the females (7-8 yrs) and continued *ad*
2371 *libitum* consumption of a low-fat chow diet that allows for increased weight gain and
2372 adiposity without promoting outright insulin resistance[347-349]. Additionally, the loss of
2373 animals in the WSD and T+WSD groups due to health issues between 3 yrs and 5 yrs of
2374 treatment included those with the greatest BMI, which would likely skew the results of the
2375 remaining animals towards a healthier metabolic phenotype.

2376 Despite the lack of metabolic differences, T treatment for greater than 5 yrs did
2377 have an overt effect on ovarian follicles, as evidenced by a higher concentration the
2378 cytokine CXCL10 in FF. CXCL10 is a pro-inflammatory cytokine[350,351] with anti-
2379 angiogenic properties[352-355], both of which could contribute to poor oocyte quality[356]. A
2380 proinflammatory environment activates natural killer (NK) cells, which in turn leads to the
2381 production of CXCL10[357]. NK cells were found to be elevated in the FF of women who
2382 underwent unsuccessful IVF cycles[358]. Increased serum CXCL10 levels were also reported
2383 in lean women with PCOS and positively correlated to insulin resistance, but not with
2384 BMI[359]. The chronic inflammation observed in women with PCOS[359-361] further supports
2385 the possibility that dysregulated cytokine synthesis leads to altered ovarian function.

2386 The observations of the current study do not fully align with the results of our
2387 previous work investigating cytokine and steroid levels in FF obtained from the dominant
2388 follicle of animals in each of the different groups[218]. In this previous study, we reported
2389 separate diet and androgen effects on the cytokine and steroid milieu in the dominant
2390 follicle. The collection of mature MI/MII oocytes was associated with reduced FF levels
2391 of the chemokine C-C motif ligand (CCL)-11 in the T+WSD group and reduced CCL2 as
2392 well as fibroblast growth factor (FGF)-2 levels in T±WSD groups. A higher FF cortisol
2393 concentration was also observed in the T group compared to the C group. None of the
2394 above differences in CCL11, CCL2, FGF2, and cortisol FF levels were observed in the
2395 present study. A possible explanation for the differences detected between these two
2396 studies could be the use of ovarian stimulations in the present study, which induces the
2397 growth of multiple follicles that are heterogeneous in terms of follicle size and cellular
2398 content[84,182,183]. Additionally, 3 T, 4 WSD, and 7 T+WSD animals could not undergo
2399 further reproductive testing due to health problems, thereby reducing statistical power. We
2400 also note that the WSD and T+WSD females that were excluded from the present study
2401 had the greatest metabolic dysfunction within these cohorts.

2402 In our previous report, significantly more degenerated oocytes were collected from
2403 the single naturally selected follicle of T, WSD, and T+WSD treated animals compared to
2404 controls[218]. Since only the dominant follicle was sampled, the number of oocytes obtained
2405 were insufficient to investigate chronic T, WSD, or T+WSD treatments on oocyte
2406 maturation and post-fertilization developmental competency. Therefore, controlled ovarian
2407 stimulations were performed here to obtain sufficient oocytes for determining if continued
2408 T, WSD, and T+WSD treatments impact the oocyte-to-embryo transition. Based on our

2409 assessments of oocyte maturation, fertilization, and embryo development, we determined
2410 that long-term consumption of a WSD alone and in conjunction with hyperandrogenemia
2411 negatively affects oocyte quality. The effects of each treatment alone (i.e., T or WSD)
2412 versus the effects of the combined treatment (i.e., T+WSD) are unique, suggesting that the
2413 treatments alone or through their interactions with one another differentially alter ovarian
2414 function. For example, the oocytes isolated from the T group appeared to be smaller
2415 compared to the oocytes obtained from animals in the other groups (data not shown). Yet,
2416 we observed the highest number of blastocysts formed per female and overall blastocyst
2417 formation rates in this group. The observed effects of chronic hyperandrogenemia in our
2418 study parallels observations of previous studies that reported increased oocyte and embryo
2419 yield in women receiving moderate amounts of T or T substrates for infertility
2420 treatments[362,363]. In contrast to the T embryos, WSD consumption was associated with a
2421 reduced percentage of blastocysts formed and the T+WSD group yielded the least number
2422 of blastocysts in spite of having the highest number of mature oocytes. A similar
2423 observation in women undergoing COS protocols with PCOS was reported wherein despite
2424 the same or greater number of oocytes obtained compared to a non-PCOS control group,
2425 post-fertilization embryo development rates were lower[331,364,365]. It should be noted,
2426 however, that these studies did not consider the effect of hyperandrogenemia and diet
2427 separately. From our analysis, we observed a significant reduction in blastocyst yield from
2428 the WSD group that was worsened by T addition. Thus, it is likely that the two treatments
2429 interact in an undefined manner to exert the greatest negative effect on oocyte competency.
2430 Assessment of cleavage stage arrested embryos revealed the presence of nuclear
2431 abnormalities in each of the groups, but the incidence of this was lower within the control

2432 group. Despite the inherent baseline level of micronuclei formation previously reported in
2433 rhesus embryos[341], DNA without nuclear envelope, chromosome-containing cellular
2434 fragments, and nuclear fragmentation were more pronounced in T, WSD and T+WSD
2435 cleavage-stage embryos. However, DNA-seq of individual blastomeres from embryos
2436 within the different treatment groups did not demonstrate significant differences in
2437 aneuploidy. As previously reported with rhesus macaque embryos, the frequency of
2438 aneuploidy in healthy control animals consuming a standard chow diet is already
2439 substantial (~74%)[341]. This high aneuploidy incidence makes it challenging to detect even
2440 modest increases in aneuploidy in embryos from the different treatment groups, especially
2441 in the WSD and T+WSD groups that had the greatest attrition of animals due to health
2442 issues.

2443 RNA-Seq of the blastocysts revealed further dysfunction in critical processes as a
2444 result of the chronic T, WSD and T+WSD treatments with possible implantation and
2445 lineage commitment dysfunction. The GO analyses of the significantly expressed genes
2446 indicated that there were both combined and unique individual effects of the treatment
2447 groups on preimplantation gene expression. The functions related to DNA replication are
2448 upregulated in the T, WSD, and T+WSD blastocysts compared to the C blastocysts. The
2449 highest differentially expressed genes were observed to be involved in upregulation of
2450 apoptosis[366], microtubule functioning[367] and trophoblast differentiation[368], and
2451 downregulation of trophoblast lipid trafficking, feto-placental growth[369] and ICM integrity
2452 [370,371] pathways in the T blastocysts. In the WSD blastocysts, the biological genes
2453 associated with microtubule function and DNA replication were upregulated whereas
2454 genes critical for implantation[372-374] were downregulated. In the T+WSD blastocysts, the

2455 highest upregulated genes were associated with microtubule functioning and apoptosis[366]
2456 while the pathways associated with TRAIL binding, TNF-α signaling, mesoderm
2457 commitment, chromatin binding, and DNA methylation were significantly downregulated.
2458 These genes have been correlated to repeated implantation failure in the endometrium[375],
2459 epigenetic changes affecting the placental development[376,377], and reducing TNF-α
2460 signaling[378] leading to obesity[379], metabolic dysfunction and hyperandrogenemia[380]. It is
2461 remarkable that in spite of having the smallest cohort of females and only 2 blastocysts
2462 included for RNA-Seq differential analysis, the T+WSD treatment had the maximum effect
2463 both in terms of fold change of gene expression and the critical pathways involved in
2464 preimplantation and peri-implantation development.

2465 In summary, rhesus macaques consuming a WSD beginning just prior to the onset
2466 of puberty and continuing through adulthood (>5 yrs) has a detrimental effect on the ability
2467 of resident oocytes to undergo preimplantation development. The WSD effect is worsened
2468 in rhesus macaques when combined with hyperandrogenemia (T+WSD). Future studies
2469 are needed to understand the molecular effects of WSD and/or T treatment on
2470 preimplantation development, including analyses of how they alter gene expression and
2471 the epigenetic state of the oocyte and embryo.

2472

2473 **Acknowledgements**

2474 We thank the Division of Comparative Medicine and NHP Core for their animal
2475 care and research support, the Surgical Services Unit for their follicular aspiration
2476 expertise, the Endocrine Technologies Core for performing the cytokine and steroid
2477 analysis assays, the Bioinformatics and Biostatistics Core for providing help with statistical

2478 analysis, and the Imaging and Morphology Core for confocal microscopy all under the
2479 auspices of the NIH/OD ONPRC core grant (P51 OD011092). We thank Jimi L.
2480 Rosenkrantz for her assistance with the DNA-sequencing. This work was supported by
2481 NIH/NICHD NCTRI grant P50 HD071836 (Project II, JDH and SLC) and NIH/OD
2482 ONPRC grant P51 OD011092.

2483

2484 **Author contributions**

2485 SR, SLC, and JDH designed the study, performed experiments, analyzed data, and
2486 wrote the manuscript. MJM and NR were two independent observers for the TLM videos.
2487 MJM also helped coordinate and schedule COS cycles. BD performed the initial data
2488 analysis for DNA-sequencing. CAT collected the data for the metabolic parameters. All
2489 authors were involved in editing the manuscript.

2490

2491 **Supplementary Table S4. 1.** Assay metrics for the cytokine analysis (Luminex 29-plex)

| Target Cytokine | Intra-Assay CV (%) |
|---|---|
| FGF-basic | 8.88 |
| IL-1beta | 5.13 |
| G-CSF | 3.51 |
| IL-10 | 11.76 |
| IL-6 | 10.42 |
| IL-12 | 6.53 |
| RANTES | 3.36 |
| Eotaxin | 18.67 |
| IL-17A | 4.62 |
| MIP-1alpha | 6.79 |
| GM-CSF | 20.16 |
| MIP-1beta | 7.04 |
| MCP-1 | 9.15 |
| IL-15 | 9.57 |
| EGF | 4.37 |
| IL-5 | 0.00 |
| HGF | 13.17 |
| VEGF | 6.43 |
| IFN-γ | 7.85 |
| MDC/CCL22 | 4.82 |
| I-TAC | 19.99 |
| MIF | 1.77 |
| IL-1RA | 5.80 |
| TNF-a | 3.55 |
| IL-2 | 18.32 |
| CXCL10 | 6.06 |
| MIG | 7.42 |
| IL-4 | 3.64 |
| IL-8 | 5.12 |

2492
2493

2494 **Supplementary Table S4. 2.** Assay metrics for the steroid analysis (LC-MS/MS)

| Steroid Hormone | Accuracy (%) | Intra-assay CV (%) |
|---|---|---|
| Cortisol | 94.9 | 2.6 |
| Cortisone | 89.3 | 3.4 |
| Testosterone | 108.5 | 8.4 |
| Estradiol | 85.0 | 1.1 |
| Estrone | 85.0 | 1.7 |
| Progesterone | 106.7 | 7.3 |
| Androstenedione | 87.3 | 10.6 |

2495

2496 **Supplementary Table S4. 3.** Log fold change of the genes upregulated or downregulated
2497 in T, WSD, as well as T+WSD group.

| Log fold change | | | |
|---|---|---|---|
| **Genes** | **T Vs. C** | **WSD Vs. C** | **T+WSD Vs. C** |
| **Upregulated genes** | | | |
| MT1H | 6.26 | 4.68 | 6.37 |
| DNAH3 | 2.67 | 2.27 | 3.80 |
| POLA1 | 2.04 | 1.89 | 3.01 |
| ANAPC1 | 1.72 | 1.59 | 2.39 |
| ARHGAP11A | 1.14 | 1.26 | 2.13 |
| CTNNA1 | 1.02 | 1.26 | 1.90 |
| CKAP5 | 1.11 | 1.18 | 1.66 |
| MCM4 | 0.75 | 0.79 | 1.20 |
| **Downregulated genes** | | | |
| SIRT7 | -2.14 | -2.11 | -2.97 |
| PAK4 | -1.49 | -1.48 | -3.40 |
| CSRNP2 | -1.52 | -1.82 | -3.52 |
| PAPSS1 | -1.94 | -1.67 | -3.67 |
| JUNB | -2.87 | -3.38 | -4.50 |
| PDLIM2 | -3.49 | -3.53 | -5.00 |
| TESK2 | -2.23 | -2.01 | -5.33 |
| SLC7A2 | -2.57 | -2.69 | -5.44 |
| RELA | -1.75 | -1.46 | -5.62 |
| CDKN1A | -4.43 | -4.69 | -9.64 |

2498
2499

2500 **Supplementary Table S4. 4.** The top upregulated and downregulated genes in T, WSD
2501 and T+WSD blastocysts when compared to C blastocysts.

| **Upregulated genes** | | | | |
|---|---|---|---|---|
| Gene ID | Log fold change | Adjusted p value | External gene name | Gene biotype |
| **T vs. C** | | | | |
| ENSMMUG00000062348 | 7.72 | 0.04 | | lncRNA |
| ENSMMUG00000061454 | 7.06 | 0.03 | | lncRNA |
| ENSMMUG00000012467 | 7.05 | 0.02 | FAM227A | protein coding |
| ENSMMUG00000060311 | 6.97 | 0.04 | | protein coding |
| ENSMMUG00000061829 | 6.97 | 0.05 | | protein coding |
| ENSMMUG00000019968 | 1.41 | 0.05 | NOSTRIN | protein coding |
| **WSD vs. C** | | | | |
| ENSMMUG00000002896 | 9.65 | 0.04 | SSTR5 | protein coding |
| ENSMMUG00000061829 | 9.64 | 0.02 | | protein coding |
| ENSMMUG00000012467 | 6.93 | 0.03 | FAM227A | protein coding |
| ENSMMUG00000061454 | 6.80 | 0.04 | | lncRNA |
| ENSMMUG00000051619 | 5.49 | 0.05 | PADI3 | protein coding |
| **T+WSD vs. C** | | | | |
| ENSMMUG00000062348 | 10.79 | 0.04 | | lncRNA |
| ENSMMUG00000060590 | 8.44 | 0.05 | | protein coding |
| ENSMMUG00000054896 | 6.37 | 0.05 | MT1H | protein coding |
| ENSMMUG00000015062 | 4.04 | 0.04 | CEP97 | protein coding |
| ENSMMUG00000016753 | 3.80 | 0.02 | DNAH3 | protein coding |
| **Downregulated genes** | | | | |
| **T vs. C** | | | | |
| ENSMMUG00000041616 | -11.05 | 0.01 | GNG11 | protein coding |
| ENSMMUG00000020979 | -10.99 | 0.01 | INKA1 | protein coding |
| ENSMMUG00000020987 | -10.96 | 0.00 | FABP4 | protein coding |
| ENSMMUG00000062083 | -10.59 | 0.00 | | pseudogene |
| ENSMMUG00000021286 | -10.51 | 0.00 | COL3A1 | protein coding |
| **WSD vs. C** | | | | |
| ENSMMUG00000049714 | -13.66 | 0.01 | HCGB | protein coding |
| ENSMMUG00000064308 | -12.62 | 0.01 | | protein coding |
| ENSMMUG00000007193 | -12.27 | 0.04 | PABPC4L | protein coding |
| ENSMMUG00000014260 | -11.82 | 0.00 | CCRL2 | protein coding |
| ENSMMUG00000013014 | -10.5 | 0.02 | IL1RN | protein coding |
| **T+WSD vs. C** | | | | |
| ENSMMUG00000059411 | -11.37 | 0.02 | PLPP6 | protein coding |
| ENSMMUG00000017842 | -11.13 | 0.00 | MOSPD2 | protein coding |
| ENSMMUG00000011847 | -11.12 | 0.04 | CDYL2 | protein coding |
| ENSMMUG00000012696 | -10.94 | 0.01 | ZNF300 | protein coding |
| ENSMMUG00000018192 | -9.88 | 0.05 | RORA | protein coding |

2502

2503

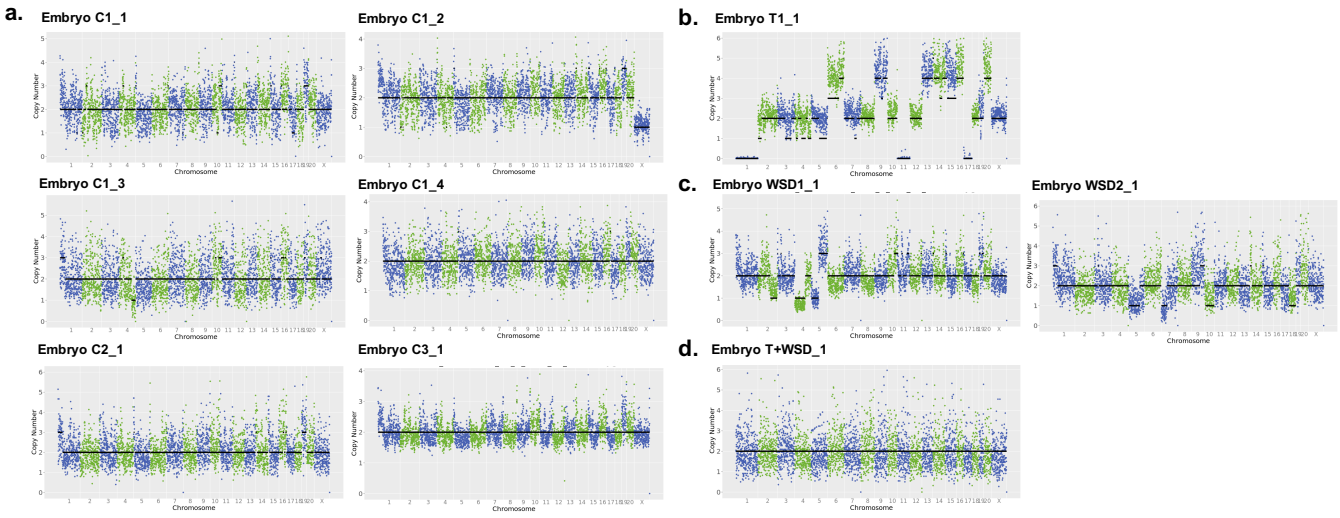


**Supplementary Figure S4. 1. DNA sequencing of single blastomeres from cleavage stage embryos.**

Copy number variation (CNV) was performed for 88 single blastomeres belonging to 16 cleavage stage embryos from the C (N=40 blastomeres from 7 embryos), T (N=21 blastomeres from 3 embryos), WSD (N=19 blastomeres from 4 embryos), T+WSD (N=8 blastomeres from 2 embryos) groups. Representative CNV plots include: **(a)** 6 single blastomeres from three embryos for the C group, **(b)** one blastomere form the T group, **(c)** 2 blastomeres from a single embryo for the WSD group, and **(d)** one blastomere for the T+WSD. No significant differences in CNV were observed between the 4 treatment groups. The chromosome number is represented on the x-axis and the copy number of the chromosome is represented on the y-axis.

2504

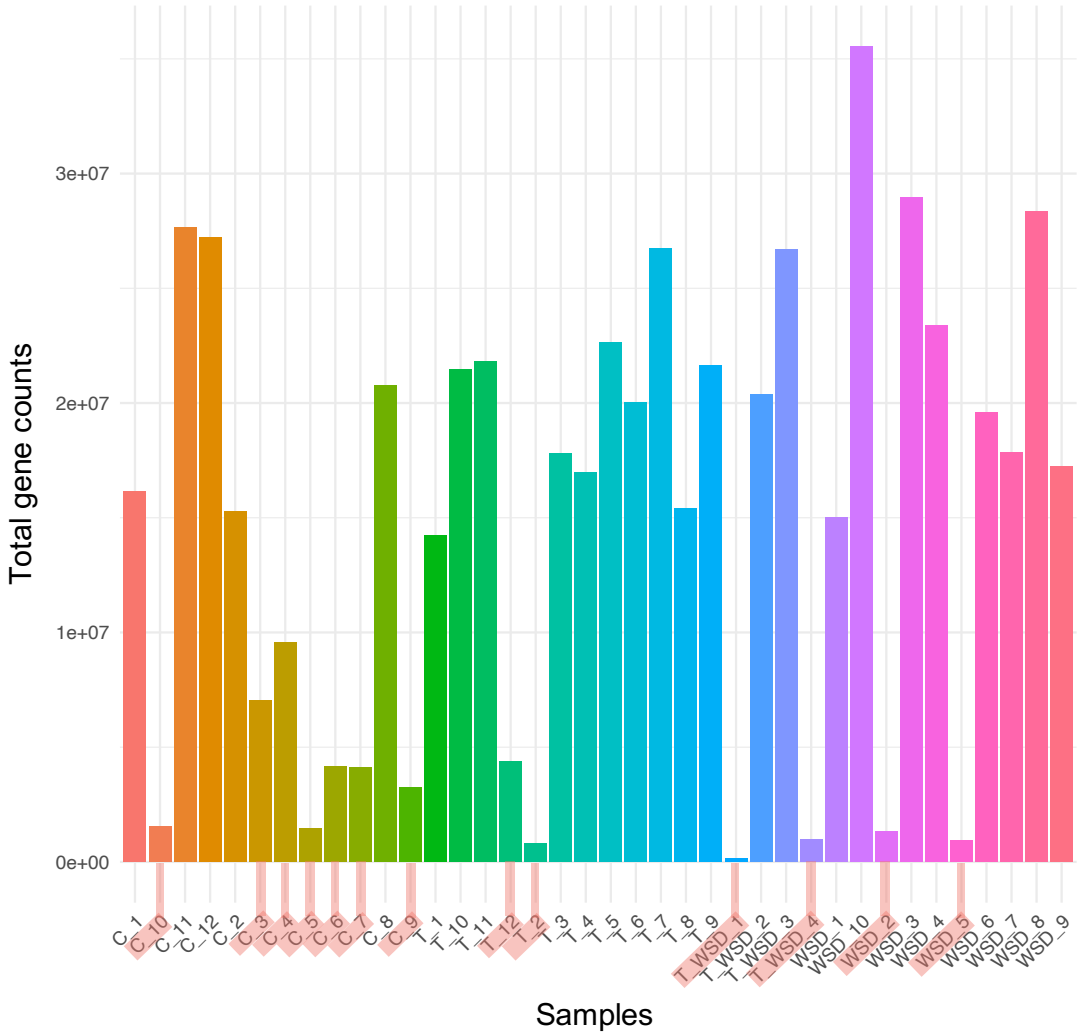


**Supplementary Figure S4. 2. DNA sequencing of single blastomeres from cleavage stage embryos.**

Total gene counts for all the blastocyst samples that underwent RNA-Sequencing. 38 blastocyst samples from the 4 treatment groups N= 38 (12 C, 12 T, 10 WSD, and 4 T+WSD) were sequenced. However, post-analysis, 13 samples has less than 10 million total gene counts represented by the pink bars in the bar graph. Hence, the remaining 25 blastocyst samples were included for analysis of differential gene expression (5 C, 10 T, 8 WSD, and 2 T+WSD).

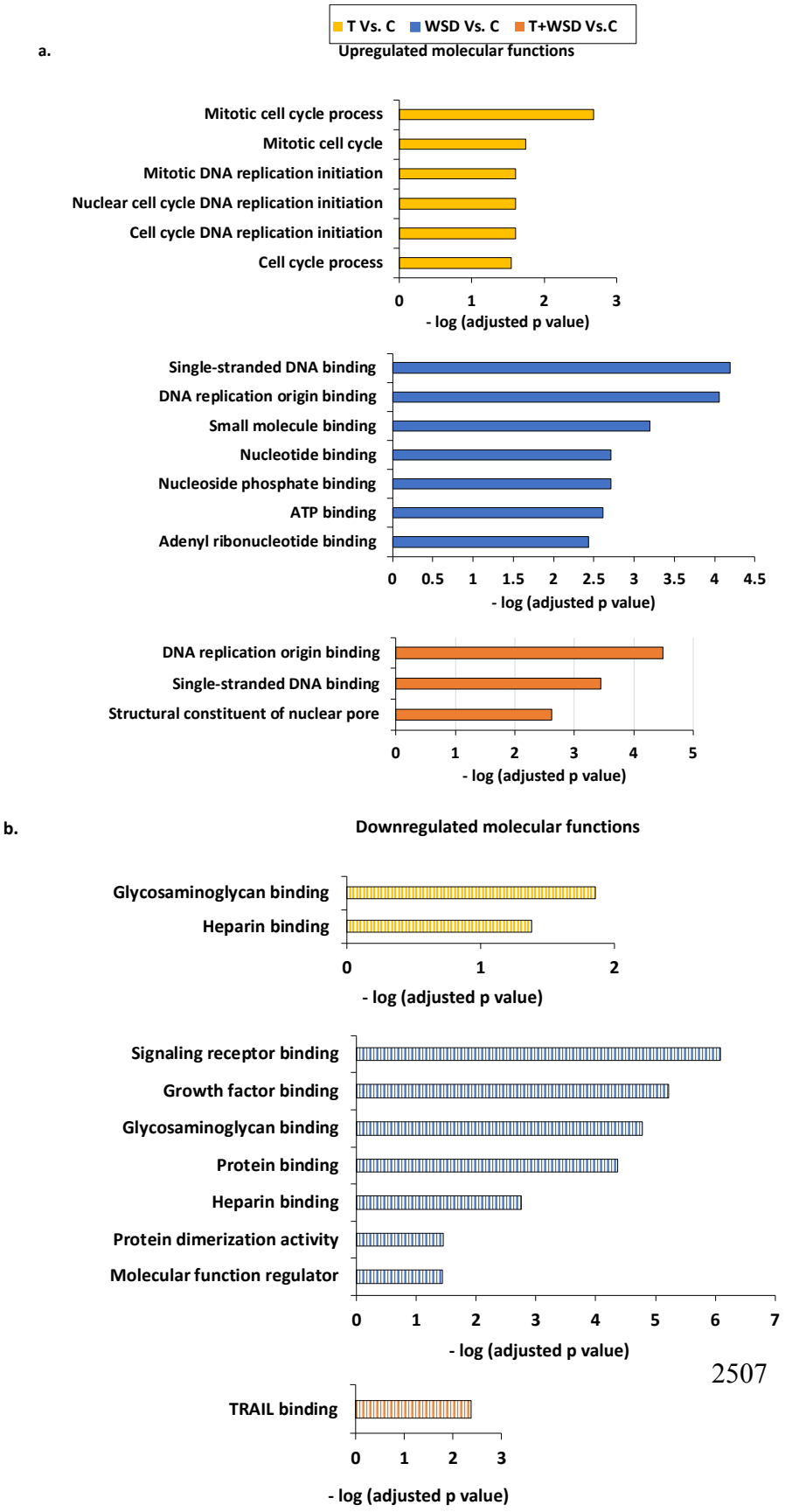


**Supplementary Figure S4. 3. Gene ontology (GO) and pathway analyses of the uniquely expressed genes in the blastocysts.**

Majority of the genes identified by RNA-Sequencing of the blastocysts that were significantly expressed (adjusted $p<0.05$) either by the T, WSD or T+WSD blastocyst compared to the C blastocysts, were unique to each treatment group. The molecular functions identified by gene ontology (GO) and pathway analyses have been represented in the bar graphs associated with T, WSD and T+WSD-induced gene (a) upregulation and (b) downregulation. The axis represents the negative log of adjusted p value.

5 blastocyst samples were included for analysis of differential gene expression (5 C, 10 T, 8 WSD, and 2 T+WSD).

# Chapter 5: Conclusion

## General Conclusions

The studies included in this dissertation utilized state-of-the-art techniques and a clinically-relevant non-human primate (NHP) model to investigate the paracrine/autocrine events within the periovulatory follicle that are responsible for the release of an oocyte capable of fertilization and preimplantation development. Further, the dissertation also demonstrated the effect of alterations in endocrine, dietary, and metabolic function on intrafollicular processes and oocyte competency. Specifically, these studies detailed the impact of exogenous pharmacological levels of gonadotropins used in infertility treatments, short-term Western-Style Diet (WSD) exposure ($WSD_S$), as well as chronic exposure to androgens (T), long-term WSD ($WSD_L$), and a combination of both conditions ($T+WSD_L$) on the ovarian follicular microenvironment during the periovulatory interval. These experiments were designed to recapitulate women that are undergoing infertility treatments, as well as those who are afflicted by diet-induced obesity ($WSD_S$, $WSD_L$) or polycystic ovary syndrome (PCOS; i.e., $T\pm WSD_L$ treatment).

The underlying factors that we determined to be important for *in vitro* fertilization (IVF) success in these studies can be broadly categorized into effects on the follicle, oocyte, and embryo, all of which are interdependent (**Fig. 5.1**). To determine the impact on the follicular microenvironment, the molecular constituents of the follicular fluid (FF) post-exogenous gonadotropin administration were analyzed in all three studies at the time of oocyte aspiration. In the metabolomics study, as well as with WSDs consumption, the ratio of cortisol to cortisone was significant in predicting the capacity of the corresponding oocyte to fertilize, cleave and form a blastocyst. We also

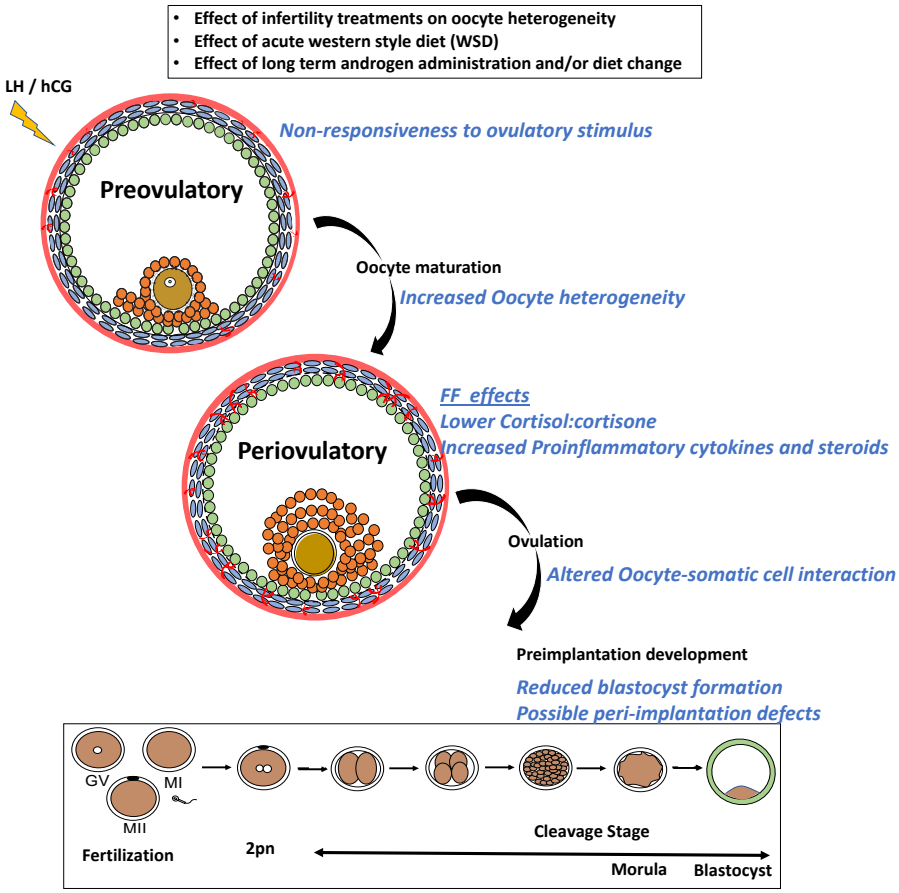


**Figure 5. 1. Alterations in endocrine, dietary, and metabolic function affect intrafollicular processes and oocyte competency.**

This schematic represents the events triggered after an ovulatory stimulus (represented by LH /hCG), which includes the preovulatory to periovulatory follicle transition, oocyte maturation, and COC expansion. This further leads to ovulation of a fertilizable oocyte that proceeds to form a preimplantation blastocyst stage embryo. These interrelated ovarian follicle, oocyte and embryo effects of infertility treatments, and diet or metabolism related changes on these processes have been highlighted in blue font. These effects are interdependent and cumulatively affect the oocyte's competency to form a preimplantation stage embryo post-fertilization in a clinically relevant model.

2547 reported, for the first time, a potential role for the nuclear glucocorticoid receptor (GR)
2548 within the oocyte during the process of oocyte maturation and cumulus cell expansion.
2549 Paracrine signaling between the oocyte and the somatic cells of the follicle is critical for
2550 the cellular events leading to ovulation[59] and our results indicate that GR deficiency in the
2551 oocyte disrupts this cumulus-oocyte complex (COC) crosstalk. We also observed the
2552 switch to a pro-inflammatory cytokine milieu in FF following $WSD_S$ and chronic T
2553 treatments. This intrafollicular proinflammatory effect of the $WSD_S$ treatment was
2554 correlated with reduced IVF success and progression to the implantation blastocyst stage
2555 in other studies[284] which was observed in the our study.

2556 As noted by the IVF experiments in the absence of dietary or steroid changes, a mature
2557 metaphase II (MII) oocyte did not always give rise to a blastocyst after IVF and further
2558 supported the concept of high oocyte heterogeneity among growing follicles following
2559 gonadotropin administration[84,182,183]. By adding the confounding factors of diet and/or
2560 elevated circulating T levels to IVF treatment, we showed that in spite of obtaining fewer
2561 immature oocytes and a higher probability of collecting mature MII oocytes, blastocyst
2562 formation was severely impaired in $WSD_S$, $WSD_L$, and $T+WSD_L$ embryos compared to
2563 their respective controls. Indicators of aneuploidy such as delayed mitotic division timing,
2564 cellular fragmentation, and multipolar divisions were also more pronounced in these
2565 treatment groups relative to the control, suggesting a potential cause for embryo arrest and
2566 reduced blastocyst formation. RNA-seq analysis of the $WSD_S$ blastocysts revealed an
2567 increase in expression of cell death genes and a decrease in genes important for lineage
2568 specification in $WSD_s$ embryos that would likely affect peri-implantation processes
2569 essential for subsequent embryonic development.

2570 **Clinical Impact**

2571 In human IVF clinics, aspirates from multiple follicles are typically combined,
2572 which prevents the assessment of oocyte heterogeneity. This heterogeneity impacts the
2573 ability of oocytes to undergo fertilization and form a blastocyst following exogenous
2574 gonadotropin administration[180-183] and likely leads to a reduction in IVF success. Our
2575 results suggest that either individual follicle aspiration techniques be implemented into
2576 clinical IVF practice or the identification of non-invasive cellular/molecular markers
2577 predictive of developmental potential be further developed. Indeed, we used time-lapse
2578 monitoring (TLM) and the measurement of imaging parameters to successfully assess
2579 differences between embryo treatment groups in the current studies. Thus, we would argue
2580 that TLM and/or other advanced techniques such as pre-implantation genetic screening
2581 (PGS), combined with analysis of FF from individual follicles, be correlated to the
2582 developmental outcome of the resident oocyte. This would enable a comprehensive
2583 assessment of oocyte and embryo heterogeneity for possible predictive modelling in future
2584 cycles, a concept that is partially supported by previous analyses of FF from individual
2585 follicle aspirations in clinical IVF settings[210,226,227].

2586 Based on our findings, we also propose testing for cortisol and cortisone
2587 concentrations in the FF from individual follicle aspirations. Because metabolomics
2588 assessments are time consuming and expensive, a quantitative ELISA for glucocorticoid
2589 levels in FF could be easily incorporated into IVF practice. Such analyses could be
2590 extended to embryo spent media and have potential for predicting IVF success as
2591 previously described[205,207]. From our experiments and previous clinical case reports of
2592 infertility in women, we know that a proinflammatory follicular environment can alter the

2593 growth and maturation of the periovulatory follicle, and therefore, IVF success[284,381]. Thus,
2594 we believe that testing FF for inflammatory cytokines such as IL-1RA and CXCL10,
2595 especially in women with infertility caused by diet-induced obesity, will also help
2596 determine oocyte competency post-fertilization. By selecting and freezing only the oocytes
2597 and embryos with high developmental potential, embryo wastage would be reduced and
2598 the indefinite storage of embryos that will never be transferred to patients potentially
2599 avoided. Although the methodologies to preserve female reproductive function are still
2600 evolving[382], especially in young girls and women with a cancer diagnosis, the selection of
2601 oocytes with the highest competency is important not only for the general IVF population,
2602 but also in more specialized circumstances such as fertility preservation prior to
2603 chemotherapy treatment.

2604 Given the etiology of maternal obesity and complexity of PCOS-like syndromes in
2605 women, our findings also take us a step closer to determining if the impaired fertility is due
2606 to the diet itself or the subsequent development of metabolic dysfunction. This will assist
2607 in adjusting strategies for treating infertility caused by these confounding factors and
2608 provide a more personalized approach to improving IVF success in these unique
2609 populations. From our studies, we demonstrate that even control females gain weight
2610 during chronic treatment, which could be age-related or due to the consumption of an *ad*
2611 *libitum* diet over-time[347,348]. Moreover, we show that the addition of WSD intake alone is
2612 sufficient to impair oocyte competency, but this condition is worsened by the addition of
2613 hyperandrogenism. Despite the lack of significant differences in metabolic parameters
2614 between the control and WSD animals utilized in our studies, the primary contribution of
2615 WSD to oocyte heterogeneity supports the idea of diet reversal as part of the infertility

2616 treatment regime. Further evidence for a switch to a low-fat diet stems from studies of diet
2617 change or weight loss improving IVF outcomes for obese women in human clinics[184,259].
2618

2619 **Future Directions**

2620 Besides cortisol and cortisone, our analysis of the periovulatory FF metabolome
2621 identified 50 other metabolites that were correlated to the post-fertilization developmental
2622 outcome of the corresponding oocyte. Although the function of most of these metabolites
2623 in ovarian follicle development is unclear and some are intermediates rather than the end
2624 products of certain metabolic pathways, further metabolomic investigation is still
2625 warranted. We note that with the exception of a few metabolites, the majority were
2626 downregulated in blastocysts compared to cleavage stage arrested embryos. Based on this,
2627 as well as findings that no significant differences in meiotic resumption, fertilization, or
2628 percentage of cleaved embryos was observed between samples cultured with or without
2629 cortisol, our results support the concept of the "quiet embryo hypothesis"[236]. Thus, a more
2630 comprehensive assessment of the endogenous resources present in the periovulatory
2631 follicular milieu will yield insight into how these metabolites and other molecular
2632 constituents promote the subsequent growth and development of an oocyte with high
2633 potential.

2634 Future studies are also needed for analyzing the exact role of GR in oocyte
2635 maturation and coordinating the events necessary for ovulation, both *in vitro* as well as *in*
2636 *vivo*. For the *in vitro* analyses, GR knockdown within the mural granulosa cells (mGCs)
2637 should be performed to determine if cortisol through GR signaling regulates factors
2638 important for ovulatory processes such as steroidogenesis. We also suggest that mGC and

2639 cumulus cell (CC) proliferation[383] and/or expansion be assessed based on the indirect
2640 effects that disrupting GR signaling in the oocyte had on cumulus-oocyte expansion.
2641 Whether culturing oocytes as intact COCs or at least with mGCs yields improved
2642 percentage of mature oocytes, thereby increasing IVF success similar to *in* vitro maturation
2643 in farm animals[384-386], should also be determined. The communication amongst the somatic
2644 cells, in addition to the crosstalk between the oocyte and somatic cells, could be assessed
2645 *in vivo* by injecting a HSD11B1 inhibitor, an adenovirus mediating HSD11B2
2646 overexpression, or an adenoviral shRNA for GR knockdown in the periovulatory follicle.
2647 Cortisol is known for its potent and wide-ranging anti-inflammatory properties[275,276], and
2648 it is now well-established that ovulation is considered an inflammatory process[381,387]. Thus,
2649 the higher concentrations of intrafollicular cortisol observed during ovulation by us and as
2650 shown by others is seemingly counter to these observations[95,237,238]. By conducting *in vivo*
2651 analyses of the periovulatory follicle, we will be able to assess how GR or HSD11B
2652 knockdown affects inflammation associated cytokines, steroids or other factors in the
2653 intrafollicular milieu.

2654 To improve our understanding of the impact of a WSD consumption with or without
2655 hyperandrogenemia on maternal obesity or under PCOS-like conditions, we suggest
2656 performing experiments for a shorter duration of time in the T, $WSD_L$, and T+$WSD_L$ group.
2657 With respect to these chronic exposures, the controls and T only group also had *ad libitum*
2658 access to food similar to the $WSD_L$ and T+$WSD_L$ females and this likely promoted weight
2659 gain and normalization of metabolic parameters across all treatments by the time our
2660 studies were performed (i.e., after more than 5 years of continuous treatment). By
2661 conducting experiments after a shorter treatment period, we will capture the effects of

2662 metabolic dysfunction that was observed at 2-3 yrs of chronic treatments. As discussed
2663 above, a study of diet reversal following $WSD_S$ or $WSD_L$ treatment should also be
2664 performed to assess whether the duration of WSD intake plays a role in impacting
2665 restoration of IVF success similar to that of the age-matched control females.

2666 Altogether, these studies have provided insight into the cellular and molecular
2667 events that are necessary for ovulation and how specific endocrine and metabolic
2668 dysfunction disrupts these processes in primates.

2669

2670 **References**


2671 1 Gougeon, A. Regulation of ovarian follicular development in primates: facts and
2672 hypotheses. *Endocr Rev* **17**, 121-155 (1996).
2673 2 Sun, Y. C. *et al.* The role of germ cell loss during primordial follicle assembly: a
2674 review of current advances. *Int J Biol Sci* **13**, 449-457 (2017).
2675 3 Baker, T. G. A quantitative and cytological study of germ cells in human ovaries.
2676 *Proc R Soc Lond B Biol Sci* **158**, 417-433 (1963).
2677 4 Wallace, W. H. & Kelsey, T. W. Human ovarian reserve from conception to the
2678 menopause. *PLoS One* **5**, e8772 (2010).
2679 5 Kurilo, L. F. Oogenesis in antenatal development in man. *Hum Genet* **57**, 86-92
2680 (1981).
2681 6 Hanna, C. B. & Hennebold, J. D. Ovarian germline stem cells: an unlimited source
2682 of oocytes? *Fertil Steril* **101**, 20-30 (2014).
2683 7 Plant, T. M. 60 years of neuroendocrinology: the hypothalamo-pituitary-gonadal
2684 axis. *J Endocrinol* **226**, T41-54 (2015).
2685 8 Plant, T. M. A comparison of the neuroendocrine mechanisms underlying the
2686 initiation of the preovulatory LH surge in the human, Old World monkey and
2687 rodent. *Front Neuroendocrinol* **33**, 160-168 (2012).
2688 9 Knobil, E. *et al.* Control of the rhesus monkey menstrual cycle: permissive role of
2689 hypothalamic gonadotropin-releasing hormone. *Science* **207**, 1371-1373 (1980).
2690 10 Krey, L. C., Butler, W. R. & Knobil, E. Surgical disconnection of the medial basal
2691 hypothalamus and pituitary function in the rhesus monkey. I. Gonadotropin
2692 secretion. *Endocrinology* **96**, 1073-1087 (1975).
2693 11 Goodman, A. L. & Hodgen, G. D. The ovarian triad of the primate menstrual cycle.
2694 *Recent Prog Horm Res* **39**, 1-73 (1983).
2695 12 McGee, E. A. & Hsueh, A. J. Initial and cyclic recruitment of ovarian follicles.
2696 *Endocr Rev* **21**, 200-214 (2000).
2697 13 Wijayarathna, R. & de Kretser, D. M. Activins in reproductive biology and beyond.
2698 *Hum Reprod Update* **22**, 342-357 (2016).

14 Barbieri, R. L. The endocrinology of the menstrual cycle. *Methods Mol Biol* **1154**, 145-169 (2014).
15 Knight, P. G., Satchell, L. & Glister, C. Intra-ovarian roles of activins and inhibins. *Mol Cell Endocrinol* **359**, 53-65 (2012).
16 Giudice, L. C. Insulin-like growth factor family in graafian follicle development and function. *J Soc Gynecol Investig* **8**, S26-29 (2001).
17 Iwashita, M. *et al.* Physiological role of insulin-like-growth-factor-binding protein-4 in human folliculogenesis. *Horm Res* **46 Suppl 1**, 31-36 (1996).
18 el-Roeiy, A. *et al.* Expression of insulin-like growth factor-I (IGF-I) and IGF-II and the IGF-I, IGF-II, and insulin receptor genes and localization of the gene products in the human ovary. *J Clin Endocrinol Metab* **77**, 1411-1418 (1993).
19 Hendriksen, P. J. *et al.* Follicular dynamics around the recruitment of the first follicular wave in the cow. *Biol Reprod* **69**, 2036-2044 (2003).
20 Mason, H. D., Cwyfan-Hughes, S., Holly, J. M. & Franks, S. Potent inhibition of human ovarian steroidogenesis by insulin-like growth factor binding protein-4 (IGFBP-4). *J Clin Endocrinol Metab* **83**, 284-287 (1998).
21 Austin, E. J. *et al.* Alterations in intrafollicular regulatory factors and apoptosis during selection of follicles in the first follicular wave of the bovine estrous cycle. *Biol Reprod* **64**, 839-848 (2001).
22 Hernandez, E. R., Roberts, C. T., Jr., LeRoith, D. & Adashi, E. Y. Rat ovarian insulin-like growth factor I (IGF-I) gene expression is granulosa cell-selective: 5'-untranslated mRNA variant representation and hormonal regulation. *Endocrinology* **125**, 572-574 (1989).
23 Grondahl, M. L. *et al.* Specific genes are selectively expressed between cumulus and granulosa cells from individual human pre-ovulatory follicles. *Mol Hum Reprod* **18**, 572-584 (2012).
24 Clarke, H. J. Regulation of germ cell development by intercellular signaling in the mammalian ovarian follicle. *Wiley Interdiscip Rev Dev Biol* **7** (2018).
25 Traver, S. *et al.* Cell-free DNA in human follicular microenvironment: New prognostic biomarker to predict in vitro fertilization outcomes. *PLoS One* **10**, e0136172 (2015).
26 Hussein, T. S., Thompson, J. G. & Gilchrist, R. B. Oocyte-secreted factors enhance oocyte developmental competence. *Dev Biol* **296**, 514-521 (2006).
27 da Silveira, J. C. *et al.* Cell-secreted vesicles containing microRNAs as regulators of gamete maturation. *J Endocrinol* **236**, R15-R27 (2018).
28 Borgbo, T. *et al.* Effect of the FSH receptor single nucleotide polymorphisms (FSHR 307/680) on the follicular fluid hormone profile and the granulosa cell gene expression in human small antral follicles. *Mol Hum Reprod* **21**, 255-261 (2015).
29 Andersen, C. Y., Westergaard, L. G., Sinosich, M. J. & Byskov, A. G. Human preovulatory follicular fluid: inhibin and free steroids related to optimal follicular maturation in ovarian stimulation regimes and possible function in ovulation. *Hum Reprod* **7**, 765-769 (1992).
30 Andersen, C. Y. *et al.* Concentrations of AMH and inhibin-B in relation to follicular diameter in normal human small antral follicles. *Hum Reprod* **25**, 1282-1287 (2010).

31 Stocco, C. *et al.* Genome-wide interactions between FSH and insulin-like growth factors in the regulation of human granulosa cell differentiation. *Hum Reprod* **32**, 905-914 (2017).
32 Freitas, C. *et al.* Follicular fluid redox involvement for ovarian follicle growth. *J Ovarian Res* **10**, 44 (2017).
33 El-Hayek, S. *et al.* Mammalian oocytes locally remodel follicular architecture to provide the foundation for germline-soma communication. *Curr Biol* **28**, 1124-1131 e1123 (2018).
34 Komatsu, K. & Masubuchi, S. Mouse oocytes connect with granulosa cells by fusing with cell membranes and form a large complex during follicle development. *Biol Reprod* **99**, 527-535 (2018).
35 Tamba, S. *et al.* Expression profiling of cumulus cells reveals functional changes during ovulation and central roles of prostaglandin EP2 receptor in cAMP signaling. *Biochimie* **92**, 665-675 (2010).
36 Mehlmann, L. M. Stops and starts in mammalian oocytes: recent advances in understanding the regulation of meiotic arrest and oocyte maturation. *Reproduction* **130**, 791-799 (2005).
37 Conti, M., Hsieh, M., Zamah, A. M. & Oh, J. S. Novel signaling mechanisms in the ovary during oocyte maturation and ovulation. *Mol Cell Endocrinol* **356**, 65-73 (2012).
38 Tsuji, T., Kiyosu, C., Akiyama, K. & Kunieda, T. CNP/NPR2 signaling maintains oocyte meiotic arrest in early antral follicles and is suppressed by EGFR-mediated signaling in preovulatory follicles. *Mol Reprod Dev* **79**, 795-802 (2012).
39 Xi, G. *et al.* Natriuretic peptide receptor 2 (NPR2) localized in bovine oocyte underlies a unique mechanism for C-type natriuretic peptide (CNP)-induced meiotic arrest. *Theriogenology* **106**, 198-209 (2018).
40 Arur, S. Signaling-mediated regulation of meiotic prophase I and transition during oogenesis. *Results Probl Cell Differ* **59**, 101-123 (2017).
41 Jaffe, L. A. & Egbert, J. R. Regulation of Mammalian Oocyte Meiosis by Intercellular Communication Within the Ovarian Follicle. *Annu Rev Physiol* **79**, 237-260 (2017).
42 Christian, C. A. & Moenter, S. M. The neurobiology of preovulatory and estradiol-induced gonadotropin-releasing hormone surges. *Endocr Rev* **31**, 544-577 (2010).
43 Amsterdam, A., Tajima, K., Frajese, V. & Seger, R. Analysis of signal transduction stimulated by gonadotropins in granulosa cells. *Mol Cell Endocrinol* **202**, 77-80 (2003).
44 Ge, W. Intrafollicular paracrine communication in the zebrafish ovary: the state of the art of an emerging model for the study of vertebrate folliculogenesis. *Mol Cell Endocrinol* **237**, 1-10 (2005).
45 Breen, S. M. *et al.* Ovulation involves the luteinizing hormone-dependent activation of G(q/11) in granulosa cells. *Mol Endocrinol* **27**, 1483-1491 (2013).
46 Hunzicker-Dunn, M. & Mayo, K. in *Knobil and Neill's Physiology of Reproduction (Fourth Edition)* (ed A.J Zeleznik T.M.Plant) 895-945 (2015).
47 Fan, H. Y. *et al.* MAPK3/1 (ERK1/2) in ovarian granulosa cells are essential for female fertility. *Science* **324**, 938-941 (2009).

48 Weick, R. F. *et al.* Periovulatory time courses of circulating gonadotropic and ovarian hormones in the rhesus monkey. *Endocrinology* **93**, 1140-1147 (1973).
49 Direito, A., Bailly, S., Mariani, A. & Ecochard, R. Relationships between the luteinizing hormone surge and other characteristics of the menstrual cycle in normally ovulating women. *Fertil Steril* **99**, 279-285 (2013).
50 Edson, M. A., Nagaraja, A. K. & Matzuk, M. M. The mammalian ovary from genesis to revelation. *Endocr Rev* **30**, 624-712 (2009).
51 Robker, R. L. & Richards, J. S. Hormone-induced proliferation and differentiation of granulosa cells: a coordinated balance of the cell cycle regulators cyclin D2 and p27Kip1. *Mol Endocrinol* **12**, 924-940 (1998).
52 Liu, W. *et al.* Estrogen receptors in granulosa cells govern meiotic resumption of pre-ovulatory oocytes in mammals. *Cell Death Dis* **8**, e2662 (2017).
53 Palter, S. F. *et al.* Are estrogens of import to primate/human ovarian folliculogenesis? *Endocr Rev* **22**, 389-424 (2001).
54 Kolibianakis, E. M., Papanikolaou, E. G., Fatemi, H. M. & Devroey, P. Estrogen and folliculogenesis: is one necessary for the other? *Curr Opin Obstet Gynecol* **17**, 249-253 (2005).
55 Wang, L. *et al.* Genetic dissection of the different roles of hypothalamic kisspeptin neurons in regulating female reproduction. *Elife* **8** (2019).
56 Fraser, H. M., Lunn, S. F., Cowen, G. M. & Saunders, P. T. Localization of inhibin/activin subunit mRNAs during the luteal phase in the primate ovary. *J Mol Endocrinol* **10**, 245-257 (1993).
57 Burger, H. G. Evidence for a negative feedback role of inhibin in follicle stimulating hormone regulation in women. *Hum Reprod* **8 Suppl 2**, 129-132 (1993).
58 Knight, P. G. & Glister, C. TGF-beta superfamily members and ovarian follicle development. *Reproduction* **132**, 191-206 (2006).
59 Richards, J. S. & Ascoli, M. Endocrine, paracrine, and autocrine signaling pathways that regulate ovulation. *Trends Endocrinol Metab* **29**, 313-325 (2018).
60 Gudermann, T., Birnbaumer, M. & Birnbaumer, L. Evidence for dual coupling of the murine luteinizing hormone receptor to adenylyl cyclase and phosphoinositide breakdown and Ca2+ mobilization. Studies with the cloned murine luteinizing hormone receptor expressed in L cells. *J Biol Chem* **267**, 4479-4488 (1992).
61 Robker, R. L., Hennebold, J. D. & Russell, D. L. Coordination of ovulation and oocyte maturation: a good egg at the right time. *Endocrinology* **159**, 3209-3218 (2018).
62 Richards, J. S. *et al.* Molecular mechanisms of ovulation and luteinization. *Mol Cell Endocrinol* **145**, 47-54 (1998).
63 Wang, Y. *et al.* CREB activity is required for luteinizing hormone-induced the expression of EGF-like factors. *Mol Reprod Dev* **83**, 1116-1127 (2016).
64 Salvador, L. M. *et al.* Acute signaling by the LH receptor is independent of protein kinase C activation. *Endocrinology* **143**, 2986-2994 (2002).
65 Chaffin, C. L., Schwinof, K. M. & Stouffer, R. L. Gonadotropin and steroid control of granulosa cell proliferation during the periovulatory interval in rhesus monkeys. *Biol Reprod* **65**, 755-762 (2001).

66 Richards, J. S. Hormonal control of gene expression in the ovary. *Endocr Rev* **15**, 725-751 (1994).
67 Gougeon, A. Ovarian follicular growth in humans: ovarian ageing and population of growing follicles. *Maturitas* **30**, 137-142 (1998).
68 McNatty, K. P. Hormonal correlates of follicular development in the human ovary. *Aust J Biol Sci* **34**, 249-268 (1981).
69 Smith, M. F., McIntush, E. W. & Smith, G. W. Mechanisms associated with corpus luteum development. *J Anim Sci* **72**, 1857-1872 (1994).
70 Chaffin, C. L., Dissen, G. A. & Stouffer, R. L. Hormonal regulation of steroidogenic enzyme expression in granulosa cells during the peri-ovulatory interval in monkeys. *Mol Hum Reprod* **6**, 11-18 (2000).
71 Richards, J. S., Hedin, L. & Caston, L. Differentiation of rat ovarian thecal cells: evidence for functional luteinization. *Endocrinology* **118**, 1660-1668 (1986).
72 Gwynne, J. T. & Strauss, J. F., 3rd. The role of lipoproteins in steroidogenesis and cholesterol metabolism in steroidogenic glands. *Endocr Rev* **3**, 299-329 (1982).
73 Voutilainen, R. *et al.* Hormonal regulation of P450scc (20,22-desmolase) and P450c17 (17 alpha-hydroxylase/17,20-lyase) in cultured human granulosa cells. *J Clin Endocrinol Metab* **63**, 202-207 (1986).
74 Miller, W. L. & Auchus, R. J. The molecular biology, biochemistry, and physiology of human steroidogenesis and its disorders. *Endocr Rev* **32**, 81-151 (2011).
75 Borman, S. M. *et al.* Progesterone promotes oocyte maturation, but not ovulation, in nonhuman primate follicles without a gonadotropin surge. *Biol Reprod* **71**, 366-373 (2004).
76 Bishop, C. V., Hennebold, J. D., Kahl, C. A. & Stouffer, R. L. Knockdown of progesterone receptor (PGR) in macaque granulosa cells disrupts ovulation and progesterone production. *Biol Reprod* **94**, 109 (2016).
77 Curry, T. E., Jr. ADAMTS1 and versican: partners in ovulation and fertilization. *Biol Reprod* **83**, 505-506 (2010).
78 Mori, T., Suzuki, A., Nishimura, T. & Kambegawa, A. Inhibition of ovulation in immature rats by anti-progesterone antiserum. *J Endocrinol* **73**, 185-186 (1977).
79 Lydon, J. P. *et al.* Mice lacking progesterone receptor exhibit pleiotropic reproductive abnormalities. *Genes Dev* **9**, 2266-2278 (1995).
80 Zelinski-Wooten, M. B. & Stouffer, R. L. Steroid receptors and action in the primate follicle. *Trends Endocrinol Metab* **7**, 177-183 (1996).
81 Hibbert, M. L., Stouffer, R. L., Wolf, D. P. & Zelinski-Wooten, M. B. Midcycle administration of a progesterone synthesis inhibitor prevents ovulation in primates. *Proc Natl Acad Sci U S A* **93**, 1897-1901 (1996).
82 Iwai, M. *et al.* Luteinizing hormone induces progesterone receptor gene expression in cultured porcine granulosa cells. *Endocrinology* **129**, 1621-1627 (1991).
83 Capalbo, A. *et al.* Human female meiosis revised: new insights into the mechanisms of chromosome segregation and aneuploidies from advanced genomics and time-lapse imaging. *Hum Reprod Update* **23**, 706-722 (2017).
84 Stouffer, R. L. & Zelinski, M. B. Overriding follicle selection in controlled ovarian stimulation protocols: Quality vs quantity. *Reproductive Biology and Endocrinology* **2**, 32 (2004).

85 Balmaceda, J. P. *et al.* Successful in vitro fertilization and embryo transfer in cynomolgus monkeys. *Fertil Steril* **42**, 791-795 (1984).
86 Bavister, B. D. *et al.* Birth of rhesus monkey infant after in vitro fertilization and nonsurgical embryo transfer. *Proc Natl Acad Sci U S A* **81**, 2218-2222 (1984).
87 Robker, R. L. *et al.* Progesterone-regulated genes in the ovulation process: ADAMTS-1 and cathepsin L proteases. *Proc Natl Acad Sci U S A* **97**, 4689-4694 (2000).
88 Peluso, J. J. Progesterone receptor membrane component 1 and its role in ovarian follicle growth. *Front Neurosci* **7**, 99 (2013).
89 Terzaghi, L. *et al.* PGRMC1 participates in late events of bovine granulosa cells mitosis and oocyte meiosis. *Cell Cycle* **15**, 2019-2032 (2016).
90 Luciano, A. M. *et al.* Progesterone receptor membrane component 1 expression and putative function in bovine oocyte maturation, fertilization, and early embryonic development. *Reproduction* **140**, 663-672 (2010).
91 Murphy, B. E. Ontogeny of cortisol-cortisone interconversion in human tissues: a role for cortisone in human fetal development. *J Steroid Biochem* **14**, 811-817 (1981).
92 Tomlinson, J. W. *et al.* 11beta-hydroxysteroid dehydrogenase type 1: a tissue-specific regulator of glucocorticoid response. *Endocr Rev* **25**, 831-866 (2004).
93 Albiston, A. L., Obeyesekere, V. R., Smith, R. E. & Krozowski, Z. S. Cloning and tissue distribution of the human 11 beta-hydroxysteroid dehydrogenase type 2 enzyme. *Mol Cell Endocrinol* **105**, R11-17 (1994).
94 Tetsuka, M., Milne, M., Simpson, G. E. & Hillier, S. G. Expression of 11beta-hydroxysteroid dehydrogenase, glucocorticoid receptor, and mineralocorticoid receptor genes in rat ovary. *Biol Reprod* **60**, 330-335 (1999).
95 Fru, K. N., VandeVoort, C. A. & Chaffin, C. L. Mineralocorticoid synthesis during the periovulatory interval in macaques. *Biol Reprod* **75**, 568-574 (2006).
96 Xu, F. *et al.* Dynamics of the transcriptome in the primate ovulatory follicle. *Mol Hum Reprod* **17**, 152-165 (2011).
97 Tetsuka, M. & Tanakadate, M. Activation of HSD11B1 in the bovine cumulus-oocyte complex during IVM and IVF. *Endocr Connect* **8**, 1029-1039 (2019).
98 Simerman, A. A. *et al.* Intrafollicular cortisol levels inversely correlate with cumulus cell lipid content as a possible energy source during oocyte meiotic resumption in women undergoing ovarian stimulation for in vitro fertilization. *Fertil Steril* **103**, 249-257 (2015).
99 Andersen, C. Y. & Hornnes, P. Intrafollicular concentrations of free cortisol close to follicular rupture. *Hum Reprod* **9**, 1944-1949 (1994).
100 Yong, P. Y. *et al.* Development-related increase in cortisol biosynthesis by human granulosa cells. *J Clin Endocrinol Metab* **85**, 4728-4733 (2000).
101 Tetsuka, M. Actions of glucocorticoid and their regulatory mechanisms in the ovary. *Animal Science Journal* **78**, 112-120 (2007).
102 Tetsuka, M. *et al.* Gene expression of 11beta-HSD and glucocorticoid receptor in the bovine (Bos taurus) follicle during follicular maturation and atresia: the role of follicular stimulating hormone. *J Reprod Dev* **56**, 616-622 (2010).

2923 103 Amweg, A. N. *et al.* Role of glucocorticoids in cystic ovarian disease: Expression
2924 of glucocorticoid receptor in the bovine ovary. *Cells Tissues Organs* **201**, 138-147
2925 (2016).
2926 104 Myers, M. *et al.* Role of luteal glucocorticoid metabolism during maternal
2927 recognition of pregnancy in women. *Endocrinology* **148**, 5769-5779 (2007).
2928 105 Gong, S. *et al.* Mechanisms for the species difference between mouse and pig
2929 oocytes in their sensitivity to glucorticoidsdagger. *Biol Reprod* (2017).
2930 106 Fateh, M. *et al.* Cortisol levels in human follicular fluid. *Fertil Steril* **51**, 538-541
2931 (1989).
2932 107 Michael, A. E. *et al.* Ovarian 11 beta-hydroxysteroid dehydrogenase activity is
2933 inversely related to the outcome of in vitro fertilization-embryo transfer treatment
2934 cycles. *Fertil Steril* **64**, 590-598 (1995).
2935 108 Zhang, Q. *et al.* Zebrafish cyp11c1 knockout reveals the roles of 11-
2936 ketotestosterone and cortisol in sexual development and reproduction.
2937 *Endocrinology* (2020).
2938 109 Yang, J. G., Chen, W. Y. & Li, P. S. Effects of glucocorticoids on maturation of
2939 pig oocytes and their subsequent fertilizing capacity in vitro. *Biol Reprod* **60**, 929-
2940 936 (1999).
2941 110 Irvine, R. F. How is the level of free arachidonic acid controlled in mammalian
2942 cells? *Biochem J* **204**, 3-16 (1982).
2943 111 Bauminger, A. & Lindner, H. R. Periovulatory changes in ovarian prostaglandin
2944 formation and their hormonal control in the rat. *Prostaglandins* **9**, 737-751 (1975).
2945 112 Bonney, R. C. & Wilson, C. A. Hormonal control of ovarian phospholipase A2
2946 activity in rats. *J Reprod Fertil* **99**, 201-208 (1993).
2947 113 Herschman, H. R. Regulation of prostaglandin synthase-1 and prostaglandin
2948 synthase-2. *Cancer Metastasis Rev* **13**, 241-256 (1994).
2949 114 Duffy, D. M. & Stouffer, R. L. The ovulatory gonadotrophin surge stimulates
2950 cyclooxygenase expression and prostaglandin production by the monkey follicle.
2951 *Mol Hum Reprod* **7**, 731-739 (2001).
2952 115 Armstrong, D. T. Prostaglandins and follicular functions. *J Reprod Fertil* **62**, 283-
2953 291 (1981).
2954 116 Duffy, D. M., Dozier, B. L. & Seachord, C. L. Prostaglandin dehydrogenase and
2955 prostaglandin levels in periovulatory follicles: implications for control of primate
2956 ovulation by prostaglandin E2. *J Clin Endocrinol Metab* **90**, 1021-1027 (2005).
2957 117 Kim, S. O., Harris, S. M. & Duffy, D. M. Prostaglandin E2 (EP) receptors mediate
2958 PGE2-specific events in ovulation and luteinization within primate ovarian
2959 follicles. *Endocrinology* **155**, 1466-1475 (2014).
2960 118 Peluffo, M. C. *et al.* A prostaglandin E2 receptor antagonist prevents pregnancies
2961 during a preclinical contraceptive trial with female macaques. *Hum Reprod* **29**,
2962 1400-1412 (2014).
2963 119 Duffy, D. M. Novel contraceptive targets to inhibit ovulation: the prostaglandin E2
2964 pathway. *Hum Reprod Update* **21**, 652-670 (2015).
2965 120 Tilley, S. L. *et al.* Reproductive failure and reduced blood pressure in mice lacking
2966 the EP2 prostaglandin E2 receptor. *J Clin Invest* **103**, 1539-1545 (1999).

121 Mikuni, M. *et al.* The selective prostaglandin endoperoxide synthase-2 inhibitor, NS-398, reduces prostaglandin production and ovulation in vivo and in vitro in the rat. *Biol Reprod* **59**, 1077-1083 (1998).
122 Duffy, D. M. & Stouffer, R. L. Follicular administration of a cyclooxygenase inhibitor can prevent oocyte release without alteration of normal luteal function in rhesus monkeys. *Hum Reprod* **17**, 2825-2831 (2002).
123 Choi, Y. *et al.* Coordinated regulation among progesterone, prostaglandins, and EGF-like factors in human ovulatory follicles. *J Clin Endocrinol Metab* **102**, 1971-1982 (2017).
124 Shimada, M., Umehara, T. & Hoshino, Y. Roles of epidermal growth factor (EGF)-like factor in the ovulation process. *Reprod Med Biol* **15**, 201-216 (2016).
125 Lyga, S. *et al.* Persistent cAMP Signaling by Internalized LH Receptors in Ovarian Follicles. *Endocrinology* **157**, 1613-1621 (2016).
126 Light, A. & Hammes, S. R. Membrane receptor cross talk in steroidogenesis: recent insights and clinical implications. *Steroids* **78**, 633-638 (2013).
127 Nielsen, H. K. *et al.* Diurnal rhythm in serum osteocalcin: relation with sleep, growth hormone, and PTH(1-84). *Calcif Tissue Int* **49**, 373-377 (1991).
128 Andric, N. & Ascoli, M. The luteinizing hormone receptor-activated extracellularly regulated kinase-1/2 cascade stimulates epiregulin release from granulosa cells. *Endocrinology* **149**, 5549-5556 (2008).
129 Conti, M., Hsieh, M., Park, J. Y. & Su, Y. Q. Role of the epidermal growth factor network in ovarian follicles. *Mol Endocrinol* **20**, 715-723 (2006).
130 Park, J. Y. *et al.* EGF-like growth factors as mediators of LH action in the ovulatory follicle. *Science* **303**, 682-684 (2004).
131 Hsieh, M. *et al.* Luteinizing hormone-dependent activation of the epidermal growth factor network is essential for ovulation. *Mol Cell Biol* **27**, 1914-1924 (2007).
132 Yarden, Y. & Sliwkowski, M. X. Untangling the ErbB signalling network. *Nat Rev Mol Cell Biol* **2**, 127-137 (2001).
133 Vaccari, S. *et al.* Cyclic GMP signaling is involved in the luteinizing hormone-dependent meiotic maturation of mouse oocytes. *Biol Reprod* **81**, 595-604 (2009).
134 Inoue, Y. *et al.* Amphiregulin is much more abundantly expressed than transforming growth factor-alpha and epidermal growth factor in human follicular fluid obtained from patients undergoing in vitro fertilization-embryo transfer. *Fertil Steril* **91**, 1035-1041 (2009).
135 Fan, H. Y., Liu, Z., Johnson, P. F. & Richards, J. S. CCAAT/enhancer-binding proteins (C/EBP)-alpha and -beta are essential for ovulation, luteinization, and the expression of key target genes. *Mol Endocrinol* **25**, 253-268 (2011).
136 Su, Y. Q. *et al.* Oocyte-dependent activation of mitogen-activated protein kinase (ERK1/2) in cumulus cells is required for the maturation of the mouse oocyte-cumulus cell complex. *Dev Biol* **263**, 126-138 (2003).
137 Shuhaibar, L. C. *et al.* Intercellular signaling via cyclic GMP diffusion through gap junctions restarts meiosis in mouse ovarian follicles. *Proc Natl Acad Sci U S A* **112**, 5527-5532 (2015).
138 Gilchrist, R. B. *et al.* Oocyte maturation and quality: role of cyclic nucleotides. *Reproduction* **152**, R143-157 (2016).

3012 139 Norris, R. P. *et al.* Luteinizing hormone causes MAP kinase-dependent
3013 phosphorylation and closure of connexin 43 gap junctions in mouse ovarian
3014 follicles: one of two paths to meiotic resumption. *Development* **135**, 3229-3238
3015 (2008).
3016 140 Moore, R. K., Otsuka, F. & Shimasaki, S. Role of ERK1/2 in the differential
3017 synthesis of progesterone and estradiol by granulosa cells. *Biochem Biophys Res*
3018 *Commun* **289**, 796-800 (2001).
3019 141 Tsafriri, A. Ovulation as a tissue remodelling process. Proteolysis and cumulus
3020 expansion. *Adv Exp Med Biol* **377**, 121-140 (1995).
3021 142 Buscher, U., Chen, F. C., Kentenich, H. & Schmiady, H. Cytokines in the follicular
3022 fluid of stimulated and non-stimulated human ovaries; is ovulation a suppressed
3023 inflammatory reaction? *Hum Reprod* **14**, 162-166 (1999).
3024 143 De Matos, D. G. *et al.* Leukemia inhibitory factor induces cumulus expansion in
3025 immature human and mouse oocytes and improves mouse two-cell rate and delivery
3026 rates when it is present during mouse in vitro oocyte maturation. *Fertil Steril* **90**,
3027 2367-2375 (2008).
3028 144 Murphy, M. J., Halow, N. G., Royer, P. A. & Hennebold, J. D. Leukemia inhibitory
3029 factor is necessary for ovulation in female rhesus macaques. *Endocrinology* **157**,
3030 4378-4387 (2016).
3031 145 Arici, A. *et al.* Interleukin-8 expression and modulation in human preovulatory
3032 follicles and ovarian cells. *Endocrinology* **137**, 3762-3769 (1996).
3033 146 Ujioka, T. *et al.* Interleukin-8 as an essential factor in the human chorionic
3034 gonadotropin-induced rabbit ovulatory process: interleukin-8 induces neutrophil
3035 accumulation and activation in ovulation. *Biol Reprod* **58**, 526-530 (1998).
3036 147 Hellberg, P. & Norstrom, A. Bradykinin induces contractions of the human ovarian
3037 follicular wall in vitro. *Hum Reprod* **5**, 387-390 (1990).
3038 148 Larson, L. *et al.* Regulation of prostaglandin biosynthesis by luteinizing hormone
3039 and bradykinin in rat preovulatory follicles in vitro. *Prostaglandins* **41**, 111-121
3040 (1991).
3041 149 Espey, L. L. Current status of the hypothesis that mammalian ovulation is
3042 comparable to an inflammatory reaction. *Biol Reprod* **50**, 233-238 (1994).
3043 150 Acosta, T. J. & Miyamoto, A. Vascular control of ovarian function: ovulation,
3044 corpus luteum formation and regression. *Anim Reprod Sci* **82-83**, 127-140 (2004).
3045 151 Stouffer, R. L., Xu, F. & Duffy, D. M. Molecular control of ovulation and
3046 luteinization in the primate follicle. *Front Biosci* **12**, 297-307 (2007).
3047 152 Boots, C. E. & Jungheim, E. S. Inflammation and human ovarian follicular
3048 dynamics. *Semin Reprod Med* **33**, 270-275 (2015).
3049 153 Trau, H. A., Davis, J. S. & Duffy, D. M. Angiogenesis in the primate ovulatory
3050 follicle is stimulated by luteinizing hormone via prostaglandin E2. *Biol Reprod* **92**,
3051 15 (2015).
3052 154 Trau, H. A., Brannstrom, M., Curry, T. E., Jr. & Duffy, D. M. Prostaglandin E2 and
3053 vascular endothelial growth factor A mediate angiogenesis of human ovarian
3054 follicular endothelial cells. *Hum Reprod* **31**, 436-444 (2016).
3055 155 Migone, F. F. *et al.* In vivo imaging reveals an essential role of vasoconstriction in
3056 rupture of the ovarian follicle at ovulation. *Proc Natl Acad Sci U S A* **113**, 2294-
3057 2299 (2016).

3058 156 Mauro, A. *et al.* Effect of antiprogesterone RU486 on VEGF expression and blood
3059 vessel remodeling on ovarian follicles before ovulation. *PLoS One* **9**, e95910
3060 (2014).
3061 157 Kim, S. O., Trau, H. A. & Duffy, D. M. Vascular endothelial growth factors C and
3062 D may promote angiogenesis in the primate ovulatory follicle. *Biol Reprod* **96**, 389-
3063 400 (2017).
3064 158 Hazzard, T. M., Xu, F. & Stouffer, R. L. Injection of soluble vascular endothelial
3065 growth factor receptor 1 into the preovulatory follicle disrupts ovulation and
3066 subsequent luteal function in rhesus monkeys. *Biol Reprod* **67**, 1305-1312 (2002).
3067 159 Xu, F. *et al.* Intraovarian actions of anti-angiogenic agents disrupt periovulatory
3068 events during the menstrual cycle in monkeys. *Contraception* **71**, 239-248 (2005).
3069 160 Xu, F. & Stouffer, R. L. Local delivery of angiopoietin-2 into the preovulatory
3070 follicle terminates the menstrual cycle in rhesus monkeys. *Biol Reprod* **72**, 1352-
3071 1358 (2005).
3072 161 Hua, V. K., Fleming, S. D. & Illingworth, P. Effects of protein kinase A and C
3073 inhibitors on follicular inhibin and activin during ovulation. *Reprod Biomed Online*
3074 **17**, 642-651 (2008).
3075 162 Chotiner, J. Y., Wolgemuth, D. J. & Wang, P. J. Functions of cyclins and CDKs in
3076 mammalian gametogenes is dagger. *Biol Reprod* **101**, 591-601 (2019).
3077 163 Shimada, M. Regulation of oocyte meiotic maturation by somatic cells. *Reprod*
3078 *Med Biol* **11**, 177-184 (2012).
3079 164 Egbert, J. R. *et al.* Luteinizing hormone causes phosphorylation and activation of
3080 the cGMP phosphodiesterase PDE5 in rat ovarian follicles, contributing, together
3081 with PDE1 activity, to the resumption of meiosis. *Biol Reprod* **94**, 110 (2016).
3082 165 Fan, H. Y. *et al.* Protein kinase C and mitogen-activated protein kinase cascade in
3083 mouse cumulus cells: cross talk and effect on meiotic resumption of oocyte. *Biol*
3084 *Reprod* **70**, 1178-1187 (2004).
3085 166 El-Hayek, S. & Clarke, H. J. Control of oocyte growth and development by
3086 intercellular communication within the follicular niche. *Results Probl Cell Differ*
3087 **58**, 191-224 (2016).
3088 167 McGrath, S. A., Esquela, A. F. & Lee, S. J. Oocyte-specific expression of
3089 growth/differentiation factor-9. *Mol Endocrinol* **9**, 131-136 (1995).
3090 168 Dong, J. *et al.* Growth differentiation factor-9 is required during early ovarian
3091 folliculogenesis. *Nature* **383**, 531-535 (1996).
3092 169 Yan, C. *et al.* Synergistic roles of bone morphogenetic protein 15 and growth
3093 differentiation factor 9 in ovarian function. *Mol Endocrinol* **15**, 854-866 (2001).
3094 170 McIntosh, C. J. *et al.* The proregion of mouse BMP15 regulates the cooperative
3095 interactions of BMP15 and GDF9. *Biol Reprod* **79**, 889-896 (2008).
3096 171 Chaves, R. N., de Matos, M. H., Buratini, J., Jr. & de Figueiredo, J. R. The
3097 fibroblast growth factor family: involvement in the regulation of folliculogenesis.
3098 *Reprod Fertil Dev* **24**, 905-915 (2012).
3099 172 McLaughlin, M., Kinnell, H. L., Anderson, R. A. & Telfer, E. E. Inhibition of
3100 phosphatase and tensin homologue (PTEN) in human ovary in vitro results in
3101 increased activation of primordial follicles but compromises development of
3102 growing follicles. *Mol Hum Reprod* **20**, 736-744 (2014).

173 Kawashima, I. & Kawamura, K. Regulation of follicle growth through hormonal factors and mechanical cues mediated by Hippo signaling pathway. *Syst Biol Reprod Med* **64**, 3-11 (2018).
174 Tscherner, A. *et al.* STAT3 signaling stimulates miR-21 expression in bovine cumulus cells during in vitro oocyte maturation. *Sci Rep* **8**, 11527 (2018).
175 Cakmak, H. *et al.* Dynamic secretion during meiotic reentry integrates the function of the oocyte and cumulus cells. *Proc Natl Acad Sci U S A* **113**, 2424-2429 (2016).
176 Wen, X. *et al.* Estradiol, progesterone, testosterone profiles in human follicular fluid and cultured granulosa cells from luteinized pre-ovulatory follicles. *Reprod Biol Endocrinol* **8**, 117 (2010).
177 Richard, S. & Baltz, J. M. Preovulatory suppression of mouse oocyte cell volume-regulatory mechanisms is via signalling that is distinct from meiotic arrest. *Sci Rep* **7**, 702 (2017).
178 Gilula, N. B., Epstein, M. L. & Beers, W. H. Cell-to-cell communication and ovulation. A study of the cumulus-oocyte complex. *J Cell Biol* **78**, 58-75 (1978).
179 Revelli, A. *et al.* Follicular fluid content and oocyte quality: from single biochemical markers to metabolomics. *Reprod Biol Endocrinol* **7**, 40 (2009).
180 Stouffer, R. L. & Zelinski-Wooten, M. B. Overriding follicle selection in controlled ovarian stimulation protocols: quality vs quantity. *Reprod Biol Endocrinol* **2**, 32 (2004).
181 Lindner, C. *et al.* Endocrine parameters of human follicular fluid and fertilization capacity of oocytes. *Horm Metab Res* **20**, 243-246 (1988).
182 Baart, E. B., Macklon, N. S. & Fauser, B. J. Ovarian stimulation and embryo quality. *Reprod Biomed Online* **18 Suppl 2**, 45-50 (2009).
183 Macklon, N. S., Stouffer, R. L., Giudice, L. C. & Fauser, B. C. The science behind 25 years of ovarian stimulation for in vitro fertilization. *Endocr Rev* **27**, 170-207 (2006).
184 Robker, R. L. Evidence that obesity alters the quality of oocytes and embryos. *Pathophysiology* **15**, 115-121 (2008).
185 Purcell, S. H. & Moley, K. H. The impact of obesity on egg quality. *J Assist Reprod Genet* **28**, 517-524 (2011).
186 True, C. A. *et al.* Chronic combined hyperandrogenemia and western-style diet in young female rhesus macaques causes greater metabolic impairments compared to either treatment alone. *Hum Reprod* **32**, 1880-1891 (2017).
187 Norman, R. J., Chura, L. R. & Robker, R. L. Effects of obesity on assisted reproductive technology outcomes. *Fertil Steril* **89**, 1611-1612 (2008).
188 Luzzo, K. M. *et al.* High fat diet induced developmental defects in the mouse: oocyte meiotic aneuploidy and fetal growth retardation/brain defects. *PLoS One* **7**, e49217 (2012).
189 Grindler, N. M. & Moley, K. H. Maternal obesity, infertility and mitochondrial dysfunction: potential mechanisms emerging from mouse model systems. *Mol Hum Reprod* **19**, 486-494 (2013).
190 Bishop, C. V. *et al.* Western-style diet, with and without chronic androgen treatment, alters the number, structure, and function of small antral follicles in ovaries of young adult monkeys. *Fertil Steril* **105**, 1023-1034 (2016).

191 Flegal, K. M., Carroll, M. D., Kit, B. K. & Ogden, C. L. Prevalence of obesity and trends in the distribution of body mass index among US adults, 1999-2010. *JAMA* **307**, 491-497 (2012).

192 Fauser, B. C. *et al.* Consensus on women's health aspects of polycystic ovary syndrome (PCOS): the Amsterdam ESHRE/ASRM-Sponsored 3rd PCOS Consensus Workshop Group. *Fertil Steril* **97**, 28-38 e25 (2012).

193 Legro, R. S. *et al.* Diagnosis and treatment of polycystic ovary syndrome: an Endocrine Society clinical practice guideline. *J Clin Endocrinol Metab* **98**, 4565-4592 (2013).

194 Rotterdam, E. A.-S. P. C. W. G. Revised 2003 consensus on diagnostic criteria and long-term health risks related to polycystic ovary syndrome. *Fertil Steril* **81**, 19-25 (2004).

195 Dunaif, A. & Finegood, D. T. Beta-cell dysfunction independent of obesity and glucose intolerance in the polycystic ovary syndrome. *J Clin Endocrinol Metab* **81**, 942-947 (1996).

196 Barthelmess, E. K. & Naz, R. K. Polycystic ovary syndrome: current status and future perspective. *Front Biosci (Elite Ed)* **6**, 104-119 (2014).

197 Phillips, K. A. *et al.* Why primate models matter. *Am J Primatol* **76**, 801-827 (2014).

198 Binelli, M. & Murphy, B. D. Coordinated regulation of follicle development by germ and somatic cells. *Reprod Fertil Dev* **22**, 1-12 (2010).

199 Gilchrist, R. B., Lane, M. & Thompson, J. G. Oocyte-secreted factors: regulators of cumulus cell function and oocyte quality. *Hum Reprod Update* **14**, 159-177 (2008).

200 Anderson, E. & Albertini, D. F. Gap junctions between the oocyte and companion follicle cells in the mammalian ovary. *J Cell Biol* **71**, 680-686 (1976).

201 Gardner, D. K. & Balaban, B. Assessment of human embryo development using morphological criteria in an era of time-lapse, algorithms and 'OMICS': is looking good still important? *Mol Hum Reprod* **22**, 704-718 (2016).

202 Rodgaard, T., Heegaard, P. M. & Callesen, H. Non-invasive assessment of in-vitro embryo quality to improve transfer success. *Reprod Biomed Online* **31**, 585-592 (2015).

203 Brison, D. R. *et al.* Identification of viable embryos in IVF by non-invasive measurement of amino acid turnover. *Hum Reprod* **19**, 2319-2324 (2004).

204 Houghton, F. D. & Leese, H. J. Metabolism and developmental competence of the preimplantation embryo. *Eur J Obstet Gynecol Reprod Biol* **115 Suppl 1**, S92-96 (2004).

205 Houghton, F. D. *et al.* Non-invasive amino acid turnover predicts human embryo developmental capacity. *Hum Reprod* **17**, 999-1005 (2002).

206 Wallace, M. *et al.* (1)H NMR based metabolic profiling of day 2 spent embryo media correlates with implantation potential. *Syst Biol Reprod Med* **60**, 58-63 (2014).

207 Seli, E. *et al.* Noninvasive metabolomic profiling of embryo culture media using Raman and near-infrared spectroscopy correlates with reproductive potential of embryos in women undergoing in vitro fertilization. *Fertil Steril* **88**, 1350-1357 (2007).

208 Seli, E. *et al.* Noninvasive metabolomic profiling as an adjunct to morphology for noninvasive embryo assessment in women undergoing single embryo transfer. *Fertil Steril* **94**, 535-542 (2010).
209 Picton, H. M. *et al.* Association between amino acid turnover and chromosome aneuploidy during human preimplantation embryo development in vitro. *Mol Hum Reprod* **16**, 557-569 (2010).
210 Castiglione Morelli, M. A. *et al.* NMR metabolic profiling of follicular fluid for investigating the different causes of female infertility: a pilot study. *Metabolomics* **15**, 19 (2019).
211 Bellver, J. *et al.* Day-3 embryo metabolomics in the spent culture media is altered in obese women undergoing in vitro fertilization. *Fertil Steril* **103**, 1407-1415 e1401 (2015).
212 de la Barca, J. M. C. *et al.* Targeted metabolomics reveals reduced levels of polyunsaturated choline plasmalogens and a smaller dimethylarginine/arginine ratio in the follicular fluid of patients with a diminished ovarian reserve. *Hum Reprod* **32**, 2269-2278 (2017).
213 Shen, X. *et al.* Proteomic analysis of human follicular fluid associated with successful in vitro fertilization. *Reprod Biol Endocrinol* **15**, 58 (2017).
214 Ruebel, M. L. *et al.* Transcriptome analysis of rhesus monkey failed-to-mature oocytes: deficiencies in transcriptional regulation and cytoplasmic maturation of the oocyte mRNA population. *Mol Hum Reprod* (2018).
215 Wang, X. *et al.* Transcriptome analyses of rhesus monkey preimplantation embryos reveal a reduced capacity for DNA double-strand break repair in primate oocytes and early embryos. *Genome Res* **27**, 567-579 (2017).
216 Lanzendorf, S. E. *et al.* Collection and quality of rhesus monkey semen. *Mol Reprod Dev* **25**, 61-66 (1990).
217 Evans, A. M. *et al.* Integrated, nontargeted ultrahigh performance liquid chromatography/electrospray ionization tandem mass spectrometry platform for the identification and relative quantification of the small-molecule complement of biological systems. *Anal Chem* **81**, 6656-6667 (2009).
218 Bishop, C. V. *et al.* Chronically elevated androgen and/or consumption of a Western-style diet impairs oocyte quality and granulosa cell function in the nonhuman primate periovulatory follicle. *J Assist Reprod Genet* **36**, 1497-1511 (2019).
219 Young, K. A., Chaffin, C. L., Molskness, T. A. & Stouffer, R. L. Controlled ovulation of the dominant follicle: a critical role for LH in the late follicular phase of the menstrual cycle. *Hum Reprod* **18**, 2257-2263 (2003).
220 Peluffo, M. C. *et al.* Systematic analysis of protease gene expression in the rhesus macaque ovulatory follicle: metalloproteinase involvement in follicle rupture. *Endocrinology* **152**, 3963-3974 (2011).
221 Foygel, K. *et al.* A novel and critical role for Oct4 as a regulator of the maternal-embryonic transition. *PLoS One* **3**, e4109 (2008).
222 Krendl, C. *et al.* GATA2/3-TFAP2A/C transcription factor network couples human pluripotent stem cell differentiation to trophectoderm with repression of pluripotency. *Proc Natl Acad Sci U S A* **114**, E9579-E9588 (2017).

3239 223 Wigglesworth, K. *et al.* Bidirectional communication between oocytes and ovarian
3240 follicular somatic cells is required for meiotic arrest of mammalian oocytes. *Proc*
3241 *Natl Acad Sci U S A* **110**, E3723-3729 (2013).
3242 224 Eppig, J. J. *et al.* Oocyte control of granulosa cell development: how and why. *Hum*
3243 *Reprod* **12**, 127-132 (1997).
3244 225 Dumesic, D. A. *et al.* Oocyte environment: follicular fluid and cumulus cells are
3245 critical for oocyte health. *Fertil Steril* **103**, 303-316 (2015).
3246 226 Wittmaack, F. M. *et al.* Effect of follicular size on oocyte retrieval, fertilization,
3247 cleavage, and embryo quality in in vitro fertilization cycles: a 6-year data
3248 collection. *Fertil Steril* **62**, 1205-1210 (1994).
3249 227 Wirleitner, B. *et al.* Relationship between follicular volume and oocyte
3250 competence, blastocyst development and live-birth rate: optimal follicle size for
3251 oocyte retrieval. *Ultrasound Obstet Gynecol* **51**, 118-125 (2018).
3252 228 Edwards, R. G. Follicular fluid. *J Reprod Fertil* **37**, 189-219 (1974).
3253 229 Emwas, A. H. The strengths and weaknesses of NMR spectroscopy and mass
3254 spectrometry with particular focus on metabolomics research. *Methods Mol Biol*
3255 **1277**, 161-193 (2015).
3256 230 Nagy, B. *et al.* Follicular fluid progesterone concentration is associated with
3257 fertilization outcome after IVF: a systematic review and meta-analysis.
3258 *Reproductive BioMedicine Online* **00**, 1-12 (2019).
3259 231 Leese, H. J. *et al.* Metabolism of the viable mammalian embryo: quietness revisited.
3260 *Mol Hum Reprod* **14**, 667-672 (2008).
3261 232 Borland, R. M., Biggers, J. D., Lechene, C. P. & Taymor, M. L. Elemental
3262 composition of fluid in the human Fallopian tube. *J Reprod Fertil* **58**, 479-482
3263 (1980).
3264 233 Lee, E. S. *et al.* Promoting effect of amino acids added to a chemically defined
3265 medium on blastocyst formation and blastomere proliferation of bovine embryos
3266 cultured in vitro. *Anim Reprod Sci* **84**, 257-267 (2004).
3267 234 Conaghan, J. *et al.* Selection criteria for human embryo transfer: a comparison of
3268 pyruvate uptake and morphology. *J Assist Reprod Genet* **10**, 21-30 (1993).
3269 235 Gardner, D. K., Lane, M., Stevens, J. & Schoolcraft, W. B. Noninvasive assessment
3270 of human embryo nutrient consumption as a measure of developmental potential.
3271 *Fertil Steril* **76**, 1175-1180 (2001).
3272 236 Leese, H. J. Quiet please, do not disturb: a hypothesis of embryo metabolism and
3273 viability. *Bioessays* **24**, 845-849 (2002).
3274 237 Acosta, T. J. *et al.* In vivo evidence that local cortisol production increases in the
3275 preovulatory follicle of the cow. *J Reprod Dev* **51**, 483-489 (2005).
3276 238 Tetsuka, M. *et al.* Glucocorticoid metabolism in the bovine cumulus-oocyte
3277 complex matured in vitro. *Reproduction* **151**, 73-82 (2016).
3278 239 Tetsuka, M. *et al.* Differential expression of messenger ribonucleic acids encoding
3279 11beta-hydroxysteroid dehydrogenase types 1 and 2 in human granulosa cells. *J*
3280 *Clin Endocrinol Metab* **82**, 2006-2009 (1997).
3281 240 Schreiber, J. R., Nakamura, K. & Erickson, G. F. Rat ovary glucocorticoid receptor:
3282 identification and characterization. *Steroids* **39**, 569-584 (1982).

3283 241 Cikos, S. *et al.* Glucocorticoid receptor isoforms and effects of glucocorticoids in
3284 ovulated mouse oocytes and preimplantation embryosdagger. *Biol Reprod* **100**,
3285 351-364 (2019).
3286 242 Oakley, R. H. & Cidlowski, J. A. The biology of the glucocorticoid receptor: new
3287 signaling mechanisms in health and disease. *J Allergy Clin Immunol* **132**, 1033-
3288 1044 (2013).
3289 243 Tsuiko, O. *et al.* Genome stability of bovine in vivo-conceived cleavage-stage
3290 embryos is higher compared to in vitro-produced embryos. *Hum Reprod* **32**, 2348-
3291 2357 (2017).
3292 244 Treff, N. R. *et al.* Next generation sequencing-based comprehensive chromosome
3293 screening in mouse polar bodies, oocytes, and embryos. *Biol Reprod* **94**, 76 (2016).
3294 245 Fadini, R. *et al.* Oocyte in vitro maturation in normo-ovulatory women. *Fertil Steril*
3295 **99**, 1162-1169 (2013).
3296 246 Hatirnaz, S. *et al.* Oocyte in vitro maturation: A sytematic review. *Turk J Obstet*
3297 *Gynecol* **15**, 112-125 (2018).
3298 247 Yoon, H. G. *et al.* Pregnancies resulting from in vitro matured oocytes collected
3299 from women with regular menstrual cycle. *J Assist Reprod Genet* **18**, 325-329
3300 (2001).
3301 248 Hess, K. A., Chen, L. & Larsen, W. J. Inter-alpha-inhibitor binding to hyaluronan
3302 in the cumulus extracellular matrix is required for optimal ovulation and
3303 development of mouse oocytes. *Biol Reprod* **61**, 436-443 (1999).
3304 249 Massey, A. J. *et al.* The association of physiological cortisol and IVF treatment
3305 outcomes: a systematic review. *Reprod Med Biol* **13**, 161-176 (2014).
3306 250 Lewicka, S. *et al.* Cortisol and cortisone in human follicular fluid and serum and
3307 the outcome of IVF treatment. *Hum Reprod* **18**, 1613-1617 (2003).
3308 251 Michael, A. E. *et al.* Relationship between ovarian cortisol:cortisone ratios and the
3309 clinical outcome of in vitro fertilization and embryo transfer (IVF-ET). *Clin*
3310 *Endocrinol (Oxf)* **51**, 535-540 (1999).
3311 252 Seravalle, G. & Grassi, G. Obesity and hypertension. *Pharmacol Res* **122**, 1-7
3312 (2017).
3313 253 Mikhail, N., Golub, M. S. & Tuck, M. L. Obesity and hypertension. *Prog*
3314 *Cardiovasc Dis* **42**, 39-58 (1999).
3315 254 Olsovsky, J. [Obesity and diabetes]. *Vnitr Lek* **49**, 956-959 (2003).
3316 255 Kulkarni, K., Karssiens, T., Kumar, V. & Pandit, H. Obesity and osteoarthritis.
3317 *Maturitas* **89**, 22-28 (2016).
3318 256 Jantaratnotai, N., Mosikanon, K., Lee, Y. & McIntyre, R. S. The interface of
3319 depression and obesity. *Obes Res Clin Pract* **11**, 1-10 (2017).
3320 257 Best, D. & Bhattacharya, S. Obesity and fertility. *Horm Mol Biol Clin Investig* **24**,
3321 5-10 (2015).
3322 258 Minge, C. E., Bennett, B. D., Norman, R. J. & Robker, R. L. Peroxisome
3323 proliferator-activated receptor-gamma agonist rosiglitazone reverses the adverse
3324 effects of diet-induced obesity on oocyte quality. *Endocrinology* **149**, 2646-2656
3325 (2008).
3326 259 Broughton, D. E. & Moley, K. H. Obesity and female infertility: potential mediators
3327 of obesity's impact. *Fertil Steril* **107**, 840-847 (2017).

3328 260 Wise, L. A. *et al.* An internet-based prospective study of body size and time-to-
3329 pregnancy. *Hum Reprod* **25**, 253-264 (2010).
3330 261 Gesink Law, D. C., Maclehose, R. F. & Longnecker, M. P. Obesity and time to
3331 pregnancy. *Hum Reprod* **22**, 414-420 (2007).
3332 262 Klenov, V. E. & Jungheim, E. S. Obesity and reproductive function: a review of
3333 the evidence. *Curr Opin Obstet Gynecol* **26**, 455-460 (2014).
3334 263 Fedorcsak, P. *et al.* Impact of overweight and underweight on assisted reproduction
3335 treatment. *Hum Reprod* **19**, 2523-2528 (2004).
3336 264 Practice Committee of American Society for Reproductive, M. Obesity and
3337 reproduction: an educational bulletin. *Fertil Steril* **90**, S21-29 (2008).
3338 265 Maheshwari, A., Stofberg, L. & Bhattacharya, S. Effect of overweight and obesity
3339 on assisted reproductive technology--a systematic review. *Hum Reprod Update* **13**,
3340 433-444 (2007).
3341 266 Carrell, D. T. *et al.* Body mass index is inversely related to intrafollicular HCG
3342 concentrations, embryo quality and IVF outcome. *Reprod Biomed Online* **3**, 109-
3343 111 (2001).
3344 267 Metwally, M. *et al.* Effect of increased body mass index on oocyte and embryo
3345 quality in IVF patients. *Reprod Biomed Online* **15**, 532-538 (2007).
3346 268 Xue, X. *et al.* Cumulative live birth rates according to maternal body mass index
3347 after first ovarian stimulation for in vitro fertilization: a single center analysis of
3348 14,782 patients. *Frontiers in Endocrinology* **11** (2020).
3349 269 Luke, B. *et al.* The effect of increasing obesity on the response to and outcome of
3350 assisted reproductive technology: a national study. *Fertil Steril* **96**, 820-825 (2011).
3351 270 Wu, L. L. *et al.* Mitochondrial dysfunction in oocytes of obese mothers:
3352 transmission to offspring and reversal by pharmacological endoplasmic reticulum
3353 stress inhibitors. *Development* **142**, 681-691 (2015).
3354 271 Jungheim, E. S. *et al.* Diet-induced obesity model: abnormal oocytes and persistent
3355 growth abnormalities in the offspring. *Endocrinology* **151**, 4039-4046 (2010).
3356 272 Stouffer, R. L. & Woodruff, T. K. Nonhuman Primates: A Vital Model for Basic
3357 and Applied Research on Female Reproduction, Prenatal Development, and
3358 Women's Health. *ILAR J* **58**, 281-294 (2017).
3359 273 Cheung, C. Y., Roberts, V. H. J., Frias, A. E. & Brace, R. A. Effects of maternal
3360 western-style diet on amniotic fluid volume and amnion VEGF profiles in a
3361 nonhuman primate model. *Physiol Rep* **6**, e13894 (2018).
3362 274 Yazdi, A. S. & Ghoreschi, K. The Interleukin-1 Family. *Adv Exp Med Biol* **941**, 21-
3363 29 (2016).
3364 275 Beck, I. M. *et al.* Crosstalk in inflammation: the interplay of glucocorticoid
3365 receptor-based mechanisms and kinases and phosphatases. *Endocr Rev* **30**, 830-882
3366 (2009).
3367 276 Baschant, U. & Tuckermann, J. The role of the glucocorticoid receptor in
3368 inflammation and immunity. *J Steroid Biochem Mol Biol* **120**, 69-75 (2010).
3369 277 Wong, C. C. *et al.* Non-invasive imaging of human embryos before embryonic
3370 genome activation predicts development to the blastocyst stage. *Nat Biotechnol* **28**,
3371 1115-1121 (2010).
3372 278 Chen, A. A. *et al.* Biomarkers identified with time-lapse imaging: discovery,
3373 validation, and practical application. *Fertil Steril* **99**, 1035-1043 (2013).

279 Leary, C., Leese, H. J. & Sturmey, R. G. Human embryos from overweight and obese women display phenotypic and metabolic abnormalities. *Hum Reprod* **30**, 122-132 (2015).
280 Robker, R. L. *et al.* Obese women exhibit differences in ovarian metabolites, hormones, and gene expression compared with moderate-weight women. *J Clin Endocrinol Metab* **94**, 1533-1540 (2009).
281 McCurdy, C. E. *et al.* Maternal high-fat diet triggers lipotoxicity in the fetal livers of nonhuman primates. *J Clin Invest* **119**, 323-335 (2009).
282 Grant, W. F. *et al.* Perinatal exposure to a high-fat diet is associated with reduced hepatic sympathetic innervation in one-year old male Japanese macaques. *PLoS One* **7**, e48119 (2012).
283 Hariri, N. & Thibault, L. High-fat diet-induced obesity in animal models. *Nutr Res Rev* **23**, 270-299 (2010).
284 Segovia, S. A., Vickers, M. H., Gray, C. & Reynolds, C. M. Maternal obesity, inflammation, and developmental programming. *Biomed Res Int* **2014**, 418975 (2014).
285 Lewicka, S. *et al.* Cortisol and cortisone in human follicular fluid and serum and the outcome of IVF treatment. *Human Reproduction* **18**, 1613-1617 (2003).
286 Hoyer, K. K., Dooms, H., Barron, L. & Abbas, A. K. Interleukin-2 in the development and control of inflammatory disease. *Immunol Rev* **226**, 19-28 (2008).
287 Kasson, B. G. & Gorospe, W. C. Effects of interleukins 1, 2 and 3 on follicle-stimulating hormone-induced differentiation of rat granulosa cells. *Mol Cell Endocrinol* **62**, 103-111 (1989).
288 Rajagopala Raja, C. A., Spicer, L. J. & Stewart, R. E. Interleukin-2 affects steroidogenesis and numbers of bovine ovarian granulosa cells but not thecal cellsin vitro. *Endocrine* **3**, 899-905 (1995).
289 Wang, L. J., Robertson, S., Seamark, R. F. & Norman, R. J. Lymphokines, including interleukin-2, alter gonadotropin-stimulated progesterone production and proliferation of human granulosa-luteal cells in vitro. *J Clin Endocrinol Metab* **72**, 824-831 (1991).
290 Wang, L. J. & Norman, R. J. Concentrations of immunoreactive interleukin-1 and interleukin-2 in human preovulatory follicular fluid. *Hum Reprod* **7**, 147-150 (1992).
291 Orvieto, R., Dratviman-Storobinsky, O. & Cohen, Y. Interleukin-2 production by cultured human granulosa cells. *Am J Reprod Immunol* **74**, 392-397 (2015).
292 Qi, S. T. *et al.* Arrested human embryos are more likely to have abnormal chromosomes than developing embryos from women of advanced maternal age. *J Ovarian Res* **7**, 65 (2014).
293 McCoy, R. C. *et al.* Tripolar chromosome segregation drives the association between maternal genotype at variants spanning PLK4 and aneuploidy in human preimplantation embryos. *Hum Mol Genet* **27**, 2573-2585 (2018).
294 Chamayou, S. *et al.* The use of morphokinetic parameters to select all embryos with full capacity to implant. *J Assist Reprod Genet* **30**, 703-710 (2013).
295 Hlinka, D. *et al.* Time-lapse cleavage rating predicts human embryo viability. *Physiol Res* **61**, 513-525 (2012).

3419 296 Ottolini, C. S. *et al.* Tripolar mitosis and partitioning of the genome arrests human
3420 preimplantation development in vitro. *Sci Rep* **7**, 9744 (2017).
3421 297 Edel, M. J. *et al.* Rem2 GTPase maintains survival of human embryonic stem cells
3422 as well as enhancing reprogramming by regulating p53 and cyclin D1. *Genes Dev*
3423 **24**, 561-573 (2010).
3424 298 Chang, T. C. *et al.* The expansion of the PRAME gene family in Eutheria. *PLoS*
3425 *One* **6**, e16867 (2011).
3426 299 Kim, J. *et al.* Imprinting and evolution of two Kruppel-type zinc-finger genes,
3427 ZIM3 and ZNF264, located in the PEG3/USP29 imprinted domain. *Genomics* **77**,
3428 91-98 (2001).
3429 300 Igosheva, N. *et al.* Maternal diet-induced obesity alters mitochondrial activity and
3430 redox status in mouse oocytes and zygotes. *PLoS One* **5**, e10074 (2010).
3431 301 Dumollard, R., Duchen, M. & Carroll, J. The role of mitochondrial function in the
3432 oocyte and embryo. *Curr Top Dev Biol* **77**, 21-49 (2007).
3433 302 Park, S., Kamegai, J. & Kineman, R. D. Role of glucocorticoids in the regulation
3434 of pituitary somatostatin receptor subtype (sst1-sst5) mRNA levels: evidence for
3435 direct and somatostatin-mediated effects. *Neuroendocrinology* **78**, 163-175 (2003).
3436 303 Kioussi, C. *et al.* Identification of a Wnt/Dvl/beta-Catenin --> Pitx2 pathway
3437 mediating cell-type-specific proliferation during development. *Cell* **111**, 673-685
3438 (2002).
3439 304 Lu, Y. C. *et al.* Structural Basis of Latrophilin-FLRT-UNC5 Interaction in Cell
3440 Adhesion. *Structure* **23**, 1678-1691 (2015).
3441 305 Assou, S. *et al.* Transcriptome analysis during human trophectoderm specification
3442 suggests new roles of metabolic and epigenetic genes. *PLoS One* **7**, e39306 (2012).
3443 306 Graham, S. J. *et al.* BMP signalling regulates the pre-implantation development of
3444 extra-embryonic cell lineages in the mouse embryo. *Nat Commun* **5**, 5667 (2014).
3445 307 Kitamura, K. *et al.* Mouse Pitx2 deficiency leads to anomalies of the ventral body
3446 wall, heart, extra- and periocular mesoderm and right pulmonary isomerism.
3447 *Development* **126**, 5749-5758 (1999).
3448 308 Fedorcsak, P. *et al.* Obesity is a risk factor for early pregnancy loss after IVF or
3449 ICSI. *Acta Obstet Gynecol Scand* **79**, 43-48 (2000).
3450 309 Bishop, C. V. *et al.* Chronic hyperandrogenemia and western-style diet beginning
3451 at puberty reduces fertility and increases metabolic dysfunction during pregnancy
3452 in young adult, female macaques. *Hum Reprod* **33**, 694-705 (2018).
3453 310 Kuo, K. *et al.* Maternal high-fat diet consumption and chronic hyperandrogenemia
3454 are associated with placental dysfunction in female rhesus macaques.
3455 *Endocrinology* **160**, 1937-1949 (2019).
3456 311 Bishop, C. V. *et al.* Chronic hyperandrogenemia in the presence and absence of a
3457 western-style diet impairs ovarian and uterine structure/function in young adult
3458 rhesus monkeys. *Hum Reprod* **33**, 128-139 (2018).
3459 312 Huang, C. C. *et al.* Symptom patterns and phenotypic subgrouping of women with
3460 polycystic ovary syndrome: association between endocrine characteristics and
3461 metabolic aberrations. *Hum Reprod* **30**, 937-946 (2015).
3462 313 Vera-Rodriguez, M. *et al.* Prediction model for aneuploidy in early human embryo
3463 development revealed by single-cell analysis. *Nat Commun* **6**, 7601 (2015).

314 Cardozo, E. R. *et al.* Reproductive outcomes in oocyte donation cycles are associated with donor BMI. *Hum Reprod* **31**, 385-392 (2016).

315 Provost, M. P. *et al.* Pregnancy outcomes decline with increasing body mass index: analysis of 239,127 fresh autologous in vitro fertilization cycles from the 2008-2010 Society for Assisted Reproductive Technology registry. *Fertil Steril* **105**, 663-669 (2016).

316 Goodarzi, M. O., Dumesic, D. A., Chazenbalk, G. & Azziz, R. Polycystic ovary syndrome: etiology, pathogenesis and diagnosis. *Nat Rev Endocrinol* **7**, 219-231 (2011).

317 Escobar-Morreale, H. F. Polycystic ovary syndrome: definition, aetiology, diagnosis and treatment. *Nat Rev Endocrinol* **14**, 270-284 (2018).

318 Rothenberg, S. S. *et al.* Polycystic ovary syndrome in adolescents. *Best Pract Res Clin Obstet Gynaecol* **48**, 103-114 (2018).

319 Rosenfield, R. L. & Ehrmann, D. A. The pathogenesis of polycystic ovary syndrome (PCOS): the hypothesis of PCOS as functional ovarian hyperandrogenism revisited. *Endocr Rev* **37**, 467-520 (2016).

320 Sam, S. & Dunaif, A. Polycystic ovary syndrome: syndrome XX? *Trends Endocrinol Metab* **14**, 365-370 (2003).

321 Dumesic, D. A. *et al.* Scientific Statement on the Diagnostic Criteria, Epidemiology, Pathophysiology, and Molecular Genetics of Polycystic Ovary Syndrome. *Endocr Rev* **36**, 487-525 (2015).

322 Jakimiuk, A. J., Weitsman, S. R. & Magoffin, D. A. 5alpha-reductase activity in women with polycystic ovary syndrome. *J Clin Endocrinol Metab* **84**, 2414-2418 (1999).

323 Agarwal, S. K., Judd, H. L. & Magoffin, D. A. A mechanism for the suppression of estrogen production in polycystic ovary syndrome. *J Clin Endocrinol Metab* **81**, 3686-3691 (1996).

324 Willis, D. S. *et al.* Premature response to luteinizing hormone of granulosa cells from anovulatory women with polycystic ovary syndrome: relevance to mechanism of anovulation. *J Clin Endocrinol Metab* **83**, 3984-3991 (1998).

325 Hu, Y., Cortvrindt, R. & Smitz, J. Effects of aromatase inhibition on in vitro follicle and oocyte development analyzed by early preantral mouse follicle culture. *Mol Reprod Dev* **61**, 549-559 (2002).

326 Qiao, J. & Feng, H. L. Extra- and intra-ovarian factors in polycystic ovary syndrome: impact on oocyte maturation and embryo developmental competence. *Hum Reprod Update* **17**, 17-33 (2011).

327 Brzyski, R. G., Grow, D. R., Sims, J. A. & Seltman, H. J. Increase in androgen:estrogen ratio specifically during low-dose follicle-stimulating hormone therapy for polycystic ovary syndrome. *Fertil Steril* **64**, 693-697 (1995).

328 Teissier, M. P., Chable, H., Paulhac, S. & Aubard, Y. Comparison of follicle steroidogenesis from normal and polycystic ovaries in women undergoing IVF: relationship between steroid concentrations, follicle size, oocyte quality and fecundability. *Hum Reprod* **15**, 2471-2477 (2000).

329 Teixeira Filho, F. L. *et al.* Aberrant expression of growth differentiation factor-9 in oocytes of women with polycystic ovary syndrome. *J Clin Endocrinol Metab* **87**, 1337-1344 (2002).

330 Franks, S., Roberts, R. & Hardy, K. Gonadotrophin regimens and oocyte quality in women with polycystic ovaries. *Reprod Biomed Online* **6**, 181-184 (2003).

331 Heijnen, E. M. *et al.* A meta-analysis of outcomes of conventional IVF in women with polycystic ovary syndrome. *Hum Reprod Update* **12**, 13-21 (2006).

332 Dumesic, D. A., Padmanabhan, V. & Abbott, D. H. Polycystic ovary syndrome and oocyte developmental competence. *Obstet Gynecol Surv* **63**, 39-48 (2008).

333 Cano, F. *et al.* Oocyte quality in polycystic ovaries revisited: identification of a particular subgroup of women. *J Assist Reprod Genet* **14**, 254-261 (1997).

334 Dumesic, D. A. *et al.* Impaired developmental competence of oocytes in adult prenatally androgenized female rhesus monkeys undergoing gonadotropin stimulation for in vitro fertilization. *J Clin Endocrinol Metab* **87**, 1111-1119 (2002).

335 Vendola, K. A. *et al.* Androgens stimulate early stages of follicular growth in the primate ovary. *J Clin Invest* **101**, 2622-2629 (1998).

336 Walters, K. A., Allan, C. M. & Handelsman, D. J. Androgen actions and the ovary. *Biol Reprod* **78**, 380-389 (2008).

337 Boudoures, A. L. *et al.* Obesity-exposed oocytes accumulate and transmit damaged mitochondria due to an inability to activate mitophagy. *Dev Biol* **426**, 126-138 (2017).

338 Silvestris, E., de Pergola, G., Rosania, R. & Loverro, G. Obesity as disruptor of the female fertility. *Reprod Biol Endocrinol* **16**, 22 (2018).

339 Eppig, J. J., O'Brien, M. J., Pendola, F. L. & Watanabe, S. Factors affecting the developmental competence of mouse oocytes grown in vitro: follicle-stimulating hormone and insulin. *Biol Reprod* **59**, 1445-1453 (1998).

340 McGee, W. K. *et al.* Elevated androgens during puberty in female rhesus monkeys lead to increased neuronal drive to the reproductive axis: a possible component of polycystic ovary syndrome. *Hum Reprod* **27**, 531-540 (2012).

341 Daughtry, B. L. *et al.* Single-cell sequencing of primate preimplantation embryos reveals chromosome elimination via cellular fragmentation and blastomere exclusion. *Genome Res* **29**, 367-382 (2019).

342 Chavez, S. L. *et al.* Dynamic blastomere behaviour reflects human embryo ploidy by the four-cell stage. *Nat Commun* **3**, 1251 (2012).

343 Vitak, S. A. *et al.* Sequencing thousands of single-cell genomes with combinatorial indexing. *Nat Methods* **14**, 302-308 (2017).

344 Olshen, A. B., Venkatraman, E. S., Lucito, R. & Wigler, M. Circular binary segmentation for the analysis of array-based DNA copy number data. *Biostatistics* **5**, 557-572 (2004).

345 Ha, G. *et al.* Integrative analysis of genome-wide loss of heterozygosity and monoallelic expression at nucleotide resolution reveals disrupted pathways in triple-negative breast cancer. *Genome Res* **22**, 1995-2007 (2012).

346 Knouse, K. A., Wu, J. & Amon, A. Assessment of megabase-scale somatic copy number variation using single-cell sequencing. *Genome Res* **26**, 376-384 (2016).

347 Gresl, T. A. *et al.* Dietary restriction and glucose regulation in aging rhesus monkeys: a follow-up report at 8.5 yr. *Am J Physiol Endocrinol Metab* **281**, E757-765 (2001).

348 Hansen, B. C., Bodkin, N. L. & Ortmeyer, H. K. Calorie restriction in nonhuman primates: mechanisms of reduced morbidity and mortality. *Toxicol Sci* **52**, 56-60 (1999).
349 Wagner, J. D., Cann, J. A., Zhang, L. & Harwood, H. J. in *Nonhuman Primates in Biomedical Research* 699-732 (2012).
350 Redinger, R. N. The pathophysiology of obesity and its clinical manifestations. *Gastroenterol Hepatol (N Y)* **3**, 856-863 (2007).
351 Gushchina, L. V., Yasmeen, R. & Ziouzenkova, O. Moderate vitamin A supplementation in obese mice regulates tissue factor and cytokine production in a sex-specific manner. *Arch Biochem Biophys* **539**, 239-247 (2013).
352 Yoshino, O. *et al.* Concentrations of interferon-gamma-induced protein-10 (IP-10), an antiangiogenic substance, are decreased in peritoneal fluid of women with advanced endometriosis. *Am J Reprod Immunol* **50**, 60-65 (2003).
353 Angiolillo, A. L. *et al.* Human interferon-inducible protein 10 is a potent inhibitor of angiogenesis in vivo. *J Exp Med* **182**, 155-162 (1995).
354 Strieter, R. M. *et al.* Interferon gamma-inducible protein 10 (IP-10), a member of the C-X-C chemokine family, is an inhibitor of angiogenesis. *Biochem Biophys Res Commun* **210**, 51-57 (1995).
355 Coughlin, C. M. *et al.* Tumor cell responses to IFNgamma affect tumorigenicity and response to IL-12 therapy and antiangiogenesis. *Immunity* **9**, 25-34 (1998).
356 Tamanini, C. & De Ambrogi, M. Angiogenesis in developing follicle and corpus luteum. *Reprod Domest Anim* **39**, 206-216 (2004).
357 Trinchieri, G. Interleukin-12: a proinflammatory cytokine with immunoregulatory functions that bridge innate resistance and antigen-specific adaptive immunity. *Annu Rev Immunol* **13**, 251-276 (1995).
358 Krizan, J. *et al.* Altered distribution of NK and NKT cells in follicular fluid is associated with IVF outcome. *J Reprod Immunol* **82**, 84-88 (2009).
359 Deng, H. *et al.* Elevated serum interferon gamma-inducible protein-10 in women with polycystic ovary syndrome. *Gynecol Endocrinol* **33**, 363-367 (2017).
360 Tarkun, I. *et al.* Endothelial dysfunction in young women with polycystic ovary syndrome: relationship with insulin resistance and low-grade chronic inflammation. *J Clin Endocrinol Metab* **89**, 5592-5596 (2004).
361 Shorakae, S. *et al.* Inter-related effects of insulin resistance, hyperandrogenism, sympathetic dysfunction and chronic inflammation in PCOS. *Clin Endocrinol (Oxf)* **89**, 628-633 (2018).
362 Saharkhiz, N. *et al.* The effect of testosterone gel on fertility outcomes in women with a poor response in in vitro fertilization cycles: A pilot randomized clinical trial. *J Res Med Sci* **23**, 3 (2018).
363 Haydardedeoglu, B., Isik, A. Z. & Bulgan Kilicdag, E. The combination of dehydroepiandrosterone, transdermal testosterone, and growth hormone as an adjuvant therapy in assisted reproductive technology cycles in patients aged below 40 years with diminished ovarian reserve. *Turk J Obstet Gynecol* **12**, 60-65 (2015).
364 Ludwig, M. *et al.* Oocyte quality and treatment outcome in intracytoplasmic sperm injection cycles of polycystic ovarian syndrome patients. *Hum Reprod* **14**, 354-358 (1999).

365 Jabara, S. & Coutifaris, C. In vitro fertilization in the PCOS patient: clinical considerations. *Semin Reprod Med* **21**, 317-324 (2003).
366 Papouli, E., Defais, M. & Larminat, F. Overexpression of metallothionein-II sensitizes rodent cells to apoptosis induced by DNA cross-linking agent through inhibition of NF-kappa B activation. *J Biol Chem* **277**, 4764-4769 (2002).
367 Tanaka, M. *et al.* Identification of candidate cooperative genes of the Apc mutation in transformation of the colon epithelial cell by retroviral insertional mutagenesis. *Cancer Sci* **99**, 979-985 (2008).
368 Chakraborty, S. & Ain, R. NOSTRIN: A novel modulator of trophoblast giant cell differentiation. *Stem Cell Res* **31**, 135-146 (2018).
369 Makkar, A. *et al.* Fatty acid binding protein-4 is expressed in the mouse placental labyrinth, yet is dispensable for placental triglyceride accumulation and fetal growth. *Placenta* **35**, 802-807 (2014).
370 Sherman, M. I., Gay, R., Gay, S. & Miller, E. J. Association of collagen with preimplantation and peri-implantation mouse embryos. *Dev Biol* **74**, 470-478 (1980).
371 Carson, D. D., Tang, J. P. & Gay, S. Collagens support embryo attachment and outgrowth in vitro: effects of the Arg-Gly-Asp sequence. *Dev Biol* **127**, 368-375 (1988).
372 Perrier d'Hauterive, S. *et al.* Dialogue between blastocyst hCG and endometrial LH/hCG receptor: which role in implantation? *Gynecol Obstet Invest* **64**, 156-160 (2007).
373 Dokras, A., Sargent, I. L., Gardner, R. L. & Barlow, D. H. Human trophectoderm biopsy and secretion of chorionic gonadotrophin. *Hum Reprod* **6**, 1453-1459 (1991).
374 Seshagiri, P. B., Vani, V. & Madhulika, P. Cytokines and Blastocyst Hatching. *Am J Reprod Immunol* **75**, 208-217 (2016).
375 Zhou, X. *et al.* Loss of CDYL Results in Suppression of CTNNB1 and Decreased Endometrial Receptivity. *Front Cell Dev Biol* **8**, 105 (2020).
376 Gonzalez, T. L. *et al.* Sex differences in the late first trimester human placenta transcriptome. *Biol Sex Differ* **9**, 4 (2018).
377 Roifman, M. *et al.* Genome-wide placental DNA methylation analysis of severely growth-discordant monochorionic twins reveals novel epigenetic targets for intrauterine growth restriction. *Clin Epigenetics* **8**, 70 (2016).
378 Migita, H. *et al.* RORalpha1 and RORalpha4 suppress TNF-alpha-induced VCAM-1 and ICAM-1 expression in human endothelial cells. *FEBS Lett* **557**, 269-274 (2004).
379 Klar, J. *et al.* RAR-related orphan receptor A isoform 1 (RORa1) is disrupted by a balanced translocation t(4;15)(q22.3;q21.3) associated with severe obesity. *Eur J Hum Genet* **13**, 928-934 (2005).
380 Thathapudi, S. *et al.* Tumor necrosis factor-alpha and polycystic ovarian syndrome: a clinical, biochemical, and molecular genetic study. *Genet Test Mol Biomarkers* **18**, 605-609 (2014).
381 Duffy, D. M. *et al.* Ovulation: Parallels With Inflammatory Processes. *Endocr Rev* **40**, 369-416 (2019).

3645 382 Rodriguez-Wallberg, K. A. & Oktay, K. Fertility preservation during cancer
3646 treatment: clinical guidelines. *Cancer Manag Res* **6**, 105-117 (2014).
3647 383 Kumar, P. & Sait, S. F. Luteinizing hormone and its dilemma in ovulation
3648 induction. *J Hum Reprod Sci* **4**, 2-7 (2011).
3649 384 Lee, S. H. *et al.* Effect of co-culture canine cumulus and oviduct cells with porcine
3650 oocytes during maturation and subsequent embryo development of parthenotes in
3651 vitro. *Theriogenology* **106**, 108-116 (2018).
3652 385 Appeltant, R. *et al.* Interactions between oocytes and cumulus cells during in vitro
3653 maturation of porcine cumulus-oocyte complexes in a chemically defined medium:
3654 effect of denuded oocytes on cumulus expansion and oocyte maturation.
3655 *Theriogenology* **83**, 567-576 (2015).
3656 386 Adeldust, H. *et al.* In vitro maturation of ovine oocyte in a modified granulosa cells
3657 co-culture system and alpha-tocopherol supplementation: effects on nuclear
3658 maturation and cleavage. *J Anim Sci Technol* **57**, 27 (2015).
3659 387 Espey, L. L. Ovulation as an inflammatory reaction--a hypothesis. *Biol Reprod* **22**,
3660 73-106 (1980).

3661